The Dissertation Committee for Yannick Bomble
certifies that this is the approved version of the following dissertation:

Development and Implementation of High Accuracy Coupled Cluster Methods for Ground and Excited States: Applications to Thermochemistry and Spectroscopy

Committee:

John F. Stanton, Supervisor

Peter J. Rossky

David A. Vanden Bout

Eric V. Anslyn

Manfred Fink

Development and Implementation of High Accuracy Coupled Cluster Methods for Ground and Excited States: Applications to Thermochemistry and Spectroscopy

by

Yannick Bomble, B.S.

DISSERTATION

Presented to the Faculty of the Graduate School of

The University of Texas at Austin

in Partial Fulfillment

of the Requirements

for the Degree of

DOCTOR OF PHILOSOPHY

THE UNIVERSITY OF TEXAS AT AUSTIN

May 2006

Dedicated to my parents

Acknowledgments

This dissertation would not have been completed without the help, patience, and guidance of my adviser, John Stanton. I cannot thank him enough for creating a stimulating research environment and teaching me the ways of rigorous quantum chemistry. The past five years have been the most intellectually challenging years of my "long" academic career, however, I was always awarded the time and freedom needed to digest the difficult concepts of coupled cluster theory. I am also indebted to my colleagues and friends at U.T for their encouragements and interesting conversations - Juana Vázquez, Mychel Varner, David Shear, Christopher Simmons, David Price, Harshal Gupta, Bradley Flowers, Craig Michoski, Thomas Doyle, and finally, my best man – who was present for one of the happiest days of my life – Michael Griffin.

Special thanks to Dr. Peter Rossky for his help, his advices, and for offering challenging statistical mechanics and quantum chemistry classes. I am also thankful to Dr. Eric Anslyn for getting me involved in some of his research projects.

This work was the result of numerous fruitful collaborations with research groups in Europe. I am deeply indebted to Mihály Kállay for his help in the development of CCSDT(Q) and also to Jürgen Gauss for inviting me several times to Mainz. The time I spent in Mainz will always be part of my best memories; I cannot thank him and his research group enough for taking

such good care of me when I was in Germany.

I would like to thank my parents, my sister, and my family for their love and support, and for providing a stable environment for my spiritual development.

Finally, none of this work would have been possible without the unconditional love and support of my wife, Florence. Thank you for standing by my side all these years and for giving me the most wonderful gift of all, a little baby girl, Olivia.

Development and Implementation of High Accuracy Coupled Cluster Methods for Ground and Excited States: Applications to Thermochemistry and Spectroscopy

Publication No. _____

Yannick Bomble, Ph.D.
The University of Texas at Austin, 2006

Supervisor: John F. Stanton

Several methods for treating ground and excited states are presented. All of them are based on the coupled cluster theory which is acknowledged to provide an excellent alternative to the correlation problem. A new approach is developed and implemented for treating the quadruple excitations in coupled cluster theory. Quadruple excitation contributions are computed from a formula based on a non-Hermitian perturbation theory analogous to that used previously to justify the usual noniterative triples correction used in the coupled cluster method known as CCSD(T). This method is similar to CCSD(T) and is known as CCSDT(Q). The latter is thoroughly tested on a set of molecules and is also used to simplify the HEAT protocol for calculating thermochemical parameters. The total energies obtained with CCSDT(Q) agree favorably with the ones obtained with coupled cluster methods including

single, double, triple, quadruple and even pentuple excitations. The enthalpies of formations calculated by combining CCSDT(Q) with the HEAT protocol are less than 1 kJ per mole of their best known values. Additionally, methods for evaluating ionization potentials with an approximate treatment of triple excitations are described. These are an extension of the existing EOMIP-CCSD method and are based on the CCSDT-X (X=1a, 1b, 2, 3) and CC3 approximations in traditional coupled cluster theory. Appropriate to their role in studying radicals, they are here tested on the first two Σ states and first Π state of the N_2^+, CO^+, CN, and BO diatomic radicals. The calculations show a tendency for the CC3 variant to overestimate the bond lengths and to underestimate the vibrational frequencies, while the CCSDT-3 variant seems to be most reliable. It is also demonstrated that the accuracy of such methods is comparable to sophisticated traditional multireference approaches and full configuration interaction. Similar methods for studying excited states (EOMEE-CC) are used in combination with traditional coupled cluster methods and the vibronic coupling model to investigate the vertical excitation energy for the lowest valence $\pi \rightarrow \pi^*$ transition in cyclopentadiene (CP).

Table of Contents

List of Tables

List of Figures

Chapter 1

Introduction

The main goal of any electronic structure method is to solve the time independent Schrödinger equation as accurately as possible within the Born-Oppenheimer approximation. The easiest alternative is to construct an antisymmetrical (with respect to interchange of electrons) wavefunction from a Hartree-Fock self consistent field (HF-SCF) procedure. The drawback of HF-SCF is that it doesn't take into account the instantaneous interactions among the electrons, meaning that any electron is considered to be moving in the average field created by the N-1 other electrons. The correlation of motion of the electrons is therefore neglected; the energy term missing within the Hartree-Fock procedure is known as "correlation energy". All ab initio methods going beyond the HF approximation are designed to recover as much of the correlation energy as possible within the basis set limitations. By considering all Slater determinants obtained by exciting all electrons to all the possible virtual orbitals one can recover the entire correlation energy. It can be achieved by applying an "infinite" string of excitation operators (with appropriate weights) on the HF slater determinant until all possible excitations are accounted for. This procedure is known as the full configuration interaction (FCI)[1,2,3] which was developed throughout the 1980's and successfully implemented by several

quantum chemistry groups. Probably some of the most recognized studies and implementations of this method were done by Nicholas C. Handy in Cambridge. While being an indisputably powerful method for benchmark purposes, it is unpractical for molecules with more than a few electrons. An obvious solution to this problem is to truncate the excitation operator to a certain level of excitation depending on the size of the system considered. While it is a good idea in order to reduce the computational cost it also causes problems; the main problem being that the solution no longer scales with the size of the system and is therefore labelled as not being "size consistent".

This size-consistency problem motivated the development of other correlated methods based on many-body perturbation theory (MBPT) [4,5,6,7]. Second-order MBPT2 - MP2 or MBPT(2) - is probably the most well-known and widely used of these methods. One of the other approaches developed in the last twenty years to solve the "correlation" problem is coupled cluster theory[8,9,10] where the excitation operator is no longer linear as in the case of full configuration interaction but rather is exponential. This is actually an infinite-order generalization of MBPT. The coupled cluster wavefunction is therefore more complicated than its full configuration interaction counterpart, but is equivalent if the maximum excitation level is equal to the number of electrons in the system. This means that the coupled cluster method can also solve the time independent Schrödinger equation exactly within the one-electron basis set limit if the excitation operator is not truncated. It is obvious that such a method is prohibitively expensive, and that a truncation of the cluster oper-

ator is required to create more usable and practical approaches. The first ab initio coupled cluster methods to be developed[11] were the coupled cluster doubles (CCD)[12,13] and the coupled cluster singles and doubles (CCSD)[14,15] where double excitations and single and double excitations are included in the cluster operator (Chapter 2), respectively. Subsequent methods such as CCSDT[16], CCSDTQ[17], CCSDTQP[18] were introduced more recently by adding higher level of excitations in order to treat the correlation problem more precisely. However, the aim of quantum chemistry should be to propose methods that are both reliable and cost effective. This can be done in practice by introducing approximate excitation operators into the Schrödinger equation allowing for a good compromise between cost and accuracy. One of the most successful of these approximations is the addition of noniterative approximate triple excitations to the already existing CCSD approach called CCSD(T)[19,20,21]. The correlation energy recovered by the latter method is close in most cases to that obtained with CCSDT, making it perhaps the most commonly used CC method. Chapter 3 deals with the addition of approximate noniterative quadruple excitations to CCSDT inspired by the same approach taken to derive the CCSD(T) method; this method is logically named CCSDT(Q)[22] because of its formal similarity to CCSD(T). The latter is compared to a similar approach where the approximation of the quadruple excitations is obtained by applying perturbation theory on a HF-SCF determinant[23,24,25,26] instead of taking the CCSDT solution as zeroth-order as is done in CCSDT(Q).

Chapter 4 provides a thorough benchmark evaluation of CCSDT(Q)

using a exhaustive set of challenging molecular systems and a vital application to thermochemistry. The CCSDT(Q) approach will be used within the now well-established HEAT protocol[27,28] to show its applicability for the evaluation of accurate thermochemical parameters.

Another important aspect of quantum chemistry is to describe potential energy surfaces of open-shell molecules and excited states accurately. This is usually a difficult task due to the proximity of other electronic states and the consequent configuration mixing. Indeed, in most open-shell molecules the energy levels are within a few eV of each other creating strong interactions and phenomena not usually seen in closed-shell molecules. Among these interactions are pseudo Jahn-Teller coupling[29] and spin contamination of the wavefunction[30]. In most cases a single reference determinant is used for radicals even though these determinants are usually the source of the problems encountered when dealing with open-shell molecules. The low-lying states can make the "true" wavefunction more "multireference-like" and it is therefore hard to achieve high accuracy with single-determinant methods. However, in recent years, the equation-of-motion coupled cluster (EOM-CC) approach[31,32,33,34,35,36] has made the study of open-shell systems easier. The EOM-CC procedure usually starts with a well-behaved closed-shell determinant that can be acted upon to obtain the target state, the latter being an excited or an ionized state for example. These states can be obtained by the action of appropriate annihilation and creation operators onto the reference wavefunction. The secret of the EOM-CC approach resides in its balanced

treatment of more than one reference because the eigenstate is obtained by diagonalization. For example, states of the CN molecule can be obtained by applying an EOM-CC calculation on the CN^- closed-shell molecule; this variant of EOM-CC is labelled as EOMIP-CC[37,38,39,40,41] where IP stands for ionization potential since an electron will be removed from the reference determinant. The other special cases of the EOM-CC theory are EOMEE-CC (excited states)[42,31] and EOMEA-CC (electron attachment)[43] where the desired state is obtained by moving an electron from an occupied orbital to a virtual orbital or by simply adding an electron to a virtual orbital in the case of EOMEA-CC. Several implementations based on these methods have been carried out for both energy and gradient theory and have been used for the study of radicals, absorption and ionization spectra. Most recently, the EOMIP-CCSDT[44] and even the EOMIP-CCSDTQ were developed by Musial *et al.* and by Hirata using the tensor contraction engine approach. Given the excitation level of the latter methods it is understandable that they can only be used for relatively small systems (two or three heavy atoms with a cc-pVDZ basis set[45]). Reflecting on the cost of these approaches, it is interesting to think of methods that are intermediate between EOMIP-CCSDT and EOMIP-CCSD but would recover most of the triples effect as it was done in traditional coupled cluster theory with the CCSDT-X (X=1a, 1b, 2, 3)[46] and CC3[47,48] approximations. Chapter 5 presents these newly formulated approaches for ionization potential and provides a thorough benchmark on some challenging radicals known to pose problems to most ab initio methods.

Chapter 6 presents an interesting study of the excitation energy corresponding to the $\pi \rightarrow \pi^*$ transition in cyclopentadiene (CP). In this chapter powerful methods, e.g. EOMEE-CC, and vibronic coupling theory are used together to simulate the absorption spectrum related to the $^1B_2 \leftarrow {}^1A_1$ transition in CP. The approach used in this chapter can be seen as a template for simulating electronic spectra for similar systems but also shows the accuracy of the EOMEE-CC methods. Also, the vibronic coupling model will be briefly covered in this chapter.

Chapter 7 shows the importance of the size consistency in ab initio methods. In this study, CCSD(T) is compared to its renormalized version, R-CCSD(T)[49,50], which is not rigourously size-consistent. A set of molecules will be used to compare the two methods, and a molecular system of increasing size will be used to show the lack of size consistency in R-CCSD(T).

Appendix A discusses the adaptation of the direct inversion of iterative subspace (DIIS) algorithm[51] used in most electronic structure theory programs to study dimerization processes followed by ^{1}H NMR titration.

Appendix B shows a proposed theoretical model for indicator-displacement assay isotherms and its simple implementation by using viète's analytical solution to third order polynomial. These isotherm binding curves are compared to experiment and the model is used for the determination of malate concentration in Pinot Noir grapes.

Finally, appendices C through L present a list of the author's publica-

tions and their corresponding abstracts.

Chapter 2

Introduction to Coupled Cluster Theory

2.1 Hartree-Fock and Configuration Interaction Theory

The starting point of electronic structure theory is the Hartree-Fock approximation in which the wavefunction is approximated by a single reference determinant of spin obitals. In this approximation the wavefunction can be represented as a product of spin orbitals know as the Hartree product

$$|\Psi_{HF}(X_1, X_2, X_3...X_n)\rangle = |\chi_1(X_1)\chi_2(X_2)\chi_3(X_3)\chi_4(X_4)...\chi_n(X_n)\rangle \qquad (2.1)$$

It is obvious that the Hartree product doesn't satisfy the antisymmetry principle; this is why in the self consistent field (SCF) approximation the Hartree Fock product is replaced by the usual n-electron slater determinant $|\Phi_0\rangle$.

$$|\Phi_0\rangle \;=\; |\chi_1\chi_2\chi_3\cdots\chi_n\rangle \equiv \sqrt{\frac{1}{n!}} \begin{vmatrix} \chi_1(X_1) & \chi_2(X_1) & \cdots & \chi_n(X_1) \\ \chi_1(X_2) & \chi_2(X_2) & \cdots & \chi_n(X_2) \\ \chi_1(X_3) & \chi_2(X_3) & \cdots & \chi_n(X_3) \\ \vdots & \vdots & \ddots & \vdots \\ \chi_1(X_n) & \chi_2(X_n) & \cdots & \chi_n(X_n) \end{vmatrix} \qquad (2.2)$$

$|\Phi_0\rangle$ is a convenient antisymmetric wavefunction that can be used to solve the Hartree-Fock equations. A wavefunction of this form gives, for a single

reference method, the lowest energy for

$$E_0 = \langle \Phi_0 | \hat{H} | \Phi_0 \rangle \tag{2.3}$$

where $\hat{H}$ is the full electronic Hamiltonian. It can be proven that the Hartree-Fock problem can be written using the one-electron Fock operator as the following eigenvalue problem

$$f\,\chi_i = \epsilon_i \chi_i \tag{2.4}$$

where the ϵ_n are assumed to be the energies of the corresponding orthonormal orbitals ϕ_n obtained by solving Equation 2.3 and are called Hartree-Fock molecular orbitals; f being the so-called one-electron Fock operator. If one introduces a basis set

$$\chi_i = \sum_{\mu}^{k} C_{\mu i} \phi_\mu \tag{2.5}$$

where ϕ_μ are atomic orbital basis functions in the Hartree-Fock equations one can obtain the Roothaan equations

$$\sum_{\nu} F_{\mu\nu} C_{\nu i} = \epsilon_i \sum_{\nu} S_{\mu\nu} C_{\nu i} \tag{2.6}$$

with $F_{\mu\nu}$ and $S_{\mu\nu}$ being

$$\begin{aligned} F_{\mu\nu} &= \int \phi_\mu^* \phi_\nu dX_1 \\ S_{\mu\nu} &= \int \phi_\mu^* f(X_1) \phi_\nu dX_1 \end{aligned} \tag{2.7}$$

It is common practice to write the Roothaan equations in the following matrix form

$$\mathbf{FC} = \epsilon \mathbf{SC} \tag{2.8}$$

where **S** is the overlap matrix. Solving this equation requires an iterative process called self-consistent procedure since the **F** matrix depends on its own eigenvectors.

The major shortcoming of Hartree-Fock theory is that it doesn't account for correlated motion of the electrons and therefore cannot produce a picture of the instantaneous interaction between electrons. The Hartree-Fock problem is solved by selecting an electron moving in a space where all the other electrons are frozen therefore only experiencing the average potential that they create. This is repeated for the whole set of electrons in the system. The difference between the exact energy and the Hartree-Fock energy is called the correlation energy.

$$E_{Corr} = \epsilon_0 - E_{HF} \tag{2.9}$$

Here, ϵ_0 is the exact non-relativistic energy and E_{HF} is the energy in the Hartree-Fock limit (Hartree-Fock energy calculated with an infinite basis set). Several approaches have been developed to overcome the lack of correlation of the Hartree-Fock solution. Among others the configuration interaction (CI) method[1,2,3] is one of the oldest and well-established methods to recover the correlation energy. The configuration interaction wavefunction is a linear combination of slater determinants where one mixes the different electronic configurations. This method can be summarized by the following equation:

$$\Psi_{FCI} = c_0|0\rangle + c_1\Phi_i^a + c_2\Phi_{ij}^{ab} + (...) \tag{2.10}$$

where $|0\rangle$ is a Slater determinant obtained by solving the Hartree-Fock equations (equivalent to Φ_0 earlier in the text). Φ_i^a and Φ_{ij}^{ab} are all the singly

and doubly excited determinants, respectively. The term singly excited means that the Φ_i^a are obtained by promoting one electron from an occupied orbital i (hole) to a virtual orbital a (particle). Using appropriate creation $\mathbf{a}^\dagger$ and annihilation $\mathbf{a}$ operators, one can rewrite Φ_i^a, Φ_{ij}^{ab} and all the other n-excited determinants as a string of creation and annihilation operators acting on the ground state slater determinant $|0\rangle$.

$$\begin{aligned} \Phi_i^a &\equiv a_a^\dagger a_i |0\rangle \\ \Phi_{ij}^{ab} &\equiv a_a^\dagger a_i a_b^\dagger a_j |0\rangle \\ \Phi_{ijk}^{abc} &\equiv a_a^\dagger a_i a_b^\dagger a_j a_c^\dagger a_k |0\rangle \end{aligned} \tag{2.11}$$

Thus we can rewrite the FCI wavefunction as

$$\Psi_{FCI} = C_0|0\rangle + C_1|0\rangle + C_2|0\rangle + (...) \tag{2.12}$$

with

$$C_0 = C_0^0 \tag{2.13}$$

$$C_1 = \sum_{ia} C_i^a a_a^\dagger a_i \tag{2.14}$$

$$C_2 = \frac{1}{4} \sum_{ijab} C_{ij}^{ab} a_a^\dagger a_i a_b^\dagger a_j \tag{2.15}$$

The following diagrams illustrate how the creation and annihilation operators act on the reference determinant $|0\rangle$ to create the singly and doubly excited determinants.

$$|S\rangle = \sum_{ia} a_a^\dagger a_i \left| \begin{array}{c} \overline{} \\ \overline{} \\ \overline{} \\ +\overline{} \\ +\overline{} \\ +\overline{} \end{array} \right\rangle \ni \left| \begin{array}{c} \overline{} \\ \overline{} \\ +\overline{} \\ +\overline{} \\ +\overline{} \\ +\overline{} \end{array} \right\rangle + \left| \begin{array}{c} \overline{} \\ +\overline{} \\ \overline{} \\ +\overline{} \\ +\overline{} \\ +\overline{} \end{array} \right\rangle + \left| \begin{array}{c} +\overline{} \\ \overline{} \\ \overline{} \\ +\overline{} \\ +\overline{} \\ +\overline{} \end{array} \right\rangle (...) \left| \begin{array}{c} +\overline{} \\ \overline{} \\ \overline{} \\ +\overline{} \\ +\overline{} \\ \overline{} \end{array} \right\rangle$$

$$|D\rangle = \sum_{ijab} a_a^\dagger a_b^\dagger a_i a_j \left| \begin{array}{c} \overline{} \\ \overline{} \\ \overline{} \\ +\overline{} \\ +\overline{} \\ +\overline{} \end{array} \right\rangle \ni \left| \begin{array}{c} \overline{} \\ \overline{} \\ +\overline{} \\ \overline{} \\ +\overline{} \\ +\overline{} \end{array} \right\rangle + \left| \begin{array}{c} \overline{} \\ +\overline{} \\ +\overline{} \\ \overline{} \\ +\overline{} \\ +\overline{} \end{array} \right\rangle + \left| \begin{array}{c} +\overline{} \\ \overline{} \\ +\overline{} \\ \overline{} \\ +\overline{} \\ +\overline{} \end{array} \right\rangle (...) \left| \begin{array}{c} +\overline{} \\ \overline{} \\ \overline{} \\ \overline{} \\ +\overline{} \\ +\overline{} \end{array} \right\rangle$$

The full configuration interaction is designed to solve the Schrödinger equation exactly within the basis set limitations.

$$H_{FCI} \equiv \begin{pmatrix} \langle 0|H|0\rangle & \langle 0|H|\Phi_i^a\rangle & (...) & \langle 0|H|\Phi_{ijk...n}^{abc...n}\rangle \\ \langle \Phi_i^a|H|0\rangle & \langle \Phi_i^a|H|\Phi_i^a\rangle & (...) & \langle \Phi_i^a|H|\Phi_{ijk...n}^{abc...n}\rangle \\ \langle \Phi_{ij}^{ab}|H|0\rangle & \langle \Phi_{ij}^{ab}|H|\Phi_i^a\rangle & (...) & \langle \Phi_{ij}^{ab}|H|\Phi_{ijk...n}^{abc...n}\rangle \\ \langle \Phi_{ijk}^{abc}|H|0\rangle & \langle \Phi_{ijk}^{abc}|H|\Phi_i^a\rangle & (...) & \langle \Phi_{ijk}^{abc}|H|\Phi_{ijk...n}^{abc...n}\rangle \\ (...) & (...) & (...) & (...) \\ (...) & (...) & (...) & (...) \\ (...) & (...) & (...) & (...) \\ (...) & (...) & (...) & (...) \\ (...) & (...) & (...) & (...) \\ (...) & (...) & (...) & (...) \\ \langle \Phi_{ijk...n}^{abc...n}|H|0\rangle & \langle \Phi_{ijk...n}^{abc...n}|H|\Phi_i^a\rangle & (...) & \langle \Phi_{ijk...n}^{abc...n}|H|\Phi_{ijk...n}^{abc...n}\rangle \end{pmatrix} \quad (2.16)$$

It should be noted that since the operator H is a two-electron operator the previous matrix assumes the following banded form

$$H_{FCI} \equiv \begin{pmatrix} H_{00} & H_{0S} & H_{0D} & 0 & 0 & (...) \\ H_{S0} & H_{SS} & H_{SD} & H_{ST} & 0 & (...) \\ H_{D0} & H_{DS} & H_{DD} & H_{DT} & H_{DQ} & (...) \\ 0 & H_{TS} & H_{TD} & H_{TT} & H_{TQ} & (...) \\ (...) & 0 & H_{QD} & H_{QT} & H_{QQ} & (...) \\ (...) & (...) & 0 & H_{PT} & H_{PQ} & (...) \\ (...) & (...) & (...) & 0 & H_{S_eQ} & (...) \\ (...) & (...) & (...) & (...) & 0 & (...) \\ (...) & (...) & (...) & (...) & (...) & (...) \\ (...) & (...) & (...) & (...) & (...) & (...) \\ 0 & 0 & 0 & 0 & 0 & (...) \end{pmatrix} \tag{2.17}$$

However, to evaluate the FCI energy the complete set of excited determinant must be diagonalized; this is really unpractical except for a few small systems. The number of determinants for the water molecule using different basis sets is shown in Table 2.1.

Table 2.1: Exponential growth of the FCI Hamiltonian for the simple example of the water molecule

Basis sets	Number of basis functions	Number of FCI determinants
STO-3G	7	1.00×10^3
6-31G	13	5.31×10^6
6-31G*	18	2.54×10^8
6-311G	19	4.73×10^8
cc-pVDZ	24	6.54×10^9
cc-pVTZ	58	8.16×10^{13}

Thus, approximations must be taken in order to evaluate the correlation en-

ergy using the CI framework. The usual approximation is to truncate the excitation level in order to be able to diagonalize the CI matrix, thus, evaluate the CI coefficients. One of the inconvenience of truncated CI methods is their lack of size consistency that has motivated quantum chemists to develop other methods. The CISD method[52] is usually used to show the lack of size consistency in truncated CI methods. In the case of CISD, the only excited determinants included are singly and doubly excited determinants. Let us assume the following CISD wavefunction

$$\Phi_{CISD} = C_0|0\rangle + C_1|0\rangle + C_2|0\rangle \tag{2.18}$$

or in a simpler form

$$\Phi_{CISD} = \phi_{HF} + \phi_S + \phi_D \tag{2.19}$$

One can define a supersystem AB (where A and B don't interact) and its corresponding CISD wavefunction as follows

$$\Phi^{AB}_{CISD} = \Phi^{A}_{CISD}\Phi^{B}_{CISD} \tag{2.20}$$

where

$$\Phi^{A}_{CISD} = \phi^{A}_{HF} + \phi^{A}_{S} + \phi^{A}_{D} \tag{2.21}$$

and similarly for system B. The CISD wavefunction corresponding the supersystem AB can be expanded in the following manner

$$\begin{aligned}\Phi^{AB}_{CISD} &= (\phi^{A}_{HF} + \phi^{A}_{S} + \phi^{A}_{D})(\phi^{B}_{HF} + \phi^{B}_{S} + \phi^{B}_{D}) \\ &= \phi^{A}_{HF}\phi^{B}_{HF} + \phi^{A}_{HF}\phi^{B}_{S} + \phi^{A}_{HF}\phi^{B}_{D} + \phi^{A}_{S}\phi^{B}_{HF} + (...) + \phi^{A}_{D}\phi^{B}_{D}.\end{aligned} \tag{2.22}$$

The arising terms can be collected by excitation orders but one can already notice that the solution will include triply and quadruply excited determinants that are not present in the traditional CISD model.

$$\begin{aligned}
\phi_{HF}^{AB} &= \phi_{HF}^{A}\phi_{HF}^{B} \\
\phi_{S}^{AB} &= \phi_{HF}^{A}\phi_{S}^{B} + \phi_{S}^{A}\phi_{HF}^{B} \\
\phi_{D}^{AB} &= \phi_{HF}^{A}\phi_{D}^{B} + \phi_{D}^{A}\phi_{HF}^{B} + \phi_{S}^{A}\phi_{S}^{B} \\
\phi_{T}^{AB} &= \phi_{S}^{A}\phi_{D}^{B} + \phi_{D}^{A}\phi_{S}^{B} \\
\phi_{Q}^{AB} &= \phi_{D}^{A}\phi_{D}^{B}
\end{aligned} \tag{2.23}$$

As mentioned earlier one would expect Φ_{CISD}^{AB} to be equal to $\Phi_{HF}^{AB} + \Phi_{S}^{AB} + \Phi_{D}^{AB}$ but this is obviously not the case; the three extra terms $(\phi_{S}^{A}\phi_{D}^{B} + \phi_{D}^{A}\phi_{S}^{B} + \phi_{D}^{A}\phi_{D}^{B})$ appearing in the expansion ruin the size consistency of this method as well as all truncated CI methods.

2.2 General Coupled Cluster Theory

The coupled cluster theory[10] was developed as an alternative to configuration interaction in order to truncate excitation operators while preserving the size consistency properties. For doing so, coupled cluster theory uses an exponential expansion of the cluster or excitation operator $\hat{T}$. Similarly to the configuration interaction operator, $\hat{T}$ is formed by a sum of well-known creation and annihilation operators weighted by the so-called coupled cluster amplitudes (t_{i}^{a}, t_{ij}^{ab}, t_{ijk}^{abc}, ...) as follows

$$\hat{T_1} \equiv \sum_{ia} t_i^a a_a^\dagger a_i \tag{2.24}$$

$$\hat{T_2} \equiv \frac{1}{4} \sum_{ijab} t_{ij}^{ab} a_a^\dagger a_b^\dagger a_j a_i \tag{2.25}$$

$$\hat{T_3} \equiv \frac{1}{36} \sum_{ijkabc} t_{ijk}^{abc} a_a^\dagger a_b^\dagger a_c^\dagger a_k a_j a_i \tag{2.26}$$

or a general n-orbital cluster operator may be defined as

$$\hat{T_n} \equiv \frac{1}{(n!)^2} \sum_{ijk...abc...} t_{ijk...}^{abc...} a_a^\dagger a_b^\dagger a_c^\dagger .....a_k a_j a_i \tag{2.27}$$

Using the cluster operator defined above the coupled cluster wavefunction is written as

$$|\Psi_{CC}\rangle = e^{\hat{T}} |\psi_0\rangle \tag{2.28}$$

where

$$\hat{T} = \hat{T_1} + \hat{T_2} + \hat{T_3} + ... + \hat{T_n} \tag{2.29}$$

and $|\psi_0\rangle$ is a Slater determinant that is usually, but not necessarily, the Hartree-Fock wavefunction.

In order to create the coupled cluster wavefunction one needs to evaluate the coupled cluster amplitudes. The starting point of the analysis is the Schrödinger equation,

$$\hat{H}|\Psi\rangle = E|\Psi\rangle \tag{2.30}$$

By introducing the coupled cluster wavefunction into the Schrödinger equation one obtains the following equation

$$\hat{H}e^{\hat{T}}|\psi_0\rangle = E_{CC}e^{\hat{T}}|\psi_0\rangle \tag{2.31}$$

which multiplied on the left by the reference determinant gives the coupled cluster energy

$$\langle\psi_0|\hat{H}e^{\hat{T}}|\psi_0\rangle = \langle\psi_0|E_{CC}e^{\hat{T}}|\psi_0\rangle \equiv E_{CC} \tag{2.32}$$

where intermediate normalization $\langle\psi_0|\Psi_{CC}\rangle = 1$ is assumed. While this equation is useful in order to understand the concepts of coupled cluster theory it is not well-suited for computer implementation. In the previous equation $\hat{H}$ can be written in second quantization as

$$\hat{H} = \sum_{pq} h_{pq}a_p^\dagger a_q + \frac{1}{4}\sum_{pqrs}\langle pq||rs\rangle a_p^\dagger a_q^\dagger a_s a_r \tag{2.33}$$

where h_{pq} is the one-electron component of the Hamiltonian and $\langle pq||rs\rangle$ the two-electron antisymmetrized counterpart.

A better way to derive the coupled cluster equations is by premultiplying Equation 2.31 by $e^{-\hat{T}}$ to obtain

$$\langle\psi_0|e^{-\hat{T}}\hat{H}e^{\hat{T}}|\psi_0\rangle = E_{CC}. \tag{2.34}$$

The following equation is also important to evaluate the amplitude of the coupled cluster operator

$$\langle\psi_{ijk\ldots}^{abc\ldots}|e^{-\hat{T}}\hat{H}e^{\hat{T}}|\psi_0\rangle = 0. \tag{2.35}$$

The last two equations are the corner-stones of coupled cluster theory and are used in derivations of coupled cluster methods. Using these two equations, the energy and cluster amplitudes are decoupled and therefore the computer implementation is simplified. The notation $\bar{H}$ is assumed from now on to define the operator $e^{-\hat{T}}\hat{H}e^{\hat{T}}$, called, similarity transformed Hamiltonian. It is somewhat unusable in this form; one can instead use the Hausdorff expansion to rewrite $\bar{H}$ as follows

$$\begin{aligned}\bar{H} =&\hat{H}_N + [\hat{H}_N, \hat{T}] + \frac{1}{2}[[\hat{H}_N, \hat{T}], \hat{T}] + \frac{1}{6}[[[\hat{H}_N, \hat{T}], \hat{T}], \hat{T}] \\ &+ \frac{1}{24}[[[[\hat{H}_N, \hat{T}], \hat{T}], \hat{T}], \hat{T}]\end{aligned} \tag{2.36}$$

where $\hat{H}_N$ is the normal-ordered Hamiltonian defined in coupled cluster theory as $\hat{H}_N \equiv \hat{F}_N + \hat{V}_N = \hat{H} - \langle\psi_0|\hat{H}|\psi_0\rangle$; the terms included in $\hat{H}_N$ are shown in Figure 2.2. The expansion truncates naturally at the quadruply-nested commutator. Similar to configuration interaction, coupled cluster theory will solve the non-relativistic Schrödinger equation exactly within the limitation of the basis set. However, coupled cluster theory offers advantages over configuration interaction theory when the excitation operator is truncated.

2.3 Coupled Cluster Singles and Doubles

Coupled cluster singles and doubles (CCSD)[14,15] is a coupled cluster based method routinely used in computational chemistry. It provides an accurate treatment of the Schrödinger equation while remaining computationally inexpensive compared to full configuration interaction. Within the CCSD

framework the cluster operator $\hat{T}$ is truncated at the double excitation level and can be written as follows

$$\hat{T} = \hat{T}_1 + \hat{T}_2. \tag{2.37}$$

Similarly, the CCSDT cluster operator can be created by adding the $\hat{T}_3$ excitation operator but for the sake of clarity and succinctness we will limit ourselves to deriving the CCSD equations in this section. The CCSD Hamiltonian assumes the following matrix form

$$\bar{H}_{CCSD} = \begin{pmatrix} E_{CCSD} & \bar{H}_{0S} & \bar{H}_{0D} \\ 0 & \bar{H}_{SS} & \bar{H}_{SD} \\ 0 & \bar{H}_{DS} & \bar{H}_{DD} \end{pmatrix} \tag{2.38}$$

where $\bar{H}_{00} = E_{CCSD}$ and $\bar{H}_{S0}$, $\bar{H}_{D0}$ disappear by virtue of the coupled cluster equations. The first part of evaluating the CCSD amplitudes and energy is to derive the second quantization expressions of the different elements of $\bar{H}$. Inserting the CCSD cluster operator defined previously ($\hat{T} = \hat{T}_1 + \hat{T}_2$) in the Hausdorff expansion defined in 2.36 one can obtain the following expression for $\bar{H}$

$$\begin{aligned} \bar{H} = \hat{H}_N &+ \hat{H}_N\hat{T}_1 + \hat{H}_N\hat{T}_2 + \frac{1}{2}\hat{H}_N\hat{T}_1{}^2 + \frac{1}{2}\hat{H}_N\hat{T}_2{}^2 + \frac{1}{2}\hat{H}_N\hat{T}_1\hat{T}_2 \\ &+ \frac{1}{6}\hat{H}_N\hat{T}_1{}^3 + \frac{1}{2}\hat{H}_N\hat{T}_1\hat{T}_2{}^2 + \frac{1}{2}\hat{H}_N\hat{T}_2\hat{T}_1{}^2 + \frac{1}{6}\hat{H}_N\hat{T}_2{}^3 + \frac{1}{24}\hat{H}_N\hat{T}_1{}^4 \\ &+ \frac{1}{6}\hat{H}_N\hat{T}_1{}^3\hat{T}_2 + \frac{1}{4}\hat{H}_N\hat{T}_1{}^2\hat{T}_2{}^2 + \frac{1}{6}\hat{H}_N\hat{T}_1\hat{T}_2{}^3 + \frac{1}{24}\hat{H}_N\hat{T}_2{}^4 \end{aligned} \tag{2.39}$$

The diagrammatic representation of $\bar{H}$ for CCSD is shown in Figure 2.3. One can now obtain the energy and amplitude equations for CCSD by inserting $\bar{H}$ into equations 2.34 and 2.35, respectively, *viz.*

$$E_{CCSD} - E_0 = \langle \psi_0 | (\hat{H}_N + \hat{H}_N \hat{T}_1 + \hat{H}_N \hat{T}_2 + \frac{1}{2}\hat{H}_N \hat{T}_1^{\,2} + \frac{1}{2}\hat{H}_N \hat{T}_2^{\,2} + ...)_c | \psi_0 \rangle \quad (2.40)$$

which simplifies to

$$E_{CCSD} - E_0 = \langle \psi_0 | (\hat{F}_N \hat{T}_1 + \hat{W}_N (\hat{T}_2 + \frac{1}{2}\hat{T}_1^{\,2}))_c | \psi_0 \rangle \quad (2.41)$$

As we mentioned earlier diagrammatic representation of the coupled cluster contributions is a convenient way to select the connected terms that insure the size consistency of coupled cluster theory. This can also be shown by using the same supersystem as in Section 2.1

$$\begin{aligned} \Phi^{AB}_{CCSD} &= \phi^A_{CCSD} \phi^B_{CCSD} \\ &= e^{(\hat{T}_1^A + \hat{T}_2^A)} \phi^A_{HF} \; e^{(\hat{T}_1^B + \hat{T}_2^B)} \phi^B_{HF} \\ &= e^{(\hat{T}_1^A + \hat{T}_2^A + \hat{T}_1^B + \hat{T}_2^B)} \phi^A_{HF} \phi^B_{HF} \end{aligned} \quad (2.42)$$

Thanks to the exponential nature of the excitation operator the level of excitation is conserved making CCSD or any truncated coupled cluster methods size consistent. The CCSD contribution to the electronic energy can be diagrammatically represented as follows

$E_{CCSD} - E_0 =$ 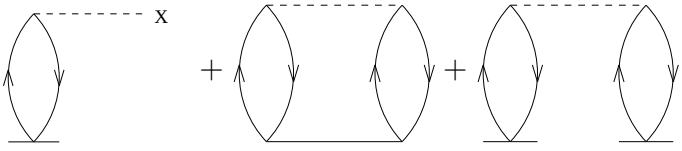

(2.43)

For the CCSD method only the $\hat{T}_1$ and $\hat{T}_2$ amplitudes have to be evaluated using the following equations

$$\langle\psi_i^a|[\hat{F}_N\hat{T}_1 + \hat{F}_N(\hat{T}_2 + \frac{1}{2}\hat{T}_1^2) + \hat{W}_N\hat{T}_1 + \hat{W}_N(\hat{T}_2 + \frac{1}{2}\hat{T}_1^2) + \hat{W}_N(\hat{T}_1\hat{T}_2 + \frac{1}{6}\hat{T}_1^3)]_c|\psi_0\rangle \tag{2.44}$$

$$\langle\psi_{ij}^{ab}|[\hat{F}_N\hat{T}_2 + \hat{F}_N(\hat{T}_1\hat{T}_2) + \hat{W}_N + \hat{W}_N\hat{T}_1 + \hat{W}_N(\hat{T}_2 + \frac{1}{2}\hat{T}_1^2) + \hat{W}_N(\hat{T}_1\hat{T}_2 + \frac{1}{6}\hat{T}_1^3) + \hat{W}_N(\frac{1}{2}\hat{T}_2^2 + \frac{1}{2}\hat{T}_1^2\hat{T}_2 + \frac{1}{24}\hat{T}_1^4)]_c|\psi_0\rangle \tag{2.45}$$

The diagrammatic representations of the CCSD amplitudes are shown in Figure 2.5 and 2.6. By solving this set of non-linear equations one can evaluate the coupled cluster amplitudes and, therefore, the CCSD energy. While this derivation of CCSD has allowed a better understanding of truncated coupled cluster theory, it is in practice not a sufficient method for most applications where high accuracy is required. Thus, it is usually necessary to go beyond the CCSD method. In the next chapters we will also present other alternative to the CCSD and CCSDT methods.

Figure 2.1: Diagrammatic representation of the cluster operators in the anti-symmetrized Brandow formalism[10].

$$\hat{T}_1 \equiv \sum_{ia} t_i^a a_a^\dagger a_i =$$

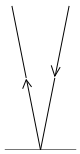

$$\hat{T}_2 \equiv \tfrac{1}{4} \sum_{ijab} t_{ij}^{ab} a_a^\dagger a_b^\dagger a_j a_i =$$

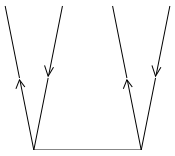

$$\hat{T}_3 \equiv \tfrac{1}{36} \sum_{ijkabc} t_{ijk}^{abc} a_a^\dagger a_b^\dagger a_c^\dagger a_k a_j a_i =$$

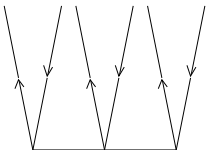

Figure 2.2: Diagrammatic representation of the one- and two-electron parts of $\hat{H}_N$ in the antisymmetrized Brandow formalism.

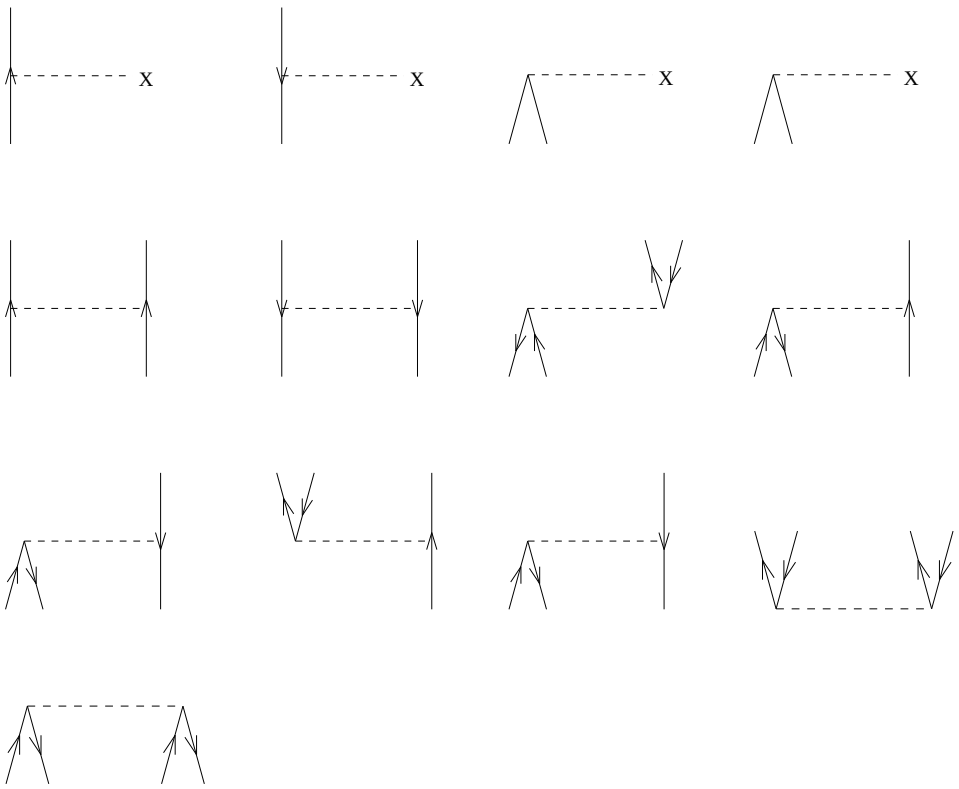

Figure 2.3: Diagrammatic representation of the one- and two-electron parts of $\bar{H}$ in the antisymmetrized Brandow formalism.

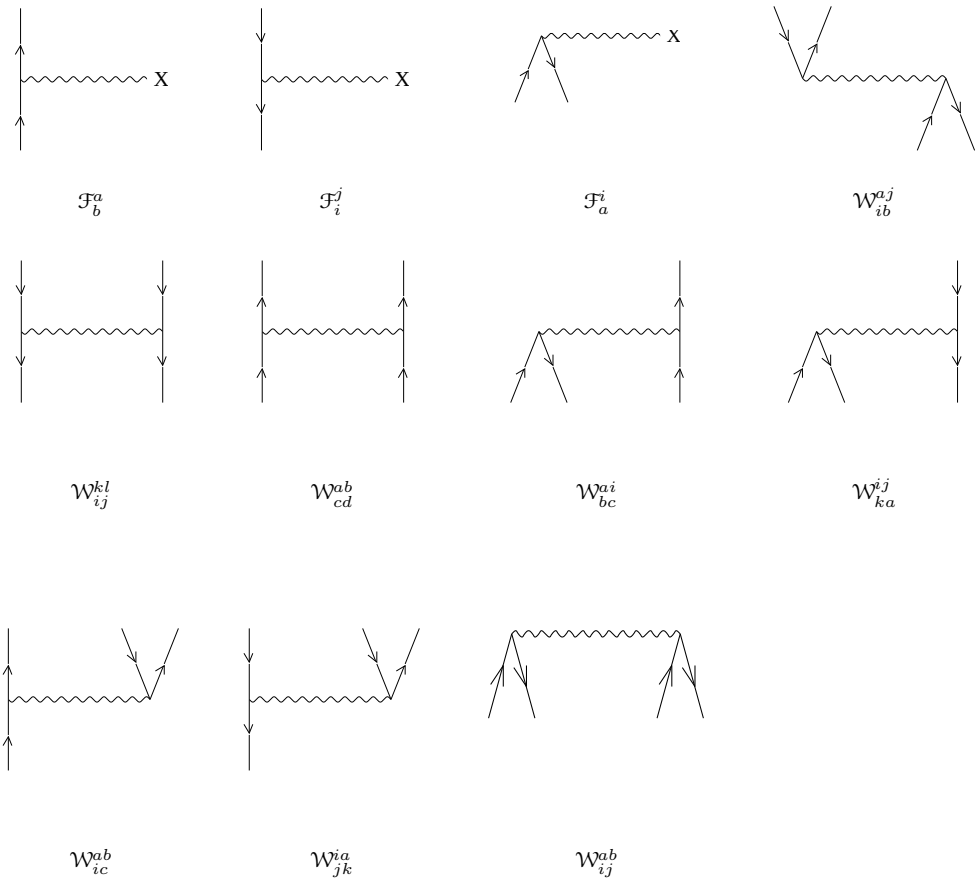

Figure 2.4: Representation of the shorthand diagrams used in Figure 2.3 to form $\bar{H}$ in the antisymmetrized Brandow formalism.

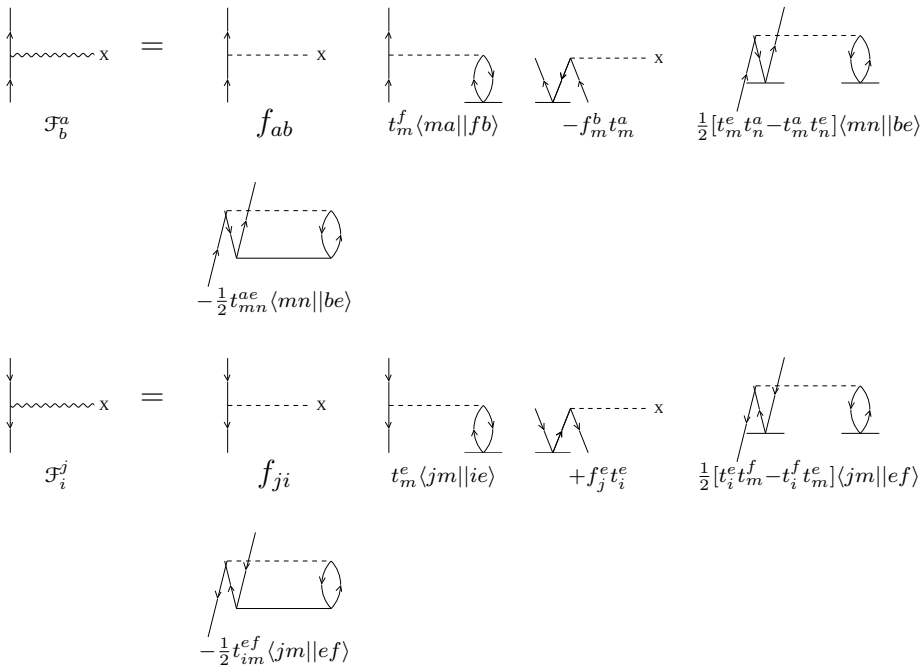

Figure 2.4 continue

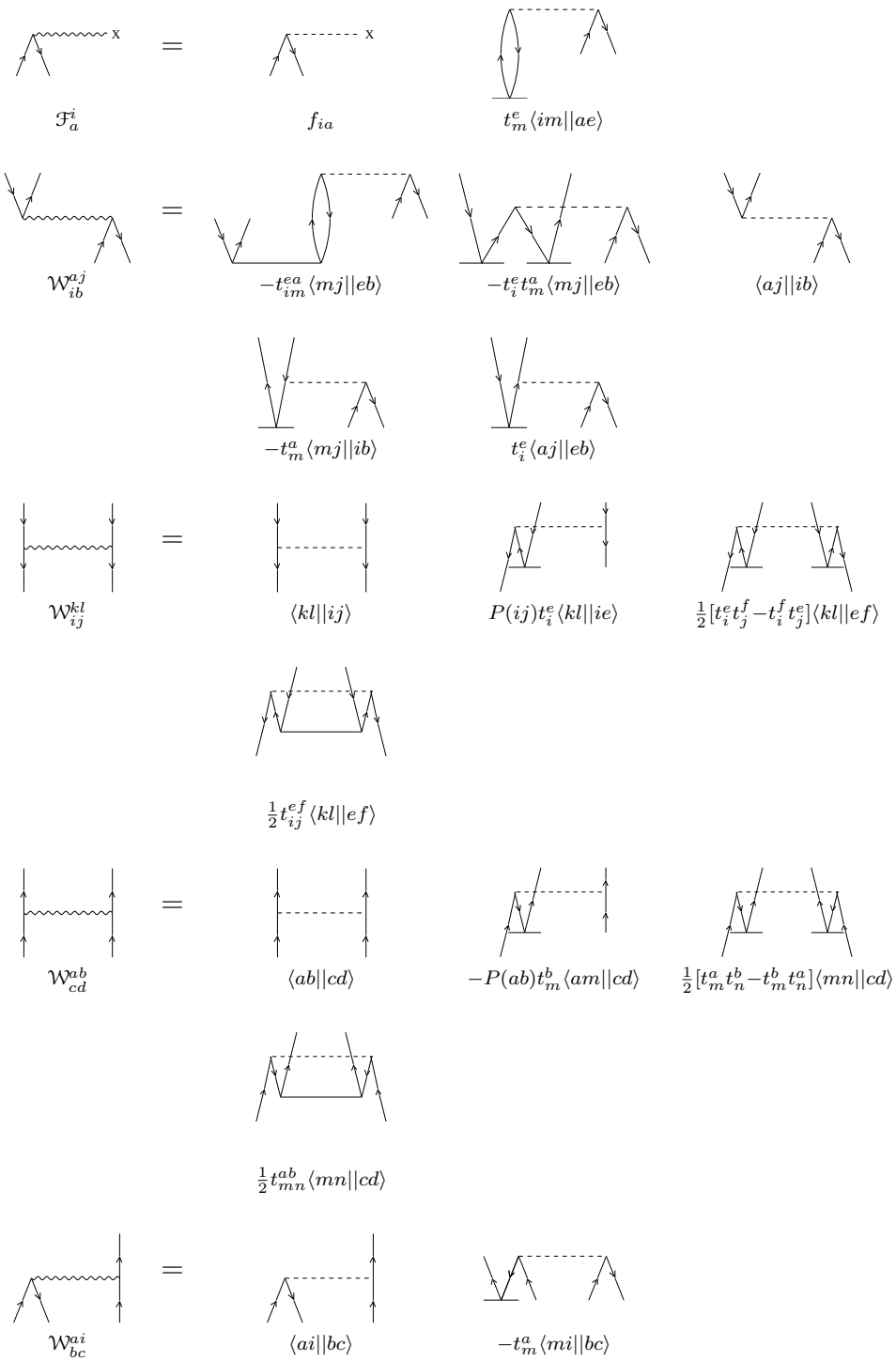

Figure 2.4 continue

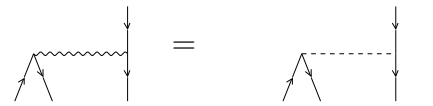

$\mathcal{W}^{ij}_{ka}$ $\langle jk||ia\rangle$ $+t^e_i\langle jk||ea\rangle$

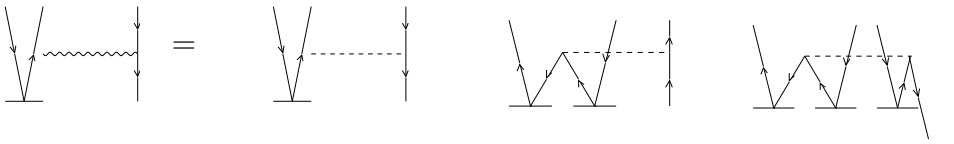

$t^a_m\,\mathcal{W}^{im}_{jk}$ $-t^e_i\langle ak||ej\rangle$ $-t^a_m t^e_i\langle mc||eb\rangle$ $+P(ij)t^a_m t^e_i t^f_j\langle mk||ef\rangle$

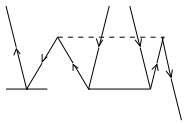

$+\frac{1}{2}t^a_m t^{ef}_{ij}\langle mk||ef\rangle$

$\mathcal{W}^{ab}_{ic}$ $\langle ab||ic\rangle$ $t^{ab}_{im}\mathcal{F}^m_c$ $t^e_i\mathcal{W}^{ab}_{ie}$

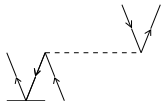

$-P(ab)t^a_m\langle mb||ci\rangle$

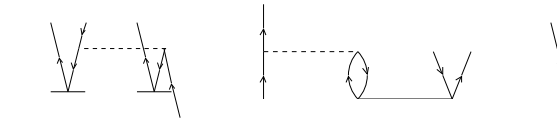

$\frac{1}{2}[t^a_m t^b_n - t^b_m t^a_n]\langle ci||mn\rangle$ $P(ab)t^{be}_{im}\langle am||ce\rangle$ $\frac{1}{2}t^{ab}_{mn}\langle ci||mn\rangle$

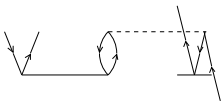

$P(ab)t^a_m t^{be}_{ni}\langle mn||ce\rangle$

Figure 2.4 continue

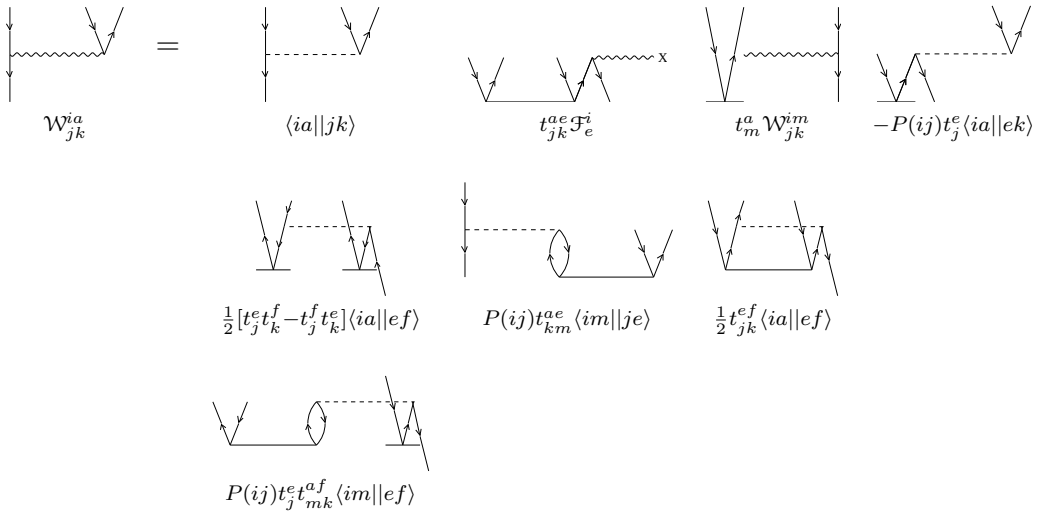

Figure 2.5: Diagrammatic representation of the singles amplitude equations for CCSD in the antisymmetrized Brandow formalism (Skeleton diagrams only).

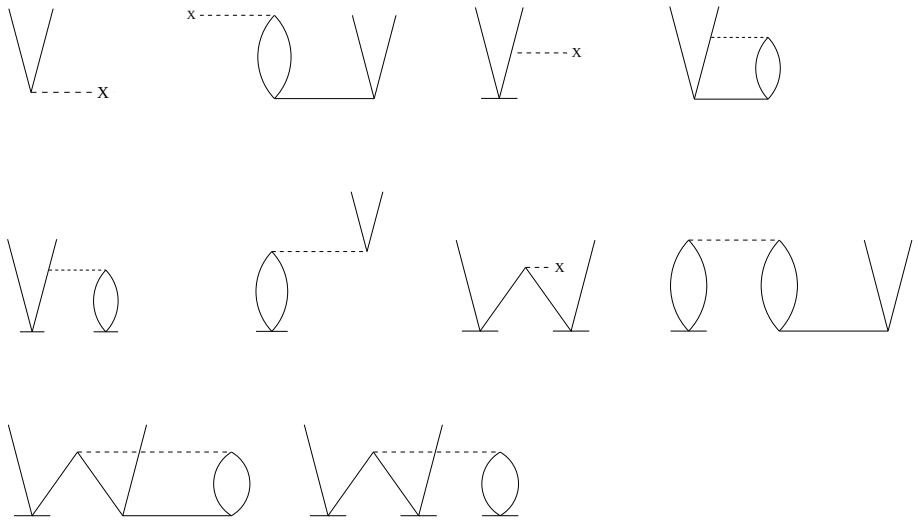

Figure 2.6: Diagrammatic representation of the doubles amplitude equations for CCSD in the antisymmetrized Brandow formalism (Skeleton diagrams only).

Chapter 3

Coupled Cluster Methods Including Noniterative Quadruple Excitations: CCSDT(Q)

3.1 Motivation Behind the Development of CCSDT(Q)

As mentioned in Chapter 1 and Chapter 2, the CCSD method although useful in some cases is often not sufficient to achieve high accuracy, making quantum chemists turn to CCSDT instead. In the last twenty years a lot of methods have been developed to approximate the CCSDT method because of its high computational cost (CCSDT scales as n^8). These methods developed to approximate the triple excitations – scaling as n^7 – fall into two categories: the so-called noniterative and iterative methods. The iterative methods are defined as CCSDT-X (X= 1a, 1b, 2, 3)[46] and CC3[47,48], they provide a improvement to CCSD but are still expensive and are not reliable except for CCSDT-3 (The details of the terms included in these methods will be given in Chapter 5). Better alternatives to CCSDT are the noniterative methods: CCSD(T)[19,20,21] and CCSD+T(CCSD)[53,54,55,56]; that can be obtained by applying perturbation theory on the CCSD wavefunction or the Hartree-Fock wavefunction, respectively. The CCSD(T) method has had a lot of success and is routinely used in quantum chemistry; it is a more balanced method

than CCSD+T(CCSD). In CCSD(T) the terms that have to be added to the CCSD energy are the following

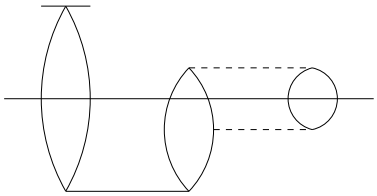

$\langle 0|\hat{T}_1 W_N D_3 W_N \hat{T}_2|0\rangle$

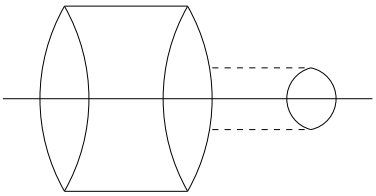

$\langle 0|\hat{T}_2 W_N D_3 W_N \hat{T}_2|0\rangle$

The second term is not present in CCSD+T(CCSD) and only comes from taking the CCSD wavefunction as "zeroth-order". We believe this additional term balances the evaluation of the triple excitations. The results obtained with CCSD(T) are remarkable and affordable since calculating these two terms only requires one n^7 step since it is a noniterative method. The only inconvenience of CCSD(T) is that it tends to overestimate the effect of triple excitations.

The impressive performance of CCSD(T) made it one of the most commonly used coupled cluster methods but there exist chemical problems that require more accuracy than CCSD(T) or even CCSDT can provide. One of the original alternative was to seek greater accuracy by using costly methods such as CCSDTQ[17], CCSDTQP[18] or even in some cases FCI[1,2,3], scaling

as n^{10}, n^{12} or $N!$, respectively. While most modern computational chemists would laugh at using methods with such scaling and would rather use DFT based methods; they are absolutely vital to solve problems in high accuracy (< 1kJ/mol) thermochemistry for example. The increase in computer power has allowed quantum chemists to perform CCSDT calculation more routinely but calculations using inclusion of quadruple excitations and beyond remain a humongous task. Thus, there has been a will to develop approximate methods following the same model as approximate methods for CCSD. Most of these are iterative methods known as CCSDTQ-X (x=1a, 1b, 2, 3)[57,58] but also several noniterative methods most of which use a clever (and approximate) factorization scheme to lower the computational cost from n^9 to n^7. The latter can be justified from the perspective of perturbation theory based on a zeroth-order HF-SCF (Hartree-Fock self consistent field) wavefunction[23,24,25,26]. From this perspective, the quadruples effect arises first at fifth order in the perturbation expansion. The noniterative method that does not exploit the factorization is similar in nature to CCSD+T(CCSD) (also known as CCSD[T]), and is perhaps most appropriately designated as CCSDT[Q][59]. Numerical results obtained with CCSDT[Q] show improvement relative to CCSDT, indicating that CCSDT[Q] provides a suitable approximation of CCSDTQ. However it is legitimate to wonder whether this method will encounter problems reminiscent to those seen with CCSD[T][60].

3.2 Matrix Form of Perturbation Theory

Let us consider the CI eigenvalue problem

$$\mathbf{HR} = \mathbf{ER} \tag{3.1}$$

R being the eigenvector of **H**. This eigenvalue problem can be written into a matrix form by partitioning the Hamiltonian. Let $|p\rangle$ be the Hartree-Fock determinant in this example (One can use any determinant to represent the ground state and not necessarily the Hartree-Fock determinant) and $|q\rangle$ the set of determinants spanning the space of singly, doubly, triply ... excited determinants.

$$\begin{aligned} |p\rangle &= |0\rangle \\ |q\rangle &= |S\rangle + |D\rangle + |T\rangle ... \end{aligned} \tag{3.2}$$

Equation 3.1 can now be represented in the following matrix form

$$\begin{pmatrix} H_{pp} & H_{pq} \\ H_{qp} & H_{qq} \end{pmatrix} \begin{pmatrix} R_p \\ R_q \end{pmatrix} = E \begin{pmatrix} R_p \\ R_q \end{pmatrix} \tag{3.3}$$

that can be expanded to the following set of equations

$$H_{pp}R_p + H_{pq}R_q = ER_p \tag{3.4}$$

$$H_{qp}R_p + H_{qq}R_q = ER_q \tag{3.5}$$

it is then straightforward to rearrange these equations to obtain an expression that only depends on R_p by inserting

$$R_q = H_{qp}(E - H_{qq})^{-1}R_p \tag{3.6}$$

into Equation 3.4.

$$H_{pp}R_p + H_{pq}(E - H_{qq})^{-1}H_{qp}R_p = ER_p \tag{3.7}$$

One can then multiply the previous equation by the left eigenvector of $\hat{H}$, L_p to obtain

$$L_pH_{pp}R_p + L_pH_{pq}(E - H_{qq})^{-1}H_{qp}R_p = EL_pR_p \tag{3.8}$$

which after being slightly rearranged gives a clean expression for the energy

$$E = \frac{L_pH_{pp}R_p}{L_pR_p} + \frac{L_pH_{pq}(E - H_{qq})^{-1}H_{qp}R_p}{L_pR_p} \tag{3.9}$$

We now assume the normalization relation $L_pR_p = 1$, consequently simplifying the expression for the energy

$$E = H_{pp} + H_{pq}(E - H_{qq})^{-1}H_{qp}. \tag{3.10}$$

Given the fact that the Hamiltonian can be written as

$$\hat{H} = \hat{H}^{(0)} + \hat{V} \tag{3.11}$$

where $\hat{H}^{(0)}$ is the zeroth-order part of the Hamiltonian and $\hat{V}$ a perturbation and by definition of $|p\rangle$ and $|q\rangle$ the energy can be rewritten in the following form

$$E = H_{00}^{(0)} + V_{00} + V_{0q}(E - H_{qq})^{-1}V_{q0} \tag{3.12}$$

Similarly to the Hamiltonian the energy can also be broken up in two parts

$$E = E^{(0)} + \Delta E \tag{3.13}$$

which allows us to rewrite Equation 3.12 as follows

$$\begin{aligned}
\Delta E &= V_{00} + V_{0q}(E - H_{qq})^{-1}V_{q0} \\
&= V_{00} + V_{0q}[(E^{(0)} - H_{qq}^{(0)})(1 - (E^{(0)} - H_{qq}^{(0)})^{-1}(V_{qq} - \Delta E))]^{-1}V_{q0} \\
&= V_{00} + V_{0q}[(1 - \mathcal{R}_0(V_{qq} - \Delta E))]^{-1}\mathcal{R}_0 V_{q0}
\end{aligned} \tag{3.14}$$

where $\mathcal{R}_0 \equiv (E^{(0)} - H_{qq}^{(0)})^{-1}$; $\mathcal{R}_0$ is usually called the resolvent. One should note that $\mathcal{R}_0$ is a diagonal matrix and a zeroth-order quantity. Most of the matrices in ΔE are too large to be inverted therefore one needs to recognize the $(1-x)^{-1} = 1 + x + x^2 + x^3...$ Taylor series expansion in order to rewrite ΔE into a usable form.

$$\begin{aligned}
\Delta E =& V_{00} + V_{0q}[1 + \mathcal{R}_0(V_{qq} - \Delta E) + (\mathcal{R}_0(V_{qq} - \Delta E))^2 \\
&+ (\mathcal{R}_0(V_{qq} - \Delta E))^3 + ...]\mathcal{R}_0 V_{q0} \\
=& V_{00} + V_{0q}\mathcal{R}_0 V_{q0} + V_{0q}\mathcal{R}_0(V_{qq} - \Delta E)\mathcal{R}_0 V_{q0} + ...
\end{aligned} \tag{3.15}$$

One can write ΔE as

$$\Delta E \equiv \Delta E^{(1)} + \Delta E^{(2)} + \Delta E^{(3)} + ... \tag{3.16}$$

allowing one to collect the righ-hand side terms by order

$$
\begin{aligned}
&\Delta E^{(1)} = V_{00} \\
&\Delta E^{(2)} = V_{0q}\mathcal{R}_0 V_{q0} \\
&\Delta E^{(3)} = V_{0q}\mathcal{R}_0 V_{qq}\mathcal{R}_0 V_{q0} - V_{0q}\mathcal{R}_0 \Delta E^{(1)}\mathcal{R}_0 V_{q0} \\
&(...)
\end{aligned}
\tag{3.17}
$$

The terms including $\Delta E^{(n)}$ could be a problem before they would spoil the size consistency of the method. However, they are diagrammatically disconnected, therefore, removed from any size consistent method reducing the previous equations to

$$
\begin{aligned}
&\Delta E^{(1)} = V_{00} \\
&\Delta E^{(2)} = V_{0q}\mathcal{R}_0 V_{q0} \\
&\Delta E^{(3)} = V_{0q}\mathcal{R}_0 V_{qq}\mathcal{R}_0 V_{q0} \\
&(...)
\end{aligned}
\tag{3.18}
$$

This derivation is used to justify the MBPT equations. For example the MBPT(2) energy is equal to $V_{0q}\mathcal{R}_0 V_{q0}$ and can be diagrammatically represented as

$$
E^{(2)} \equiv \frac{1}{4}\sum_{ijab}\frac{\langle ij||ab\rangle\langle ab||ij\rangle}{D_{ij}^{ab}} =
\tag{3.19}
$$

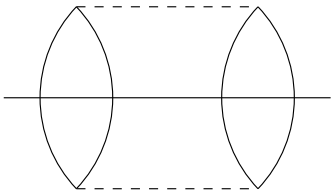

3.3 Many-body Perturbation and Coupled Cluster Theory

Many-body perturbation theory was developed like coupled cluster theory to account for correlation energy; within the framework of MBPT, the correlation energy is treated as a perturbation of the Hartree-Fock wavefunction. In the following discussion we will present MBPT in the context of coupled cluster theory in order to show how existing coupled cluster methods can be improved. For the sake of clarity, a few definitions and assumptions have to be presented (The idea presented in this section are similar to those in section 3.2). In MBPT the normal-ordered Hamiltonian, $\hat{H}_N$, can be partitioned so that its one- and two-electron parts are taken as zeroth- and first-order, respectively, *viz.*

$$\begin{aligned} \hat{H}_N &= \hat{F}_N + \hat{V}_N \\ &= \hat{H}^{(0)} + \hat{H}^{(1)} \end{aligned} \tag{3.20}$$

using this definition for $\hat{H}_N$ and the fact that we will considerer the set of canonical Hartree-Fock orbitals (RHF or UHF) one can obtain the Møller-Plesset variant of many-body perturbation theory. In this context the matrix $\hat{F}_N$ is diagonal and the only excitation operator with a non-zero first-order contribution is $\hat{T}_2$; meaning that the other operators such as $\hat{T}_1$ and $\hat{T}_3$ will be second-order quantities. In fact any cluster operator can be written as a sum of first-, second-, ... order operators

$$\hat{T}_n \equiv \hat{T}_n^{(0)} + \hat{T}_n^{(1)} + \hat{T}_n^{(2)} + \hat{T}_n^{(3)} + ... \tag{3.21}$$

Similarly the contributions to the similarity transformed Hamiltonian are as follows

$$\bar{H} \equiv \bar{H}^{(0)} + \bar{H}^{(1)} + \bar{H}^{(2)} + ... \tag{3.22}$$

where one can notice that

$$\begin{aligned}
\bar{H}^{(0)} &\equiv \hat{H}_N^{(0)} = \hat{F}_N \\
\bar{H}^{(1)} &\equiv \hat{H}_N^{(1)} + (\hat{H}_N^{(0)}\hat{T}_n^{(1)})_c = \hat{V}_N + (\hat{F}_N\hat{T}_2^{(1)})_c \\
\bar{H}^{(2)} &\equiv (\hat{H}_N^{(0)}\hat{T}_n^{(2)})_c + (\hat{H}_N^{(1)}\hat{T}_n^{(1)})_c + (\hat{H}_N^{(0)}\hat{T}_n^{(1)}\hat{T}_n^{(1)})_c = (\hat{F}_N\hat{T}_1^{(2)})_c \\
&\quad + (\hat{V}_N\hat{T}_2^{(1)})_c + (\hat{F}_N\hat{T}_2^{(1)}\hat{T}_2^{(1)})_c \\
&(...)
\end{aligned} \tag{3.23}$$

Using the definition of $\bar{H}^{(n)}$ presented in the equations above and the general coupled cluster equation

$$E = \langle\psi_0|\bar{H}|\psi_0\rangle \tag{3.24}$$

it is straightforward to define the second order correction to the Hartree-Fock energy $E^{(2)}$ as

$$\begin{aligned}
E^{(2)} &= \langle\psi_0|\bar{H}^{(2)}|\psi_0\rangle \\
&= \langle\psi_0|(\hat{F}_N\hat{T}_1^{(2)})_c + (\hat{V}_N\hat{T}_2^{(1)})_c + (\hat{F}_N\hat{T}_2^{(1)}\hat{T}_2^{(1)})_c|\psi_0\rangle
\end{aligned} \tag{3.25}$$

and in the same manner define a general expression for any MBPT energy

correction $\mathrm{E}^{(n)}$ as

$$E^{(n)} = \langle\psi_0|\bar{H}^{(n)}|\psi_0\rangle. \tag{3.26}$$

Equation 3.25 reduces to

$$E^{(2)} = \langle\psi_0|(\hat{V}_N\hat{T}_2^{(1)})_c|\psi_0\rangle \tag{3.27}$$

since $\hat{F}_N$ is diagonal due to the choice of HF orbitals. The MBPT(2) correction to the energy has the following diagrammatic representation

$E^{(2)} =$ 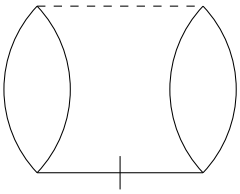 (3.28)

In order to evaluate $\hat{T}_2^{(1)}$ one needs to go back to the equation defining the coupled cluster amplitudes *i.e.*

$$\langle\psi_{ij}^{ab}|\bar{H}^{(1)}|\psi_0\rangle \equiv \langle\psi_{ij}^{ab}|\hat{V}_N|\psi_0\rangle + \langle\psi_{ij}^{ab}|(\hat{F}_N\hat{T}_2^{(1)})_c|\psi_0\rangle = 0 \tag{3.29}$$

Once again some of the terms included in $\hat{F}_N$ with the use of canonical orbitals disappear ($f_{ia} = 0$ and $f_{ai} = 0$ thus the only non-vanishing terms are f_{ii}, f_{jj}, f_{aa}, and f_{bb}); therefore, the amplitude of $\hat{T}_2^{(1)}$ is reduced to

$$t_{ij}^{ab(1)} = \frac{\langle ab||ij\rangle}{D_{ij}^{ab}}. \tag{3.30}$$

Consequently the diagrammatic representation of the first order contribution to the $\hat{T}_2$ cluster operator is

$$\hat{T}_2^{(1)} \equiv$$  $$=$$ 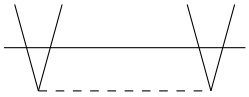 (3.31)

meaning that the second order correction to the energy is simply

$$E^{(2)} \equiv \frac{1}{4}\sum_{ijab}\frac{\langle ij||ab\rangle\langle ab||ij\rangle}{D_{ij}^{ab}} =$$ 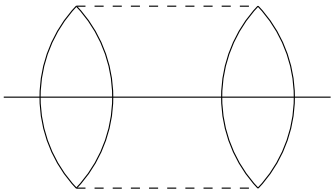 (3.32)

which is exactly what one would get by using the matrix form of perturbation theory on the Hartree-Fock determinant as we saw in section 3.2.

The same technique can be used to evaluate the third-, fourth-, and nth-order contribution to the energy. In this discussion we are especially interested in analyzing how to improve existing coupled cluster methods. Thus, an order by order comparison of the MBPT contribution and the existing CCSD method would be useful to know the terms missing from the latter method to be complete up to a certain order of perturbation. It can be found that CCSD is complete up to third order of perturbation theory but is lacking the triple excitations contribution to be complete up to fourth order of perturbation.

Let us consider the fourth order correction to the energy

$$E^{(4)} \equiv \langle\psi_0|\bar{H}^{(4)}|\psi_0\rangle = \langle\psi_0|(\hat{V}_N\hat{T}_2^{(3)})_c|\psi_0\rangle \tag{3.33}$$

where $\hat{T}_2^{(3)}$ can be found using the following amplitude equation

$$\langle\psi_{ij}^{ab}|(\hat{V}_N\hat{T}_1^{(2)})_c + (\hat{F}_N\hat{T}_2^{(3)})_c + (\hat{V}_N\hat{T}_2^{(2)})_c + (\frac{1}{2}\hat{V}_N\hat{T}_2^{(1)}\hat{T}_2^{(1)})_c + (\hat{V}_N\hat{T}_3^{(2)})_c|\psi_0\rangle = 0 \tag{3.34}$$

in this discussion were are only interested in the effects involving the triple excitations since these are not included in CCSD we will then limit ourself to the following expression for $\hat{T}_2^{(3)}$

$\hat{T}_2^{(3)} =$ 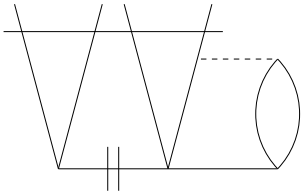 (3.35)

with the second-order contribution to the triple excitation operators being

$\hat{T}_3^{(2)} =$ 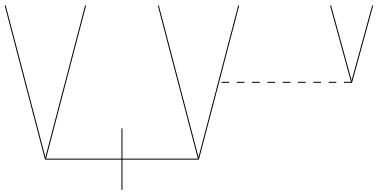 (3.36)

It is now straightforward to evaluate the energy contribution associated with the $\hat{T}_2^{(3)}$ excitation term; we will label the contribution as $E_T^{(4)}$ for the time being

$E_T^{(4)} =$ 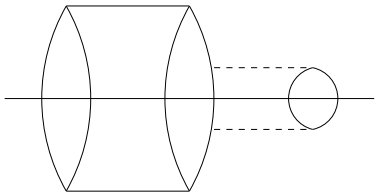 (3.37)

This energy correction was originally named CCSD+T(CCSD) in the literature requiring the noniterative evaluation of only one energy term on top of CCSD. As we said earlier, while easily proven from the former order by order perturbation theory, this method is not well-balanced. Indeed, a fifth-order term has to be added to CCSD+T(CCSD) in order to reproduce the effects of the triple excitations correctly. The method including the former fourth-order term and an additional fifth-order term is formally known as CCSD(T) and can be obtained by applying perturbation theory on the CCSD wavefunction; this additional term is

$E_T^{(5)} =$ 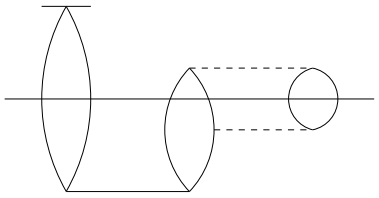 (3.38)

As described previously CCSD(T) allows a more accurate treatment of triple excitations. In the following section we will discuss the development of a similar method but providing a noniterative alternative to CCSDTQ and CCS-

DTQP.

3.4 Derivation of the CCSDT(Q) Method

The CCSD(T) method can be justified by applying perturbation theory on the similarity transformed Hamiltonian corresponding to CCSD as it was shown in section 3.2 for the regular Hamiltonian.

In the following discussion we will give an overview of the newly developed CCSDT(Q) method. Let us assume that we have formed the CCSDT similarity transformed Hamiltonian in the same manner it was done in Chapter 2 and that we can then write the right eigenvector as simply the reference determinant $|\psi_0\rangle$, whereas the left eigenvalue condition is[61]

$$\langle\psi_0|\hat{\mathfrak{L}}\bar{H} = \langle\psi_0|\hat{\mathfrak{L}}E_{CCSDT}. \tag{3.39}$$

We can then write the following eigenvalue problem where the energy is written as a transition expectation value

$$\langle\psi_0|\hat{\mathfrak{L}}\bar{H}|\psi_0\rangle = E_{CCSDT}. \tag{3.40}$$

In the basis of Slater determinants obtained by distributing electrons amongst the occupied and virtual orbitals in all possible ways, $\bar{H}$ admits to the matrix representation

$$\begin{pmatrix} E_{CCSDT} & \bar{H}_{0p} & \bar{H}_{0q} \\ 0 & \bar{H}_{pp} & \bar{H}_{pq} \\ \bar{H}_{q0} & \bar{H}_{qp} & \bar{H}_{qq} \end{pmatrix}. \tag{3.41}$$

In the previous equation p is the set of determinants obtained by promotion of one, two or three electrons from the reference wavefunction $|\psi_0\rangle$ ($|S\rangle$, $|D\rangle$, and $|T\rangle$) 0 represents $|\psi_0\rangle$, and q all other determinants ($|Q\rangle + |P\rangle + ...$). If one were to restrict the p space to be the set of only singly and doubly excited determinants then one could derive the well-known CCSD(T) equations as it was done in Ref. 21 and Sections 3.2-3.3. The reason why $\bar{H}_{p0}$ vanishes in equation 3.41 comes from the fact that the following amplitude equations have to be satisfied:

$$0 = \bar{H}_{p0} = \begin{cases} \langle S|e^{-\hat{T}}\hat{H}e^{\hat{T}}|\psi_0\rangle \\ \langle D|e^{-\hat{T}}\hat{H}e^{\hat{T}}|\psi_0\rangle \\ \langle T|e^{-\hat{T}}\hat{H}e^{\hat{T}}|\psi_0\rangle \end{cases}$$

Following the same model as in Ref. 21 and section 3.2; the Löwdin partitioning technique[63] can be used to write the exact energy as

$$E_{exact}\langle\mathcal{L}|\mathcal{R}\rangle = \langle\mathcal{L}|\bar{H}|\mathcal{R}\rangle + \langle 0|\mathcal{L}\bar{H}|q\rangle[\langle q|E_{exact} - \bar{H}|q\rangle]^{-1}\langle q|\bar{H}\mathcal{R}|0\rangle \qquad (3.42)$$

Here, $\mathcal{L}$ and $\mathcal{R}$ are the p space projections of the exact left and right eigenvectors of $\bar{H}$.

Without truncation of the p space, the energy would be the same as the FCI energy. Thus, solving the non-relativistic Schrödinger equation exactly within the basis set limitations. Using the same expansion as in section 3.2 the difference between the exact energy and the "zeroth-order" energy can be written as $\Delta E = E_{exact} - E_{CCSDT} \equiv \Delta E = \Delta E^{[4]} + \Delta E^{[5]} + ...$ where orders are assigned as in Ref. 21.

It is assumed here that the effect of quadruple excitations will be mainly found

in the fourth-order terms of the previous expansion. The first non-vanishing contribution in the aforementioned expansion is

$$\Delta E^{[4]} = \langle 0|\hat{\mathfrak{L}}\bar{H}^{[1]}|q\rangle[\langle q|H_N^{[0]}|q\rangle]^{-1}\langle q|\bar{H}^{[3]}|0\rangle. \tag{3.43}$$

Note that, $\langle q|H_N^{[0]}|q\rangle$ are the usual (diagonal) Møller-Plesset energy differences, $\langle q|H_N^{[0]}|q\rangle = \langle q|[H^{[0]} - \langle 0|H^{[0]}|0\rangle]|q\rangle$.

Since only terms of at least third-order are needed to connect the reference state with the space of quadruple and higher excitations the low-order contributions to $\langle q|\bar{H}\hat{\mathfrak{R}}|0\rangle$ vanish.

There are two fourth-order contributions to the energy

$$\Delta E^{[4]} = \langle 0|\hat{\mathfrak{L}}|D\rangle\langle D|\bar{H}^{[1]}|Q\rangle D_4\langle Q|\bar{H}^{[3]}|0\rangle + \langle 0|\hat{\mathfrak{L}}|T\rangle\langle T|\bar{H}^{[1]}|Q\rangle D_4\langle Q|\bar{H}^{[3]}|0\rangle \tag{3.44}$$

Here, we have used the shorthand notation $D_4 = [\langle Q|H_N^{[0]}|Q\rangle]^{-1}$. Comparing the method developed by Kucharski *et al.* a few years ago, CCSDT[Q], one can notice that only one of the two terms is present. The second term appears within the context of the present type of perturbation analysis; it is therefore analogous to the extra "fifth-order" term that distinguishes CCSD(T) from CCSD[T]. The diagrammatic representation of the additional $\Delta E^{[4]}$ energy terms in the antisymmetrized Brandow formalism[10,55] with their corresponding operator equations is:

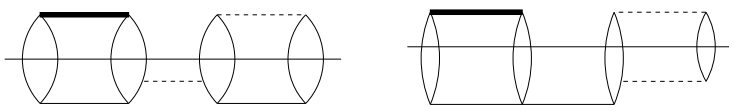

$$\langle 0|\hat{\mathcal{L}}_2 W_N D_4 \hat{T}_2 W_N \hat{T}_2|0\rangle \quad + \quad \langle 0|\hat{\mathcal{L}}_2 W_N D_4 W_N \hat{T}_3|0\rangle$$

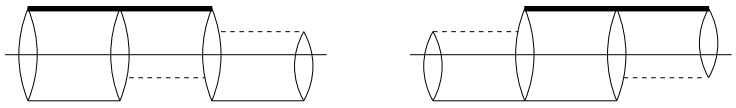

$$\langle 0|\hat{\mathcal{L}}_3 W_N D_4 \hat{T}_2 W_N \hat{T}_2|0\rangle \quad + \quad \langle 0|\hat{\mathcal{L}}_3 W_N D_4 W_N \hat{T}_3|0\rangle \quad = \quad E_Q^{[4]}$$

The dashed and long solid lines represent integrals and the D_4 denominators, respectively, while the thick and thin amplitude vertices correspond to the $\hat{\mathcal{L}}$ and $\hat{T}$ operators. While a correction that makes use of both $\hat{\mathcal{L}}$ and $\hat{T}$ amplitudes seems natural in the context of this formalism, the cost of evaluating $\hat{\mathcal{L}}$ is comparable to that of an additional CCSDT calculation. Instead, we follow the practice of replacing the $\hat{\mathcal{L}}$ amplitudes with those of the $\hat{T}^\dagger$ operator, as is done in CCSD(T). Since these operators are equivalent in lowest order, this pragmatic simplification is justified. We note, however, that the use of $\hat{\mathcal{L}}$ has been studied in the context of noniterative corrections[64,65,66]; a numerical investigation of its use in CCSDT(Q) is an appropriate subject for further study.

Approximating $\hat{\mathcal{L}}$ by $\hat{T}^\dagger$, one obtains the diagrammatic representations and

their corresponding operator equations shown below

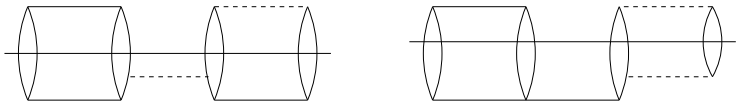

$$\langle 0|\hat{T}_2^{\dagger} W_N D_4 W_N \hat{T}_2^{2}|0\rangle \quad + \quad \langle 0|\hat{T}_2^{\dagger} W_N D_4 W_N \hat{T}_3|0\rangle$$

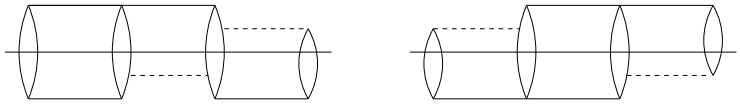

$$\langle 0|\hat{T}_3^{\dagger} W_N D_4 W_N \hat{T}_2^{2}|0\rangle \quad + \quad \langle 0|\hat{T}_3^{\dagger} W_N D_4 W_N \hat{T}_3|0\rangle \quad = \quad E_Q^{[4]}$$

It is important to note that the first two terms above are fifth-order in the context of HF-SCF-based perturbation theory, while the other two terms occur at sixth-order in that formalism. All terms have connected diagrammatic representations, and therefore both CCSDT[Q] (first two terms) and the proposed CCSDT(Q) method (all terms) are rigorously size-extensive.

3.5 Implementation of CCSDT(Q) and CCSDT[Q]

When implementing computationally expensive methods such as CCSDT(Q) the choice of intermediates and loop structures is crucial. As we mentioned earlier both CCSDT[Q] and CCSDT(Q) scale as n^9 with the right implementation. Logically the implementation of these two methods was done

within the framework of the well-know quantum chemistry package ACES II[67] which already provides robust implementations of coupled cluster methods. One of the two $\hat{T}_4$ contributions has to be calculated using intermediates in order to reduce the computational cost. The diagrammatic representation of the $\hat{T}_4$ excitation operators are the following

$T^{(4)} =$ 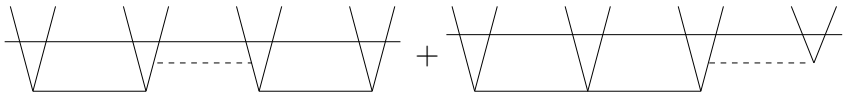 $+$

In order to evaluate the first term one has to first compute the following intermediate

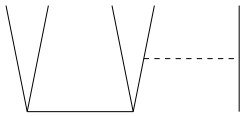

which only requires a n^7 step. The next step is to contract the previous intermediate with the $\hat{T}_2$ operator; this is computationally equivalent to forming the second $\hat{T}_4$ term both scaling as n^9. The remaining contractions for evaluating the contribution to the energy are rather inexpensive. One needs to multiply the terms obtained in the n^9 step by the denominator with an n^8 step.

$D \times$ 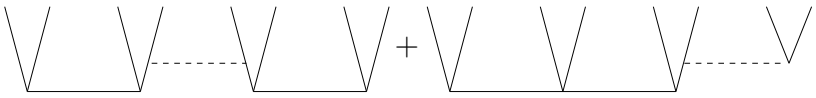 $+$

The final contraction with $\hat{T}^\dagger$ and $\hat{V}_N$ are negligible. Consequently, the overall scaling is indeed n^9 compared to n^{10} or n^{12} for CCSDTQ and CCSDTQP, respectively. Also, as mentioned earlier in the discussion, what makes the

CCSDT(Q) method powerful besides its scaling is its noniterative nature. A parallel version of this method was also implemented using the message passing interface (MPI) framework; within this implementation the CCSDT(Q) method scales almost linearly with the number of processors used in the calculation making CCSDT(Q) amenable to studying larger systems.

In the next chapter we will provide convincing benchmark of the CCSDT(Q) method and some interesting applications of this powerful method where the latter is used in the framework of the HEAT protocol[27,28] to evaluate thermochemical properties. As a check on the correctness of the program, the same two methods were also coded in the string-based many-body package of Kállay[68]. The fact that these very different implementations yield identical energies provide support for the contention that results presented in the next chapter are correct.

Chapter 4

Benchmark and Application to Ab Initio Thermochemistry

4.1 Introduction

In this chapter, we will present a thorough benchmark of CCSDT(Q) by comparison with CCSDT, CCSDT[Q], CCSDTQ, CCSDTQP and even FCI when possible in which we will analyze the strengths and weaknesses of CCSDT(Q). In order to do so, we selected a set of challenging molecular systems including closed- and open-shell molecules; some of them known to pose pathological problems to most ab initio methods. The benchmark will be based on the comparison of correlation energies in the first place but will then include careful comparison with experimental data. We will use the framework of the recently developed HEAT method[27,28] to calculate important thermochemical properties such as atomization energies and enthalpies of formation that will then be compared to a highly reliable set of thermochemical data: Ruscic's Active Thermochemical Tables (ATcT)[69,70]. Mostly, we will analyse if the CCSDT(Q) method can be used as a reliable method when higher correlation methods are needed, thereby avoiding the large computational cost of CCSDTQ, CCSDTQP, or FCI.

4.2 Benchmark of CCSDT(Q)

The noniterative correction proposed in Chapter 3 has been benchmarked for a challenging test suite that comprises atoms and small molecules. In this work, we compare CCSDT, CCSDT[Q] and higher "complete" CC methods that include quadruple (CCSDTQ)[17,68] and pentuple (CCSDTQP)[68,18] excitations with the proposed CCSDT(Q) model. The CCSDTQ and CCSDTQP energies presented here were obtained with the program of Kállay[68] (the remaining calculations were carried out on a local version of ACES II). All of the calculations (unless stated otherwise) used the cc-pVDZ and cc-pVTZ[45] basis sets, and correlation of the core electrons were excluded. The molecular geometries used in this study can be found in Ref. 27.

The principal numerical results of this work are collected in Tables 4.1-4.8 and Figures 4.1-4.5. From Table 4.1 and Figure 4.1, it can be seen that addition of the noniterative quadruple corrections defined by both CCSDT(Q) and CCSDT[Q] systematically gives energies that are superior to CCSDT. Both CCSDT[Q] and CCSDT(Q) perform well compared to CCSDTQ. A trend is exhibited whereby CCSDT[Q] and CCSDT(Q) underestimate and overestimate the magnitude of the CCSDTQ correlation energy, respectively. The poor performance of CCSDT[Q] and CCSDT(Q) for the CN radical is almost certainly due to large spin contamination in the HF-SCF wavefunction, a well-known problem of this molecule[71,72]. Even though the mean absolute error is larger for CCSDT[Q] (0.145 mE_H) than for CCSDT(Q) (0.100 mE_H), the difference is so small as to prevent any conclusion to be drawn about the

relative merits of the two approaches. The maximum absolute errors are also comparable; 0.616 mE_H and 0.582 mE_H for CCSDT[Q] and CCSDT(Q), respectively[73]. However, CCSDT(Q) is evidently vastly superior to CCSDT[Q] in some cases. For example, in the case of the CF radical, CCSDT[Q] is even inferior to CCSDT.

The same species are studied in Table 4.2 and Figure 4.2, but now with the cc-pVTZ basis set. And here a major curiosity is noted : while CCSDT(Q) performs as well as it did with the cc-pVDZ basis set, the accuracy of CCSDT[Q] is significantly degraded. For the latter method, the results are less satisfactory in every case, with substantial worsening in some cases. The mean absolute error almost triples from 0.145 mE_H to 0.405 mE_H; the worst performance is seen for CO where the error is greater than 1 mE_H. On the other hand, the mean absolute error for CCSDT(Q) doesn't change significantly (0.100 mE_H with cc-pVDZ vs. 0.136 mE_H with cc-pVTZ). For CCSDT(Q) the worst performance is again for CN because of spin contamination (0.685 mE_H). It is clear from these results that the behavior of the two methods with respect to basis set is totally different; CCSDT[Q] seems to be lacking an important balancing contribution that CCSDT(Q) appears to possess. In the course of this research, we have noted a similar property of the CCSD[T] and the CCSD(T) methods. For the same set of molecules and atoms the error with respect to CCSDT in CCSD[T] grows with the size of the basis set, while that of CCSD(T) becomes slightly smaller. The magnitude of

this effect is not as large as in the corresponding quadruples methods, but is still significant: respective errors are 0.450 and 0.482 mE_H with cc-pVDZ and 0.624 and 0.452 mE_H with cc-pVTZ for CCSD[T] and CCSD(T).

The importance of the "sixth order" (from the HF-SCF perspective) terms are especially evident when the cc-pVTZ basis is used; a majority of the quadruples contribution comes for the sixth-order terms whereas the fifth-order terms dominate when the smaller cc-pVDZ basis set is used (See Table 4.5). It is important to note that the fifth-order correction tends to become smaller as the basis set size increases. Another manifestation of this basis set phenomenon is seen in Figures 4.3 and 4.4 where CCSDT(Q) and CCSDT[Q] methods were used for the ground (singlet) and first excited (triplet) state of the beryllium atom with four basis sets of increasing size; all four electrons of the beryllium atom were correlated. Here one observes that CCSDT[Q] becomes less and less satisfactory as the basis set size increases. On the other hand, CCSDT(Q) performs comparably with all four basis sets. Even though the errors introduced are of the order of a fraction of millihartree they are representative of the trend of these two methods. The quality of both methods is comparable when using the cc-pVDZ basis set but the quality of CCSDT[Q] quickly degrades as the basis increases while CCSDT(Q) remains an excellent approximation.

In the preceding, we compared CCSDT[Q] and CCSDT(Q) to CCSDTQ. However, a better test is perhaps to compare them to the exact (FCI) energies. Nevertheless, since FCI calculations are not possible for most mem-

bers of the test suite, a comparison with CCSDTQP is a pragmatic alternative. In Tables 4.7-4.8 and Figure 4.5 we compare CCSDT, CCSDT[Q], CCSDT(Q), and CCSDTQ to CCSDTQP using an even larger number of atomic and molecular states. The performance of CCSDT(Q) is again impressive, with a mean absolute error relative to CCSDTQP (0.055 mE_H) that is even lower than CCSDTQ (0.061 mE_H) (!) while CCSDT[Q] performs less well than either method (0.198 mE_H) (It should be stressed, however, that CCSDTQ is more consistent than CCSDT(Q), in the sense that its energy is higher than the one of CCSDTQP in all cases except for CF). The only significant problem for CCSDT(Q) is again the CN radical. However, for CCSDT[Q], discrepancies of 0.554 mE_H, 0.590 mE_H, and 0.670 mE_H are seen for HCO, CF and CO, respectively, while the corresponding CCSDT(Q) errors are on the order of 0.1 mE_H in all cases.

Table 4.1: Total energies in E_H with the cc-pVDZ basis set

Species	CCSDT	CCSDT[Q]	CCSDT(Q)	CCSDTQ
N_2	−109.275374	−109.276773	−109.277059	−109.276831
F_2	−199.097717	−199.099315	−199.099411	−199.099253
O_2	−149.985875	−149.987648	−149.987783	−149.987605
C	−37.760688	−37.760708	−37.760710	−37.760717
F	−99.527650	−99.527761	−99.527760	−99.527765
N	−54.478631	−54.478663	−54.478664	−54.478673
O	−74.910062	−74.910130	−74.910131	−74.910140
CO	−113.054887	−113.055222	−113.055979	−113.055839
CCH	−76.400169	−76.400780	−76.401147	−76.401099
CH_2	−39.041567	−39.041616	−39.041638	−39.041647
CH	−38.380164	−38.380204	−38.380225	−38.380239
CH_3	−39.715944	−39.716018	−39.716057	−39.716064
H_2O	−76.241180	−76.241615	−76.241662	−76.241634
HCO	−113.576393	−113.576830	−113.577505	−113.577323
HF	−100.228220	−100.228599	−100.228632	−100.228612
NO	−129.598350	−129.599354	−129.599819	−129.599605
OH	−75.559425	−75.559652	−75.559673	−75.559683
CN	−92.491172	−92.492299	−92.493159	−92.492577
HCN	−93.188522	−93.189600	−93.189954	−93.189752
CF	−137.475514	−137.475429	−137.476115	−137.476036
NH_2	−55.732843	−55.733026	−55.733060	−55.733066
NH_3	−56.402181	−56.402457	−56.402513	−56.402498
NH	−55.091573	−55.091668	−55.091681	−55.091697
OF	−174.499043	−174.499746	−174.500248	−174.500028

Figure 4.1: Comparison to the total energies calculated with CCSDTQ and cc-pVDZ in mE_H

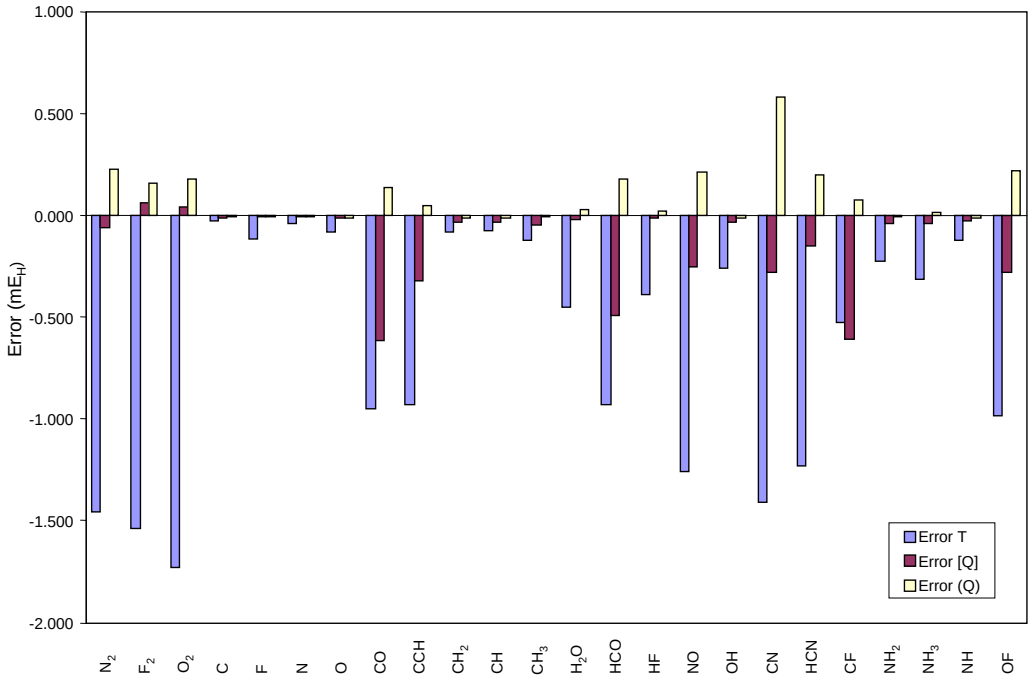

Table 4.2: Total energies in E_H with the cc-pVTZ basis set

Species	CCSDT	CCSDT[Q]	CCSDT(Q)	CCSDTQ
N_2	−109.373571	−109.374597	−109.375364	−109.375134
F_2	−199.296092	−199.297208	−199.297669	−199.297478
O_2	−150.128943	−150.130198	−150.130769	−150.130565
C	−37.781226	−37.781242	−37.781259	−37.781267
F	−99.620540	−99.620546	−99.620606	−99.620599
N	−54.515027	−54.515044	−54.515066	−54.515069
O	−74.974252	−74.974262	−74.974303	−74.974302
CO	−113.155614	−113.155580	−113.156728	−113.156585
CCH	−76.468768	−76.469131	−76.469957	−76.469895
CH_2	−39.078318	−39.078316	−39.078390	−39.078396
CH	−38.411007	−38.411013	−38.411083	−38.411097
CH_3	−39.761416	−39.761403	−39.761527	−39.761534
H_2O	−76.332267	−76.332419	−76.332620	−76.332585
HCO	−113.684388	−113.684416	−113.685517	−113.686472
HF	−100.338382	−100.338466	−100.338622	−100.338590
NO	−129.717046	−129.717609	−129.718554	−129.718316
OH	−75.638009	−75.638077	−75.638184	−75.638174
CN	−92.567909	−92.568705	−92.570229	−92.569544
HCN	−93.274977	−93.275711	−93.276561	−93.276367
CF	−137.605096	−137.604672	−137.605633	−137.605543
NH_2	−55.794002	−55.794058	−55.794196	−55.794196
NH_3	−56.473359	−56.473437	−56.473658	−56.473647
NH	−55.141117	−55.141144	−55.141214	−55.141218
OF	−174.671034	−174.671218	−174.672168	−174.671871

Figure 4.2: Comparison to the total energies calculated with CCSDTQ and cc-pVTZ in mE_H

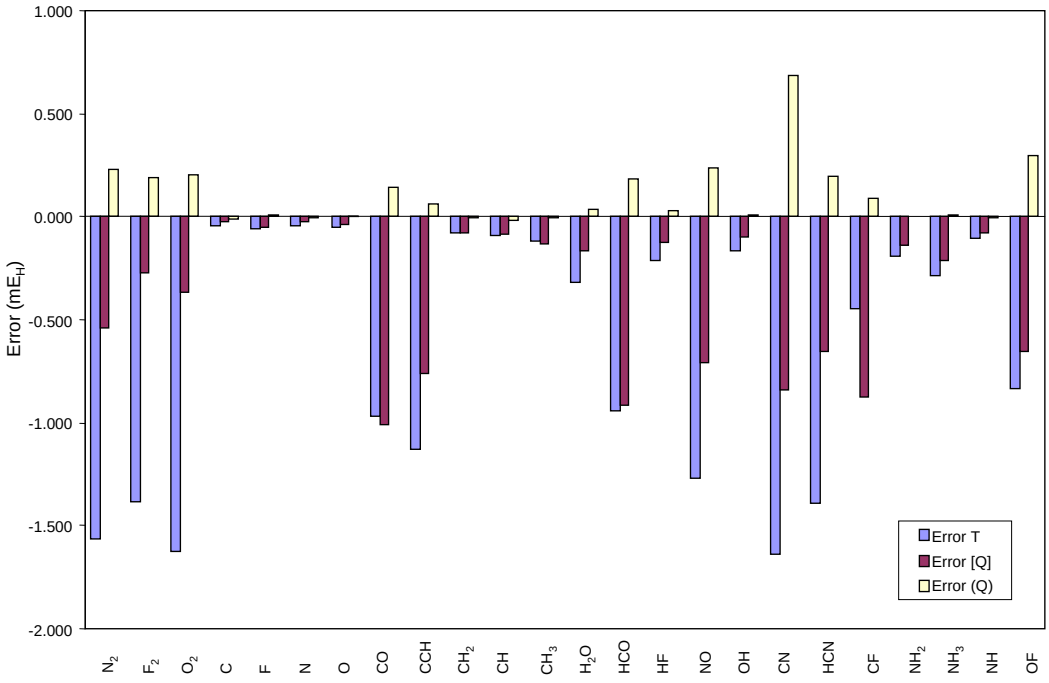

Table 4.3: Statistical analysis in mE_H with cc-pVDZ basis set

Methods	CCSDT	CCSDT[Q]	CCSDT(Q)
MAE (in mE_H)	0.635	0.145	0.100
MSE (in mE_H)	−0.635	−0.136	0.092
MER (in mE_H)	1.730	0.616	0.582

Table 4.4: Statistical analysis in mE_H with cc-pVTZ basis set

Methods	CCSDT	CCSDT[Q]	CCSDT(Q)
MAE (in mE_H)	0.663	0.405	0.136
MSE (in mE_H)	−0.663	−0.405	0.049
MER (in mE_H)	2.084	2.056	0.955

MAE: Mean absolute error, MSE: Mean signed error, MER: Maximum error

Table 4.5: Contributions to the total energies of the 5^{th}- and 6^{th}-order terms in mE_H with cc-pVDZ$^{(a)}$ and cc-pVTZ$^{(b)}$ basis sets

Species	$E_Q^{[5]^{(a)}}$	$E_Q^{[6]^{(a)}}$		$E_Q^{[5]^{(b)}}$	$E_Q^{[6]^{(b)}}$
N_2	−1.399	−0.285		−1.026	−0.767
F_2	−1.598	−0.096		−1.116	−0.461
O_2	−1.773	−0.135		−1.256	−0.571
C	−0.020	−0.002		−0.017	−0.017
F	−0.111	0.001		−0.007	−0.059
N	−0.032	0.000		−0.016	−0.022
O	−0.068	0.000		−0.010	−0.041
CO	−0.335	−0.757		0.034	−1.148
CCH	−0.611	−0.367		−0.363	−0.826
CH_2	−0.050	−0.021		0.002	−0.074
CH	−0.040	−0.022		−0.005	−0.071
CH_3	−0.073	−0.039		0.014	−0.125
H_2O	−0.435	−0.047		−0.152	−0.201
HCO	−0.438	−0.674		−0.028	−1.101
HF	−0.378	−0.033		−0.085	−0.156
NO	−1.004	−0.465		−0.563	−0.945
OH	−0.227	−0.021		−0.068	−0.107
CN	−1.127	−0.860		−0.796	−1.524
HCN	−1.078	−0.354		−0.734	−0.850
CF	0.085	−0.686		0.424	−0.962
NH_2	−0.183	−0.034		−0.056	−0.138
NH_3	−0.275	−0.056		−0.077	−0.221
NH	−0.095	−0.014		−0.027	−0.069
OF	−0.703	−0.502		−0.184	−0.950

Table 4.6: Total energies of the singlet and triplet states of the Beryllium atom in E_H with various basis sets

Methods	CCSDT[Q]	CCSDT(Q)	FCI
Singlet State			
cc-pVDZ	−14.61740963	−14.61740969	−14.61740951
cc-pVTZ	−14.62380892	−14.62380989	−14.62380994
cc-pVQZ	−14.64012126	−14.64012358	−14.64012388
cc-pV5Z	−14.64633059	−14.64633327	−14.64633366
Triplet State			
cc-pVDZ	−14.51630276	−14.51630276	−14.51630273
cc-pVTZ	−14.52344787	−14.52344794	−14.52344793
cc-pVQZ	−14.54002289	−14.54002306	−14.54002306
cc-pV5Z	−14.54642500	−14.54642521	−14.54642521

Figure 4.3: Comparison to the total energies calculated with FCI in mE_H for the singlet state of the beryllium atom.

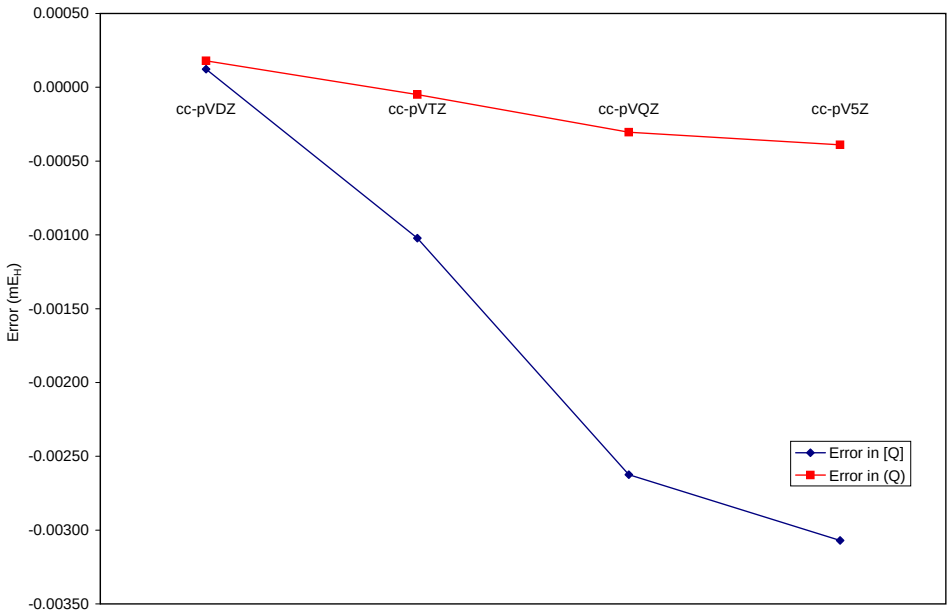

Figure 4.4: Comparison to the total energies calculated with FCI in mE_H for the triplet state of the beryllium atom.

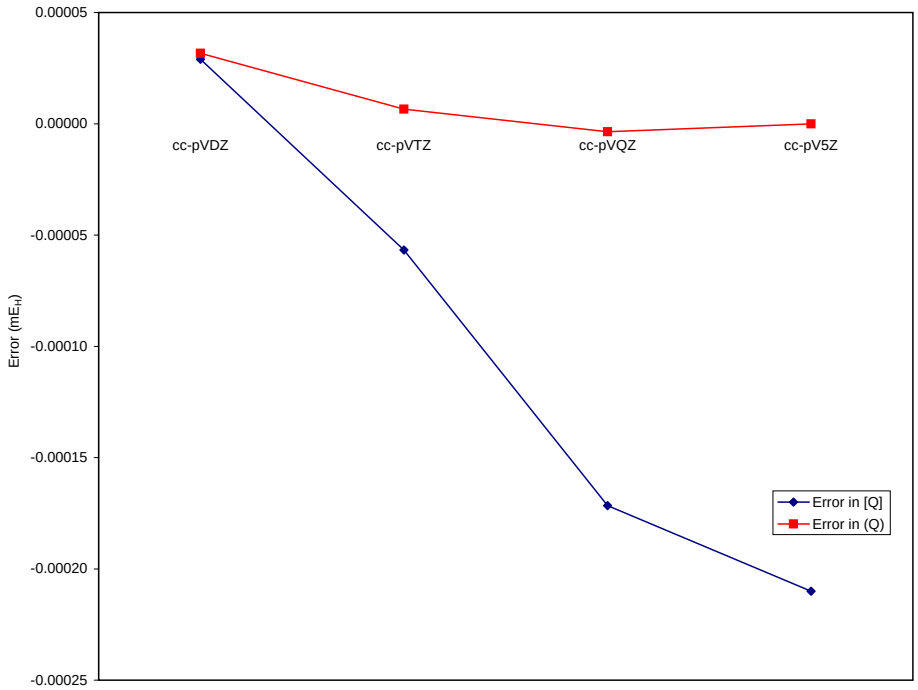

Table 4.7: Total energies in E_H with the cc-pVDZ basis set

Species	CCSDT[Q]	CCSDT(Q)	CCSDTQ	CCSDTQP
N_2	−109.276773	−109.277059	−109.276831	−109.277012
F_2	−199.099315	−199.099411	−199.099253	−199.099328
O_2	−149.987648	−149.987783	−149.987605	−149.987773
C	−37.760708	−37.760710	−37.760717	−37.760717
F	−99.527761	−99.527760	−99.527765	−99.527772
N	−54.478663	−54.478664	−54.478673	−54.478673
O	−74.910130	−74.910131	−74.910140	−74.910143
CO	−113.055222	−113.055979	−113.055839	−113.055892
C_2H_2	−77.110330	−77.110663	−77.110554	−77.110678
CCH	−76.400780	−76.401147	−76.401099	−76.401217
CH_2	−39.041616	−39.041638	−39.041647	−39.041650
CH	−38.380204	−38.380225	−38.380239	−38.380241
CH_3	−39.716018	−39.716057	−39.716064	−39.716070
H_2O_2	−151.195141	−151.195317	−151.195183	−151.195266
H_2O	−76.241615	−76.241662	−76.241634	−76.241649
HCO	−113.576830	−113.577505	−113.577323	−113.577384
HF	−100.228599	−100.228632	−100.228612	−100.228622
HO_2	−150.560131	−150.560452	−150.560296	−150.560380
NO	−129.599354	−129.599819	−129.599605	−129.599737
OH	−75.559652	−75.559673	−75.559683	−75.559689
HNO	−130.172606	−130.172966	−130.172772	−130.172906
CN	−92.492299	−92.493159	−92.492577	−92.492760
HCN	−93.189600	−93.189954	−93.189752	−93.189910
CF	−137.475429	−137.476115	−137.476036	−137.476019
NH_2	−55.733026	−55.733060	−55.733066	−55.733076
NH_3	−56.402457	−56.402513	−56.402498	−56.402517
NH	−55.091668	−55.091681	−55.091697	−55.091700
OF	−174.499746	−174.500248	−174.500028	−174.500090

Figure 4.5: Comparison to the total energies calculated with CCSDTQP and cc-pVDZ in mE_H

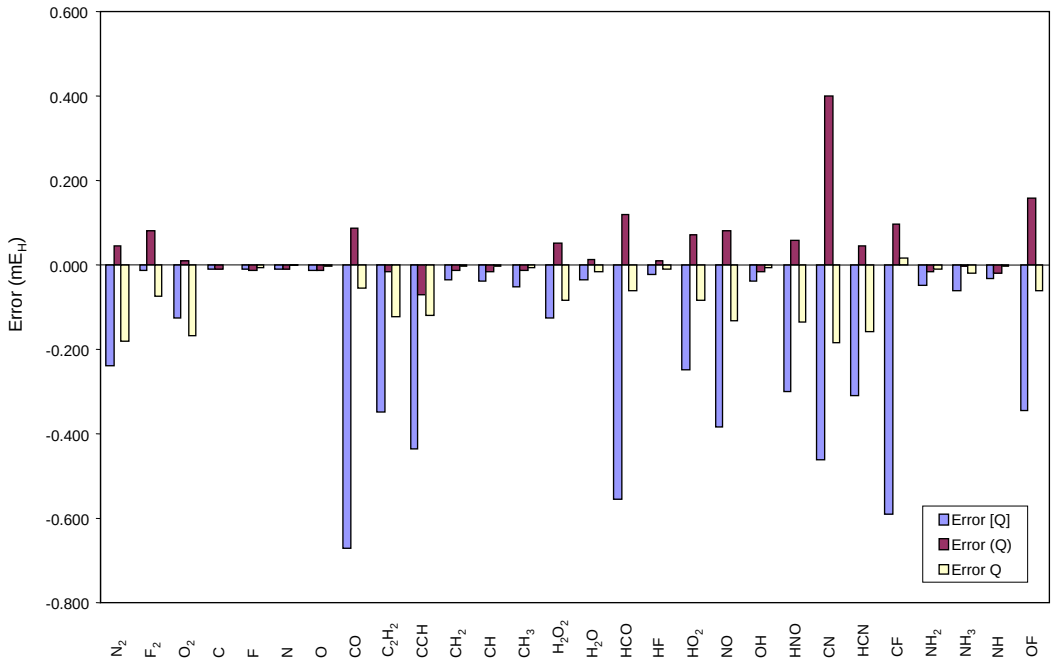

Table 4.8: Statistical analysis in mE_H with cc-pVDZ basis set

Methods	CCSDT	CCSDT[Q]	CCSDT(Q)	CCSDTQ
MAE (in mE_H)	0.775	0.198	0.055	0.058
MSE (in mE_H)	−0.775	−0.198	0.040	−0.059
MER (in mE_H)	1.898	0.670	0.399	0.183

MAE: Mean absolute error, MSE: Mean signed error, MER: Maximum error

4.3 Application to Ab Initio Thermochemistry

In this section we will present a brief summary of the HEAT II method used to calculate the atomization energies and enthalpies of formation. The CCSDTQ and CCSDTQP methods are used as higher-order excitation methods in this protocol. Although, we will demonstrate that the newly developed CCSDT(Q) method can be used while preserving the same accuracy but at a modest computational cost.

The HEAT energies are obtained by a sum of several terms refining the total energies for each atom or molecule

$$\begin{aligned} E_{HEAT} =& E^{\infty}_{HF} + \Delta E^{\infty}_{CCSD(T)} + \Delta E_{CCSDT} + \Delta E_{HLC} + \Delta E_{rel} + \Delta E_{DBOC} \\ &+ \Delta E_{SO} + \Delta E_{ZPE}. \end{aligned} \tag{4.1}$$

The various contributions to E_{HEAT} are described below:

E^{∞}_{HF}: An estimate of the Hartree-Fock limit energy, approximated by extrapolating HF-SCF energies calculated with the aug-cc-pCVXZ hierarchy[74] of basis sets (X=T,Q and 5) using the formula suggested by Feller[75],

$$E^{X}_{HF} = E^{\infty}_{HF} + a \exp(-bX), \tag{4.2}$$

where E^{X}_{HF} is the HF-SCF energy obtained with the aug-cc-pCVXZ basis set, and a and b are parameters fit to the calculated energies.

$\Delta E^{\infty}_{CCSD(T)}$: An estimate of the CCSD(T)[19,20] correlation energy at the basis

set limit, through extrapolation of energies obtained with the aug-cc-pCVQZ and aug-cc-pCV5Z basis sets using the approach advocated by Helgaker[76], which has a somewhat tenuous basis in the atomic partial wave expansion of the correlation energy,

$$\Delta E^{X}_{CCSD(T)} = \Delta E^{\infty}_{CCSD(T)} + \frac{a}{X^3}. \tag{4.3}$$

Here, $\Delta E^{X}_{CCSD(T)}$ is the CCSD(T) correlation energy obtained with the aug-cc-pCVXZ basis sets. Note that through CCSD(T), core and valence correlation effects are not assumed additive; the CCSD(T) calculations above are done for all electrons, using (quite large) basis sets that are appropriate for the treatment of both core and valence correlation effects.

ΔE_{CCSDT}: An estimate of the difference between full CCSDT[16] and CCSD(T) correlation energies at the basis set limit, obtained by extrapolating CCSDT and CCSD(T) energies with the cc-pVTZ and cc-pVQZ basis sets with the extrapolation scheme above (Eq. 4.3) for the CCSDT and CCSD(T) energies. Core correlation effects are *not* included at this stage of the calculation; it is thus implicitly assumed that they are converged at the CCSD(T) level of theory.

ΔE_{HLC}: This "higher-level correlation" contribution attempts to account, approximately, for deficiences in the CCSDT method and is the most expensive step involved in the HEAT protocol[77]. Numerically, it is given by the difference between CCSDT and any higher correlation energies (CCSDT(Q), CCSDTQ,

CCSDTQP ...), both of these obtained in valence-only calculations using the cc-pVDZ basis set. It is understood that this step is one of the most expensive in the HEAT protocol and is therefore the focal point of this section. Any way of making this step computationally cheaper would be highly beneficial to the HEAT method.

ΔE_{rel}: An estimate of the relativistic contribution to the total energy, in which the one-electron Darwin and mass-velocity terms[78,79] are calculated using perturbation theory at the CCSD(T)/aug-cc-pCVTZ level. The relativistic corrections used in the original HEAT protocol[78,79] are obtained via a perturbative treatment based on the one-electron mass-velocity and Darwin terms using the CCSD(T)/cc-pCVTZ basis. In the present work, this treatment is expanded to include the corresponding two-electron Darwin term[80,81]. In addition some calculations have been performed to check on the basis set sensitivity. However, as those were found to be negligible (on the order of 0.01 kJ mol^{-1}), this work focuses on corrections obtained at the CCSD(T)/cc-pCVTZ level.

ΔE_{DBOC}: An estimate of the diagonal Born-Oppenheimer correction[82,83,84,85], which is the expectation value of the nuclear kinetic energy operator, taken over the electronic (clamped-nucleus) wavefunction. This contribution is calculated at the HF-SCF level of theory using the aug-cc-pVTZ basis set.

ΔE_{SO}: This refers to the difference between the true ground state level for radi-

cals in degenerate electronic states and the weighted average that corresponds to the results calculated with non-relativistic electronic structure programs. In HEAT, ΔE_{SO} is calculated using a spin-orbit CI program and relativistic effective core potentials, using the cc-pVDZ basis set.

ΔE_{ZPE}: The zero-point vibrational contribution to the energy. This is calculated from the CCSD(T)/cc-pVQZ quartic force field, using the formula[86]

$$\Delta E_{ZPE} = \sum_i \frac{\omega_i}{2} + \frac{1}{4}\sum_{i<j} x_{ij}, \tag{4.4}$$

which includes a contribution from vibrational anharmonicity.

The zero-point energy formula (Eq. 4.4) used in the original HEAT paper is based on second-order vibrational perturbation theory (VPT2). This equation suffices to calculate energy differences, and is therefore entirely sufficient for spectroscopic analyses, but it neglects a constant contribution to the energy levels. The correct equation is

$$\Delta E_{ZPE} = G_0 + \sum_i \frac{\omega_i}{2} + \frac{1}{4}\sum_{i<j} x_{ij}. \tag{4.5}$$

Formulas for the G_0 term have been derived independently by three groups[27,87,88] in the past few years and, apart from some apparent misprints[89], all three agree.

All calculations are performed at the geometry obtained by minimizing the CCSD(T)/cc-pVQZ all-electron energy and can be found in Ref. 27. It should be noted that the purpose of this section is to show the importance of

the CCSDT(Q) method therefore we will not discuss the effects of the other contributions to the HEAT energy in great details. This work is the result of an extensive collaboration between several research groups to which the author's contribution was the evaluation of the "higher-level correlation" single-point energies.

We already demonstrated the potential of the CCSDT(Q) approach in the previous section, however, using the latter in the context of calculating thermochemical parameters will demonstrate its robustness and stability in comparison to the its inferior CCSDT[Q] rival. In order to make this study more interesting we only calculated the enthalpies of formation using the cc-pVDZ basis set for the higher-level correlation calculations as using the cc-pVTZ basis set would be impossible to handle for CCSDTQ and CCSDTQP for some of the larger systems (H_2O_2, C_2H_2 ...). The first obvious benchmark for CCSDT(Q) and CCSDT[Q] is to compare them to CCSDTQ (as in section 4.2) since they should be able to reproduce the quadruple excitation effects included in CCSDTQ. This is summarized in Tables 4.9-4.10 and Figure 4.6; it is clear that CCSDT[Q] and CCSDT(Q) improve the CCSDT enthalpies of formation. The mean absolute error is 1.92 kJ mol^{-1} for CCSDT while it is only 0.51 and 0.36 kJ mol^{-1} for CCSDT[Q] and CCSDT(Q), respectively. However, CCSDT[Q] is clearly not as reliable as CCSDT(Q) and can generate errors that are over 3 kJ mol^{-1} compared to less than 1.6 kJ mol^{-1} in the case of CCSDT(Q). The performance of CCSDT is disastrous and clearly illustrates the necessity of higher-level corrections. From now we will focus

only on methods including at least quadruple excitations and will no longer worry about the performance of CCSDT. While comparing the two noniterative methods to CCSDTQ is interesting in principle it is even more pertinent to compare them to a method that is close to FCI ("exact" solution of the Schrödinger equation); in this case CCSDTQP. In Tables 4.11-4.12 and Figure 4.7 we compare the three quadruple excitation based methods (CCSDT[Q], CCSDT(Q), CCSDTQ) to CCSDTQP that one can assume to be close to the exact energy (It should be noted that calculating total energies with FCI is impossible for most of these systems). In Section 4.2 it was mentioned that CCSDT(Q) has the same behavior as CCSD(T) i.e. it tends to overestimate the quadruple excitation correction by recovering some of the pentuple effects; this is not seen in the case of CCSDT[Q]. This behavior is seen in the evaluation of the enthalpies of formation; the errors introduced by CCSDT(Q) are now noticeably smaller than in Table 4.10 where we compared CCSDT(Q) to CCSDTQ. The performance of CCSDT(Q) is similar to the one of CCSDTQ with a mean absolute error of about 0.20 kJ mol^{-1} and a RMS of about 0.30 kJ mol^{-1}.

Now that we demonstrated the superiority of CCSDT(Q) when a noniterative treatment of the quadruple excitations is required we can compare the enthalpies of formation obtained with the latter to experimental results and assess its accuracy against the theoretically superior CCSDTQ and CCSDTQP (Tables 4.13-4.14 and Figure 4.8). At first glance, the results are not that im-

pressive; the RMS are around 4.2 kJ mol^{-1} and the maximum errors close to 18 kJ mol^{-1}. Although, one should keep in mind that some of the experimental references used in this comparison have error bars sometimes larger than 15 kJ mol^{-1} and that most predictions are within the experimental errors except for the NH molecule. While the comparison to experimental enthalpies of formation with such errors seems somewhat useless, it is at the contrary a great example of the importance of highly accurate theoretical thermochemistry models. In fact, theoretical approaches can help refining these experimental numbers as it is done in the active thermochemical tables (ATcT) of Ruscic and co-workers. The ATcT database is generated from the most up-to-date experimental and theoretical thermochemical data reported in the literature and can optimize – using a sophisticated self consistency check – the absolute value of a given thermochemical property with appropriate error bars. All the experimental enthalpies of formation – up to the OH molecule – given in Table 4.13 come from the ATcT database; considering that these values are now considered more reliable than their NIST-JANAF counterparts, it seems more logical to benchmark the accuracy of the previously mentioned theoretical methods against these "experimental" values. This is shown in Tables 4.15-4.16 and Figure 4.9. The results are astonishing for all three methods, the mean absolute errors are only 0.29, 0.31 and 0.25 kJ mol^{-1} and the RMS are 0.37, 0.37, 0.29 for CCSDT(Q), CCSDTQ and the CCSDTQP, respectively. It is obvious that CCSDTQP offers the best results but at a more than prohibitive computational cost. The CCSDTQP method is not a valuable option

for larger systems. Another encouraging fact is the brilliant performance of the "cheap" CCSDT(Q); CCSDTQ performs barely if at all better than the latter on more than fifteen theoretically-tricky systems. As a reminder, one should keep in mind that the scaling of CCSDT(Q) is only n^9 compared to n^{10} and n^{12} for CCSDTQ and CCSDTQP, respectively. Also, most importantly, it is conducted in a noniterative manner, thus, only requiring one n^9 step after CCSDT is performed. This usually means hours or days of processor time saved. The largest error for CCSDT(Q) is in the case of F_2, CO_2 and HO_2 but is always below 0.75 kJ mol^{-1}.

Table 4.9: Enthalpies of formation (0 K, in kJ mol^{-1}) calculated with CCSDT, CCSDT[Q], CCSDT(Q), and CCSDTQ.

Species	HEAT345-T	HEAT345-[Q]	HEAT345-(Q)	HEAT345-Q
N_2	3.66	0.16	−0.59	0.05
H_2	−0.31	−0.31	−0.31	−0.31
F_2	3.17	−0.44	−0.70	−0.26
O_2	4.73	0.43	0.08	0.60
CO	−111.22	−111.87	−113.85	−113.44
C_2H_2	231.57	229.87	229.01	229.34
CCH	566.41	564.91	563.95	564.12
CH_2	391.28	391.20	391.15	391.15
CH	593.05	593.00	592.95	592.93
CH_3	150.31	150.17	150.07	150.07
CO_2	−388.71	−389.42	−393.74	−392.83
H_2O_2	−126.11	−129.00	−129.46	−129.06
H_2O	−238.34	−239.30	−239.42	−239.32
HCO	44.26	43.34	41.57	42.10
HF	−272.10	−272.80	−272.89	−272.83
HO_2	17.51	15.38	14.54	15.01
NO	94.25	91.87	90.65	91.27
OH	37.23	36.81	36.76	36.76
HNO	114.09	110.93	109.99	110.54
CN	441.32	438.49	436.24	437.81
HCN	133.02	130.33	129.40	129.98
CF	244.18	244.75	242.95	243.19
NH_2	189.21	188.82	188.73	188.74
NH_3	−38.14	−38.78	−38.92	−38.86
NH	359.04	358.88	358.84	358.83
OF	112.47	111.09	109.77	110.39

Table 4.10: Statistical analysis of errors from Table 4.9 in comparison to HEAT345-Q

Methods	HEAT345-T	HEAT345-[Q]	HEAT345-(Q)
Mean Absolute Error	1.92	0.51	0.36
Mean Signed Error	1.92	0.48	−0.35
RMS	2.36	0.89	0.50
Maximum Error	4.13	3.41	1.57

Figure 4.6: Errors in the enthalpies of formation for HEAT345-T, HEAT345-[Q], and HEAT345-(Q) with respect to HEAT345-Q in kJ mol^{-1}.

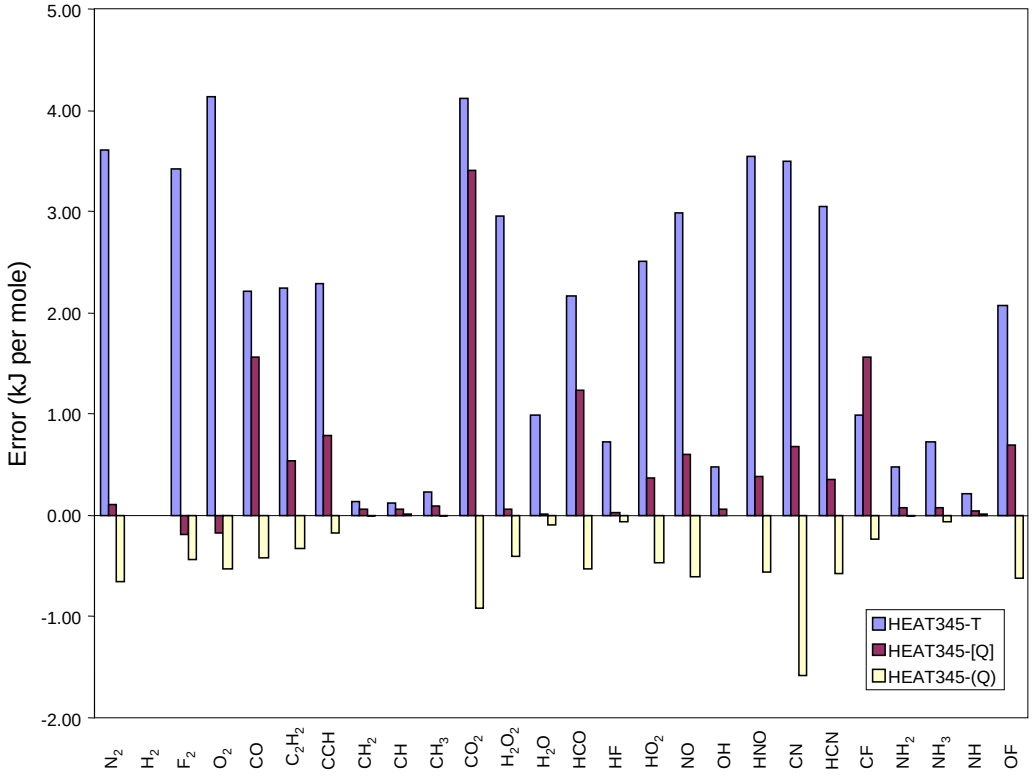

Table 4.11: Enthalpies of formation (0 K, in kJ mol^{-1}) calculated with CCSDT[Q], CCSDT(Q), CCSDTQ, and CCSDTQP.

Species	HEAT345-[Q]	HEAT345-(Q)	HEAT345-Q	HEAT345-QP
N_2	0.16	−0.59	0.05	−0.42
H_2	−0.31	−0.31	−0.31	−0.31
F_2	−0.44	−0.70	−0.26	−0.42
O_2	0.43	0.08	0.60	0.17
CO	−111.87	−113.85	−113.44	−113.57
C_2H_2	229.87	229.01	229.34	229.01
CCH	564.91	563.95	564.12	563.81
CH_2	391.20	391.15	391.15	391.14
CH	593.00	592.95	592.93	592.93
CH_3	150.17	150.07	150.07	150.05
CO_2	−389.42	−393.74	−392.83	−392.99
H_2O_2	−129.00	−129.46	−129.06	−129.26
H_2O	−239.30	−239.42	−239.32	−239.36
HCO	43.34	41.57	42.10	41.94
HF	−272.80	−272.89	−272.83	−272.84
HO_2	15.38	14.54	15.01	14.80
NO	91.87	90.65	91.27	90.93
OH	36.81	36.76	36.76	36.75
HNO	110.93	109.99	110.54	110.20
CN	438.49	436.24	437.81	437.33
HCN	130.33	129.40	129.98	129.56
CF	244.75	242.95	243.19	243.25
NH_2	188.82	188.73	188.74	188.71
NH_3	−38.78	−38.92	−38.86	−38.91
NH	358.88	358.84	358.83	358.82
OF	111.09	109.77	110.39	110.25

Table 4.12: Statistical analysis of errors from Table 4.11 in comparison to HEAT345-QP.

Methods	HEAT345-[Q]	HEAT345-(Q)	HEAT345-Q
Mean Absolute Error	0.65	0.20	0.17
Mean Signed Error	0.65	−0.19	0.17
RMS	1.01	0.32	0.24
Maximum Error	3.57	1.09	0.48

Figure 4.7: Errors in the enthalpies of formation for HEAT345-[Q], HEAT345-(Q), and HEAT345-Q with respect to HEAT345-QP in kJ mol^{-1}.

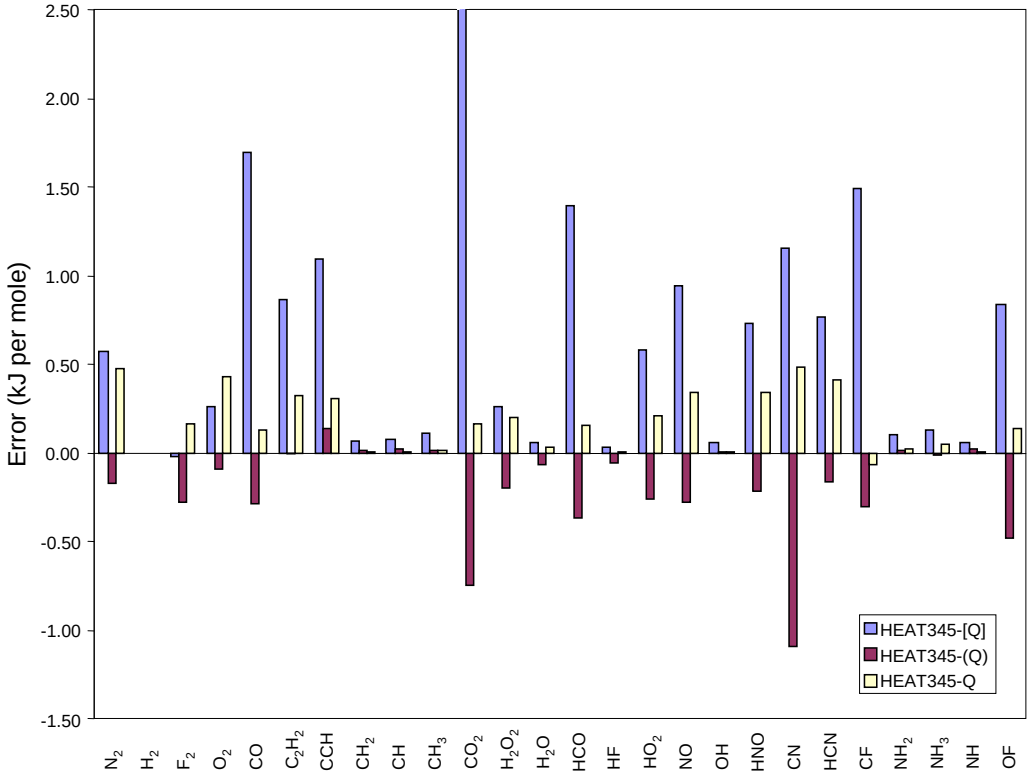

Table 4.13: Enthalpies of formation (0 K, in kJ mol^{-1}) calculated with CCSDT(Q), CCSDTQ, CCSDTQP, and their experimental estimates (ATcT tables and NIST-JANAF[a]).

Species	HEAT345-(Q)	HEAT345-Q	HEAT345-QP	EXP
N_2	−0.59	0.05	−0.42	0.00 ± 0.00
H_2	−0.31	−0.31	−0.31	0.00 ± 0.00
F_2	−0.70	−0.26	−0.42	0.00 ± 0.00
O_2	0.08	0.60	0.17	0.00 ± 0.00
CO	−113.85	−113.44	−113.57	−113.82 ± 0.03
C_2H_2	229.01	229.34	229.01	228.82 ± 0.30
CCH	563.95	564.12	563.81	563.94 ± 0.31
CH_2	391.15	391.15	391.14	390.96 ± 0.27
CH	592.95	592.93	592.93	592.96 ± 0.25
CH_3	150.07	150.07	150.05	149.97 ± 0.10
CO_2	−393.74	−392.83	−392.99	−393.11 ± 0.01
H_2O_2	−129.46	−129.06	−129.26	−129.78 ± 0.07
H_2O	−239.42	−239.32	−239.36	−238.91 ± 0.03
HCO	41.57	42.10	41.94	41.92 ± 0.26
HF	−272.89	−272.83	−272.84	−272.73 ± 0.24
HO_2	14.54	15.01	14.80	15.21 ± 0.25
NO	90.65	91.27	90.93	90.59 ± 0.08
OH	36.76	36.76	36.75	37.09 ± 0.05
HNO	109.99	110.54	110.20	102.50 ± 0.42[a]
CN	436.24	437.81	437.33	436.80 ± 10.00[a]
HCN	129.40	129.98	129.56	135.53 ± 8.40[a]
CF	242.95	243.19	243.25	251.60 ± 8.00[a]
NH_2	188.73	188.74	188.71	193.25 ± 6.30[a]
NH_3	−38.92	−38.86	−38.91	−38.91 ± 0.40[a]
NH	358.84	358.83	358.82	376.51 ± 16.70[a]
OF	109.77	110.39	110.25	108.00 ± 10.00[a]

Table 4.14: Statistical analysis of errors from Table 4.13 in comparison to experiment.

Methods	HEAT345-(Q)	HEAT345-Q	HEAT345-QP
Mean Absolute Error	1.82	1.86	1.80
Mean Signed Error	−1.03	−0.68	−0.85
RMS	4.15	4.17	4.15
Maximum Error	17.67	17.68	17.69

Figure 4.8: Errors in the enthalpies of formation for HEAT345-(Q), HEAT345-Q, and HEAT345-QP with respect to experiment in kJ mol^{-1}.

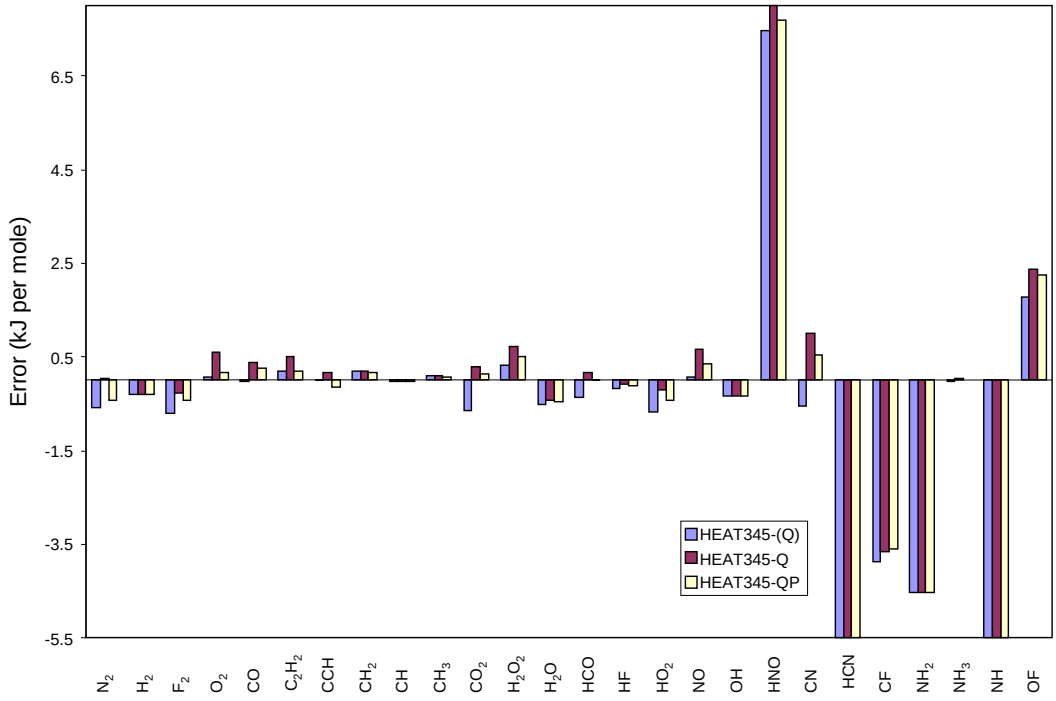

Table 4.15: Enthalpies of formation (0 K, in kJ mol^{-1}) calculated with CCSDT(Q), CCSDTQ, CCSDTQP, and their best "experimental" estimates (ATcT tables).

Species	HEAT345-(Q)	HEAT345-Q	HEAT345-QP	ATcT
N_2	−0.59	0.05	−0.42	0.00 ± 0.00
H_2	−0.31	−0.31	−0.31	0.00 ± 0.00
F_2	−0.70	−0.26	−0.42	0.00 ± 0.00
O_2	0.08	0.60	0.17	0.00 ± 0.00
CO	−113.85	−113.44	−113.57	−113.82 ± 0.03
C_2H_2	229.01	229.34	229.01	228.82 ± 0.30
CCH	563.95	564.12	563.81	563.94 ± 0.31
CH_2	391.15	391.15	391.14	390.96 ± 0.27
CH	592.95	592.93	592.93	592.96 ± 0.25
CH_3	150.07	150.07	150.05	149.97 ± 0.10
CO_2	−393.74	−392.83	−392.99	−393.11 ± 0.01
H_2O_2	−129.46	−129.06	−129.26	−129.78 ± 0.07
H_2O	−239.42	−239.32	−239.36	−238.91 ± 0.03
HCO	41.57	42.10	41.94	41.92 ± 0.26
HF	−272.89	−272.83	−272.84	−272.73 ± 0.24
HO_2	14.54	15.01	14.80	15.21 ± 0.25
NO	90.65	91.27	90.93	90.59 ± 0.08
OH	36.76	36.76	36.75	37.09 ± 0.05

Table 4.16: Statistical analysis of errors from Table 4.15 in comparison to the ATcT tables.

Methods	HEAT345-(Q)	HEAT345-Q	HEAT345-QP
Mean Absolute Error	0.29	0.31	0.25
Mean Signed Error	−0.19	0.12	−0.04
RMS	0.37	0.37	0.29
Maximum Error	0.70	0.72	0.52

Figure 4.9: Errors in the enthalpies of formation for HEAT345-(Q), HEAT345-Q, and HEAT345-QP with respect to the ATcT tables in kJ mol^{-1}.

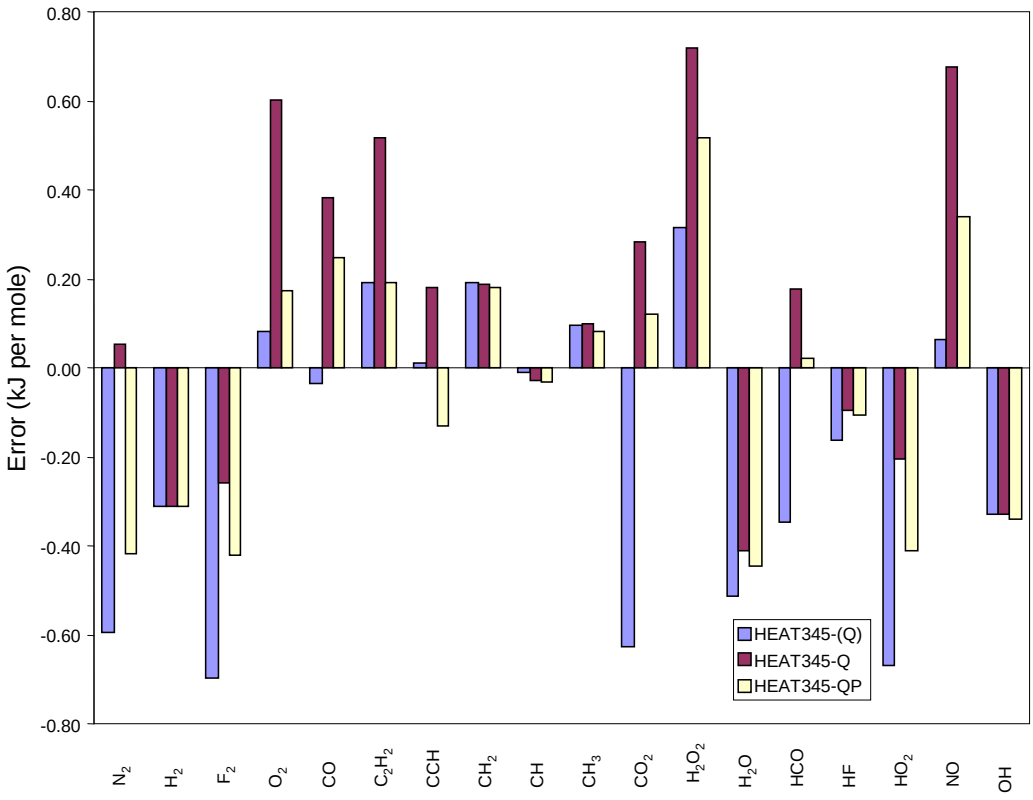

4.4 Conclusion

The tremendous impact that CCSD(T) has had on computational quantum chemistry is sometimes not fully appreciated. The CCSD method, while reasonably accurate and remarkably robust, is not adequate for applications that demand relatively high accuracy. At the time of its development, CCSD(T) offered the only practical coupled cluster approach for treating triple excitation effects. It was quickly shown to be decidedly superior to the noniterative CCSD[T] approach[91]. An unexpected finding was that CCSD(T) is more accurate than the more expensive iterative CCSDT-X treatments[92], and indeed performs just as well as the expensive CCSDT approach for most applications.

Continued advances in computational power have facilitated even more ambitious applications of quantum chemistry to problems that demand very high accuracy; one such area of interest to us is thermochemistry. It has been shown empirically that so-called subchemical accuracy (< 1 kJ mol^{-1}) in thermochemical calculations requires correlation treatments that go beyond CCSD(T) and CCSDT. Similar to the situation that existed in 1989, the full CCSDTQ method, while available in some programs, is simply not feasible for routine applications at this time. There is a consequent need for noniterative treatment of quadruple excitations, and we have developed an approach here that, in a formal sense, is to CCSDTQ what CCSD(T) is to CCSDT. Numerical tests of this method are highly encouraging, and suggest that this CCSDT(Q) method is better than the previously suggested method and has an accuracy that is comparable to CCSDTQ itself. The performance of CCSDT(Q) for cal-

culating thermochemical properties is impressive and there is no doubt that more and more quantum chemists will use this method when looking for the best cost/efficiency ratio. We believe that CCSDT(Q) will see wide applications in the future and is destined to become the method of choice for those seeking very high accuracy at a reasonable computational cost.

Chapter 5

Recent Advances in Equation-of-Motion Coupled Cluster Theory

5.1 Introduction

Advances in general coupled cluster theory have taken quantum chemistry to a level of accuracy that few if any other methods could achieve with an acceptable scaling and while preserving the size consistency of the wavefunction. However, there are cases where general coupled cluster theory and most other quantum chemistry methods can fail. This is especially true when one studies radicals or generally speaking, open-shell molecules. In fact, a lot of these molecules are associated with ground state wavefunction having an abnormal behavior. The first coupled cluster methods used for studying open-shell molecules were based on a UHF wavefunction. However, these method can be plagued with spin contamination[30]. With both UHF and restricted open-shell HF (ROHF) methods, the wavefunction is prone to symmetry breaking (or related phenomena that appear when the molecule lacks appropriate elements of symmetry)[93,94,95], which can make studies of the potential energy surface essentially impossible. In addition, when there are low-lying excited states of the radical, "real" symmetry breaking of the pseudo-Jahn-Teller type can occur, and the ability of various quantum chemical methods

to treat such situations varies widely[29].

To solve the problems mentioned above several single-determinant methods were developed. Among these are quasirestricted Hartree-Fock coupled cluster (QRHF-CC)[96] and equation-of-motion ionization potential coupled cluster (EOMIP-CC)[37,38,39,40,41] methods. These approaches are in nature pretty similar because they both use a closed-shell reference state, but still differ in a lot of ways. In the QRHF framework the coupled cluster equations are solved using the orbitals of the closed-shell system therefore avoiding the problem of reference spin contamination and symmetry breaking. However, when a "true" multireference picture of the molecule has to be used – meaning that there are a lot of interactions between states for example vibronic coupling or pseudo-Jahn-Teller effects – it doesn't perform as well as EOMIP-CC that offers a better treatment of the interacting state due to the choice of the Hamiltonian. Indeed, even if EOMIP-CC seems like a single-determinant method in appearance it is really a multireference approach in the sense that it doesn't have a bias towards any particular molecular orbital configuration. The only problem with the EOMIP-CC approaches is that the treatment of dynamic correlation is not as good as it is in general coupled cluster methods (for the same excitation level).

The EOMIP-CC methods are part of the recently developed equation-of-motion coupled cluster methods as mentioned earlier. There are two other types of EOM-CC approaches – equation-of-motion for excited states[42,31] and equation-of-motion for electron attachment[43]. These methods were developed

for several reasons, first to overcome the single-reference bias of general coupled cluster theory when a multireference method would be more appropriate and secondly to reduce the computational cost of studying the state of interest (ionized, excited). For example a naive approach for studying ionized states or excited states would be to carry out two calculations, one for the ground state of the molecule and the other one for the state of interest. While it seems like a reasonable alternative to treating this problem it isn't actually the best option. First of all, both calculations are as expensive, and second of all, it is usually more than tricky to determine a suitable wavefunction for the excited state (we mentioned earlier that these wavefunctions are prone to symmetry breaking, spin contamination ...). In the case of EOM-CC methods the reference determinant is almost always a well-behaved closed-shell determinant thus avoiding the complication of using an open-shell reference function.
In this chapter we will present the general EOM-CC method while focusing on the recent advances in EOMIP-CC.

5.2 Equation-of-Motion Coupled Cluster Theory

In the EOM-CCSD formalism, the final state wavefunction is defined as

$$|\Psi_f\rangle = \hat{\mathcal{R}}|\Psi_r\rangle \tag{5.1}$$

where f and r correspond to the final and reference (usually closed-shell) states, respectively. $\mathcal{R}$ is the second quantized operator

$$\hat{\mathcal{R}} = \hat{\mathcal{R}}_1 + \hat{\mathcal{R}}_2 \tag{5.2}$$

In the EOM-CC framework, the reference state wavefunction is given by the coupled cluster approximation

$$|\Psi_r\rangle = e^{\hat{T}}|\psi_0\rangle \tag{5.3}$$

where $|\psi_0\rangle$ is the zeroth-order Slater determinant that describes the reference state.

Truncated to single and double excitations, the cluster operator $\hat{T}$ takes the form

$$\hat{T} \equiv \hat{T}_1 + \hat{T}_2 = \sum_{ia} t_i^a a_a^\dagger a_i + \frac{1}{4}\sum_{ijab} t_{ij}^{ab} a_a^\dagger a_b^\dagger a_j a_i \tag{5.4}$$

as defined in Chapter 2. In CCSD, equations for the amplitudes are obtained by inserting Eq. 5.3 into the electronic Schrödinger equation, premultiplying by $e^{-\hat{T}}$ and projecting onto the spaces of single and double excitations. The resulting amplitude equations are as follows

$$\langle \Phi_i^a | e^{-\hat{T}} \hat{H} e^{\hat{T}} | \psi_0 \rangle = 0$$
$$\langle \Phi_{ij}^{ab} | e^{-\hat{T}} \hat{H} e^{\hat{T}} | \psi_0 \rangle = 0$$

where $e^{-\hat{T}} \hat{H} e^{\hat{T}} = \bar{H}$ (See Chapter 2). Equations for determining the final state energies in EOM methods can be derived in a few different ways for CCSD or any complete coupled cluster methods like CCSDT, CCSDTQ, *etc.* One conceptually appealing approach that led to the EOM designation is to insert the wavefunction ansatz into the Schrödinger equation, which leads to

an eigenvalue problem involving the similarity transformed Hamiltonian ($\bar{H}$),

$$\bar{H}\hat{\mathcal{R}}|\psi_0\rangle = E\hat{\mathcal{R}}|\psi_0\rangle \tag{5.5}$$

It should be noted that a more general approach is provided by linear response theory and is more appropriate for approximate methods such as CC3, CCSDT-X *etc.* The operator $\hat{\mathcal{R}}$ can assume different forms depending if one is deriving the EOM-CCSD equations for ionized states ($\hat{\mathcal{R}}^{IP}$), excited states ($\hat{\mathcal{R}}^{EE}$) or electron attachment states ($\hat{\mathcal{R}}^{EA}$). These corresponding forms of the $\hat{\mathcal{R}}$ operator and their diagrammatic representations are as follows

$$\hat{\mathcal{R}}^{IP} \equiv \hat{\mathcal{R}}_1^{IP} + \hat{\mathcal{R}}_2^{IP} = \sum_i r_i a_i + \frac{1}{2}\sum_{ija} r_{ij}^a a_a^\dagger a_i a_j \tag{5.6}$$

$=$ 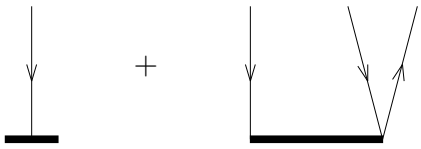 $+$

$$\hat{\mathcal{R}}^{EE} \equiv \hat{\mathcal{R}}_1^{EE} + \hat{\mathcal{R}}_2^{EE} = \sum_{ia} r_i^a a_a^\dagger a_i + \frac{1}{4}\sum_{ijab} r_{ij}^{ab} a_a^\dagger a_b^\dagger a_i a_j \tag{5.7}$$

$=$ 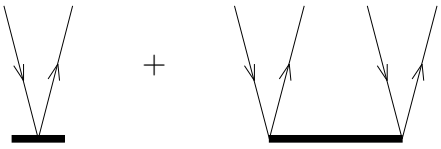

$$\hat{\Re}^{EA} \equiv \hat{\Re}_1^{EA} + \hat{\Re}_2^{EA} = \sum_a r^a a_a^\dagger + \frac{1}{2}\sum_{iab} r_i^{ab} a_a^\dagger a_b^\dagger a_i \tag{5.8}$$

In the following discussion we will only derive the EOMIP-CCSD equations since we are for the time being only interested in adding higher excitation terms to this method (triple excitations have already been added to EOMEE). However, one can also derive the EOM-CCSD method using another deexcitation operator, $\mathcal{L}$. In this case the final state wavefunction is defined as

$$\langle \Psi_f | = \langle \Psi_r | \hat{\mathcal{L}} \tag{5.9}$$

therefore Equation 5.5 becomes

$$\langle \Psi_0 | \hat{\mathcal{L}} \bar{H} = \langle \Psi_0 | \hat{\mathcal{L}} E \tag{5.10}$$

The $\mathcal{L}$ operators corresponding to the $\hat{\Re}^{IP}$, $\hat{\Re}^{EE}$, $\hat{\Re}^{EA}$ operators can be defined as being

$$\hat{\mathcal{L}}^{IP} \equiv \hat{\mathcal{L}}_1^{IP} + \hat{\mathcal{L}}_2^{IP} = \sum_i l^i a_i^\dagger + \frac{1}{2}\sum_{ija} l_a^{ij} a_i^\dagger a_j^\dagger a_a \tag{5.11}$$

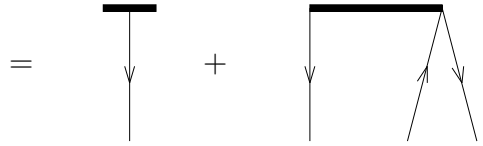

$$\hat{\mathfrak{L}}^{EE} \equiv \hat{\mathfrak{L}}_1^{EE} + \hat{\mathfrak{L}}_2^{EE} = \sum_{ia} l_a^i a_i^\dagger a_a + \frac{1}{4} \sum_{ijab} l_{ab}^{ij} a_i^\dagger a_j^\dagger a_a a_b \tag{5.12}$$

$=$ 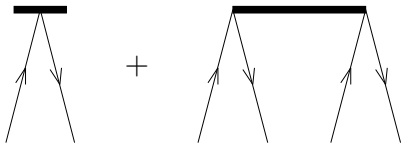 $+$

$$\hat{\mathfrak{L}}^{EA} \equiv \hat{\mathfrak{L}}_1^{EA} + \hat{\mathfrak{L}}_2^{EA} = \sum_{a} l_a a_a + \frac{1}{2} \sum_{iab} l_{ab}^{i} a_i^\dagger a_a a_b \tag{5.13}$$

$=$ 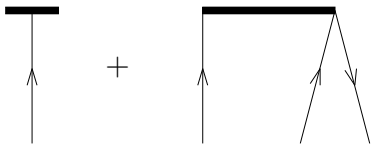 $+$

For evaluating the EOM-CC energies one only needs to form either the $\bar{H}\hat{\mathfrak{R}}$ or $\hat{\mathfrak{L}}\bar{H}$ quantity therefore evaluating both would be a waste of processor time. This is not the case when evaluating the density matrices (as needed to calculate final state properties or gradients) in which case both $\bar{H}\hat{\mathfrak{R}}$ and $\hat{\mathfrak{L}}\bar{H}$ have to be formed. These equations are the following

$$\begin{aligned}\bar{H}\mathcal{R} =& -\sum_{m} r_m \mathcal{F}_i^m - \frac{1}{2}\sum_{nem} r_{nm}^e \mathcal{W}_{ie}^{mn} + \sum_{me} r_{mi}^e \mathcal{F}_e^m \\ & - P(ij)\sum_{me} r_{im}^e \mathcal{W}_{je}^{ma} - P(ij)\sum_{m} r_{mj}^a \mathcal{F}_i^m + \sum_{e} r_{ij}^e \mathcal{F}_e^a \\ & + \frac{1}{2}\sum_{mn} r_{mn}^a \mathcal{W}_{ji}^{nm} - \frac{1}{2}\sum_{mnef} r_{nm}^e t_{ij}^{af} \langle mn||fe\rangle - \sum_{m} r_m \mathcal{W}_{ji}^{ma}\end{aligned} \tag{5.14}$$

and

$$\begin{aligned}\mathcal{L}\bar{H} =& -\sum_{m} l^m \mathcal{F}_m^i - \frac{1}{2}\sum_{nem} l_e^{nm} \mathcal{W}_{mn}^{ie} + \sum_{me} l_e^{mi} \mathcal{F}_m^e \\ & - P(ij)\sum_{me} l_e^{im} \mathcal{W}_{ma}^{je} - P(ij)\sum_{m} l_a^{mj} \mathcal{F}_m^i + \sum_{e} l_e^{ij} \mathcal{F}_a^e \\ & + \frac{1}{2}\sum_{mn} l_a^{mn} \mathcal{W}_{nm}^{ji} - \frac{1}{2}\sum_{mnef} l_e^{nm} t_{ij}^{af} \langle fe||mn\rangle - \sum_{m} l^m \mathcal{W}_{ma}^{ji}\end{aligned} \tag{5.15}$$

where $\mathcal{W}$ and $\mathcal{F}$ are intermediates (parts of $\bar{H}$ defined in Chapter 2). In the previous equations, the antisymmetric permutation operator P(pq) is defined *via* $P(pq)Z(pq) = Z(pq) - Z(qp)$. The diagrammatic representations of $\bar{H}\hat{\mathcal{R}}$ and $\hat{\mathcal{L}}\bar{H}$ with corresponding algebraic expressions can be found in Figures 5.1-5.2.

The equations for EOMEE-CCSD and EOMEA-CCSD can be derived in the same manner by using the corresponding $\hat{\mathcal{R}}$ and $\hat{\mathcal{L}}$. These methods including EOMIP-CCSD have been successful in studying open-shell systems. However, singles and doubles are usually not enough to describe the molecules of interest with quantitative accuracy, and one might like to include triple excitations. In the following section we will derive a scheme to insert triple excitations to the EOMIP-CC method while avoiding the cost of EOMIP-CCSDT[44].

Figure 5.1: Diagrammatic representation of $\bar{H}\hat{\mathfrak{R}}$ for the EOMIP-CCSD method in the antisymmetrized Brandow formalism together with corresponding algebraic expressions.

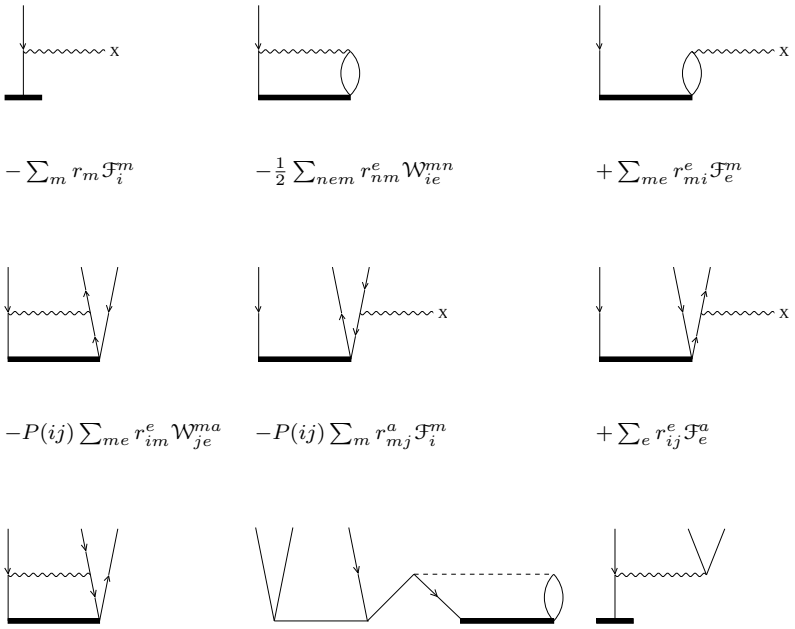

The squiggly lines and the dashed lines represent intermediates and integrals (defined in Chapter 2), respectively, while the thick and thin amplitude vertices correspond to the $\hat{\mathfrak{R}}$ and $\hat{T}$ operators.

Figure 5.2: Diagrammatic representation of $\hat{\mathfrak{L}}\bar{H}$ for the EOMIP-CCSD method in the antisymmetrized Brandow formalism together with corresponding algebraic expressions.

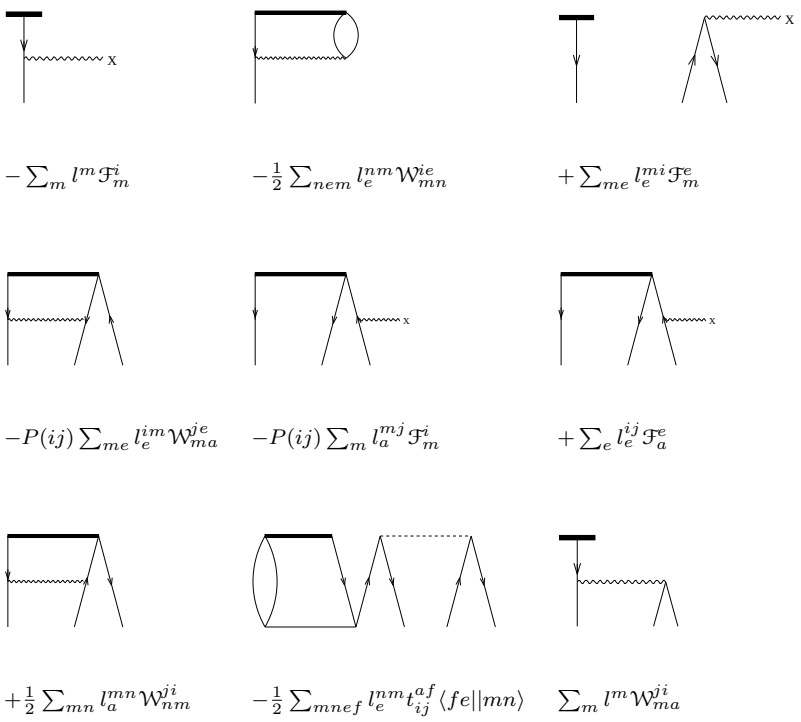

$-\sum_m l^m \mathcal{F}^i_m$ $\quad -\frac{1}{2}\sum_{nem} l^{nm}_e \mathcal{W}^{ie}_{mn}$ $\quad +\sum_{me} l^{mi}_e \mathcal{F}^e_m$

$-P(ij)\sum_{me} l^{im}_e \mathcal{W}^{je}_{ma}$ $\quad -P(ij)\sum_m l^{mj}_a \mathcal{F}^i_m$ $\quad +\sum_e l^{ij}_e \mathcal{F}^e_a$

$+\frac{1}{2}\sum_{mn} l^{mn}_a \mathcal{W}^{ji}_{nm}$ $\quad -\frac{1}{2}\sum_{mnef} l^{nm}_e t^{af}_{ij} \langle fe||mn\rangle$ $\quad \sum_m l^m \mathcal{W}^{ji}_{ma}$

The squiggly lines and the dashed lines represent intermediates and integrals (defined in Chapter 2), respectively, while the thick and thin amplitude vertices correspond to the $\hat{\mathfrak{L}}$ and $\hat{T}$ operators.

5.3 Equation-of-Motion Coupled Cluster Singles Doubles with Inclusion of Approximate Triple Excitations

The EOMIP-CCSDT method was recently developed by Musial *et al.*, this is a powerful approach in theory but using this method for large systems is unfeasible because it requires a CCSDT – scaling as N^8 – calculation on a $N+1$ electron reference state. Hence, it is interesting to develop methods to go beyond EOMIP-CCSD while avoiding the cost of EOMIP-CCSDT. The same idea was used about twenty years ago in general coupled cluster theory to approximate triples effects using a new class of iterative methods; the so-called CCSDT-X (X=1a, 1b, 2, 3)[46] and CC3[47,48] which was developed more recently. Some of these methods are known to perform relatively well while others are not so reliable. The most expensive of them, CCSDT-3 and CC3, perform well in most cases but the more complete CCSDT-3 method is more reliable. Indeed, the CC3 approximation breaks down in a lot of cases, even if it is not acknowledged by the whole "coupled cluster community". The other approximations are not expected to perform as well since a lot of terms are neglected but they are cheaper. One can expect the same behavior when these approximations are included into the EOMIP framework or any of the EOM approaches for that matter.

Deriving the EOMIP equations for the CCSD level of theory seemed somewhat straightforward although when dealing with approximated triple excitations the matrix equivalent to the similarity transformed Hamiltonian $\bar{H}$ is

not complete with respect to triple excitations and is different for each approximate methods. It is easier to define $\bar{H}$ to be the same as in EOMIP-CCSD and consider the additional contributions separately. The usual approach to figure out the terms that will be included in these approximate methods is to differentiate the amplitude equations corresponding to the various methods (this is also referred to as time independent linear response theory[97]) with respect to some perturbation. These amplitude equations are given in Table 5.1 and now include the amplitudes projected onto the triples space. Common to all of these approaches is the exclusion of $\hat{T}_3$ in the triples equations apart from the essential $\hat{F}_N\hat{T}_3$ contribution where $\hat{F}_N$ is the one-electron part of the normal-ordered Hamiltonian. If only these terms are removed, one obtains the CCSDT-3 model. The strategy of CC3 is to treat the single and double excitations as zeroth- and first-order, respectively, and to include only those terms in the triples equations that are overall second-order. Hence, $\langle\Phi_{ijk}^{abc}|\frac{1}{2}\hat{W}_N\hat{T}_2{}^2 + \frac{1}{2}\hat{W}_N\hat{T}_1\hat{T}_2{}^2|0\rangle$ is excluded from CC3, where $\hat{W}_N$ is the two-electron part of the normal-ordered Hamiltonian.

Let us take the example of the singles amplitude equations corresponding to the simplest CCSDT-1a contribution for the sake of clarity

$$\langle S|\bar{H} + \hat{W}_N\hat{T}_3|0\rangle = 0. \tag{5.16}$$

One can differentiate the latter with respect to some arbitrary perturbation X

$$\langle S|\bar{H}\frac{\partial\hat{T}}{\partial X} - \frac{\partial\hat{T}}{\partial X}\bar{H} + \bar{H}^X + \hat{W}_N^X + \hat{W}_N\frac{\partial\hat{T}_3}{\partial X}|0\rangle = 0 \tag{5.17}$$

since

$$\frac{\partial \bar{H}}{\partial X} = [\bar{H}, \frac{\partial \hat{T}}{\partial X}] + \bar{H}^X \tag{5.18}$$

where $\bar{H}^X$ is the part of $\bar{H}$ depending on the perturbation X. This equation can be rearranged by putting the terms that depend on X in the right hand side of the equation as follows

$$\langle S|\bar{H}\frac{\partial \hat{T}}{\partial X} - \frac{\partial \hat{T}}{\partial X}\bar{H} + \hat{W}_N\frac{\partial \hat{T}_3}{\partial X}|0\rangle = -\langle S|\bar{H}^X + \hat{W}_N^X|0\rangle \tag{5.19}$$

From now on we will label $-\langle S|\bar{H}^X + \hat{W}_N^X|0\rangle$ as X_S (a quantity depending on the perturbation X). By inserting $|0\rangle\langle 0|$ into the previous equation one can recognize the CCSD energy $\langle 0|\bar{H}|0\rangle$.

$$\langle S|\bar{H}\frac{\partial \hat{T}}{\partial X} + \hat{W}_N\frac{\partial \hat{T}_3}{\partial X}|0\rangle - \langle S|\frac{\partial \hat{T}}{\partial X}|0\rangle\langle 0|\bar{H}|0\rangle = X_s \tag{5.20}$$

which rearranged gives the following equation

$$\langle S|(\bar{H} - E)\frac{\partial \hat{T}}{\partial X}|0\rangle + \langle S|\hat{W}_N\frac{\partial \hat{T}_3}{\partial X}|0\rangle = X_s \tag{5.21}$$

Let's now insert the identities $|S\rangle\langle S|$, $|D\rangle\langle D|$ and $|T\rangle\langle T|$ where appropriate.

$$\langle S|(\bar{H}-E)|S\rangle\langle S|\frac{\partial \hat{T}_1}{\partial X}|0\rangle+\langle S|(\bar{H}-E)|D\rangle\langle D|\frac{\partial \hat{T}_2}{\partial X}|0\rangle+\langle S|\hat{W}_N|T\rangle\langle T|\frac{\partial \hat{T}_3}{\partial X}|0\rangle = X_s \tag{5.22}$$

The terms $\langle S|(\bar{H} - E)|S\rangle$ can be written as $\langle S|(\bar{H}_{open})|S\rangle$ meaning that only the open diagrams will be kept since the diagrams corresponding to an energy are always closed. In the case of $\langle S|(\bar{H}-E)|D\rangle$ there are no such energy terms since they wouldn't correspond to topologically closed diagrams.

The same derivation can be done for the doubles and triples amplitude equations and the complete corresponding system of equations can be written in the following matrix form.

$$\begin{pmatrix} \langle S|\bar{H}_{open}|S\rangle & \langle S|\bar{H}|D\rangle & \langle S|\hat{W}_N|T\rangle \\ \langle D|\bar{H}|S\rangle & \langle D|\bar{H}_{open}|D\rangle & \langle D|\hat{W}_N|T\rangle \\ \langle T|\bar{H}|S\rangle & \langle T|\bar{H}+\hat{W}_N|D\rangle & \langle T|\hat{F}_N|T\rangle \end{pmatrix} \begin{pmatrix} \frac{\partial \hat{T}_1}{\partial X} \\ \frac{\partial \hat{T}_2}{\partial X} \\ \frac{\partial \hat{T}_3}{\partial X} \end{pmatrix} = \begin{pmatrix} X_S \\ X_D \\ X_T \end{pmatrix} \tag{5.23}$$

This problem is equivalent to the one found in Ref. 98 where the previous matrix system is seen as being $\mathbf{A}\frac{\partial \hat{T}}{\partial X} = X_{S,D,T}$.

To solve this eigenvalue problem, the iterative diagonalization approach of Hirao and Nakatsuji[99] (which is a straightforward generalization of the Davidson method[100], adapted for non-Hermitian matrices) was used. Thus, the most computationally demanding step is the multiplication of the $\mathbf{A}$ matrix and a trial vector; in the current context $\bar{H}\hat{\mathfrak{R}}$. The same procedure can be done to evaluate the $\hat{\mathfrak{L}}$ operator as well. All these approximate methods can be derived in the same manner starting from the amplitude equations. For the most expensive but therefore more reliable EOMIP-CCSDT-3, and also for all the other methods besides CCSDT-1a, the derivation is quite straightforward if one realizes that their amplitude equations can be written as

$$\begin{aligned} \langle S|\bar{H}+\hat{H}\hat{T}_3|0\rangle &= 0 \\ \langle D|\bar{H}+\bar{H}\hat{T}_3|0\rangle &= 0 \\ \langle T|\bar{H}+\hat{F}_N\hat{T}_3|0\rangle &= 0 \end{aligned} \tag{5.24}$$

and the resulting $\mathbf{A}$ matrix can therefore be seen as being

$$\mathbf{A} = \begin{pmatrix} \langle S|\bar{H}_{open}|S\rangle & \langle S|\bar{H}|D\rangle & \langle S|\hat{H}|T\rangle \\ \langle D|\bar{H} + \hat{H}\hat{T}_3|S\rangle & \langle D|\bar{H}_{open}|D\rangle & \langle D|\hat{H}|T\rangle \\ \langle T|\bar{H}|S\rangle & \langle T|\bar{H}|D\rangle & \langle T|\hat{F}_N|T\rangle \end{pmatrix} \tag{5.25}$$

where only the appropriate terms will be kept in the derivation of the corresponding methods. Note that the diagrammatic approach to deriving coupled cluster methods makes this process relatively straightforward and pain-less. For all the methods mentioned above, the contributions to the sub-block associated to the projection of triples onto the triples space come from $\hat{F}_N$ which is the denominator mentioned in Chapter 3 therefore they all scale as n^7 instead of n^8 for EOMIP-CCSDT and no triple excitation operators have to be stored on disk. These approximate methods are really attractive for the latter reasons. The algebraic form of the $\mathbf{A}\hat{\mathcal{R}}$ equations are given below for EOMIP-CCSDT-3 and CC3 since they are the only reliable methods out of the set described above, and their diagrammatic representations are shown in Figure 5.3 and 5.4.

CCSDT-3:

$$
\begin{aligned}
\mathbf{A}\hat{\mathfrak{R}} = &- \sum_{m} r_m \mathcal{F}_i^m - \frac{1}{2}\sum_{nem} r_{nm}^{e} \mathcal{W}_{ie}^{mn} + \sum_{me} r_{mi}^{e} \mathcal{F}_e^m + \frac{1}{4}\sum_{mnef} r_{mni}^{ef} \langle mn||ef\rangle \\
&- P(ij)\sum_{me} r_{im}^{e} \mathcal{W}_{je}^{ma} - P(ij)\sum_{m} r_{mj}^{a} \mathcal{F}_i^m + \sum_{e} r_{ij}^{e} \mathcal{F}_e^a - \sum_{m} r_m \mathcal{W}_{ji}^{ma} \\
&+ \frac{1}{2}\sum_{mn} r_{mn}^{a} \mathcal{W}_{ji}^{nm} - \frac{1}{2}\sum_{mnef} r_{nm}^{e} t_{ij}^{af} \langle mn||fe\rangle + \sum_{me} r_{mij}^{ea} \mathcal{F}_e^m \\
&- \frac{1}{2}P(ij)\sum_{mne} r_{min}^{ea} \mathcal{W}_{ej}^{mn} - \frac{1}{2}\sum_{mnef} r_n t_{imj}^{aef} \langle mn||ef\rangle + \frac{1}{2}\sum_{mef} r_{mij}^{ef} \mathcal{W}_{ef}^{ma} \\
&+ P(jk/i)\sum_{mn} r_m t_{ni}^{ba} \mathcal{W}_{kj}^{mn} - P(ij/k)P(ab)\sum_{em} r_m t_{ji}^{ea} \mathcal{W}_{ke}^{mb} \\
&- P(ij/k)P(ab)\sum_{m} r_{mk}^{b} \mathcal{W}_{ji}^{ma} + P(jk/i)\sum_{e} r_{jk}^{e} \mathcal{W}_{ei}^{ba} \\
&+ P(ij/k)P(ab)\sum_{mef} r_{mk}^{e} t_{ji}^{fa} \mathcal{W}_{ef}^{mb} - P(jk/i)P(jk)\sum_{mne} r_{mk}^{e} t_{ni}^{ba} \mathcal{W}_{ej}^{mn} \\
&+ \frac{1}{2}P(ik/j)P(ab)\sum_{mne} r_{nm}^{b} t_{ki}^{ea} \mathcal{W}_{je}^{nm} - P(jk/i)\sum_{m} r_{mjk}^{ab} \mathcal{F}_i^m \\
&+ P(ab)\sum_{e} r_{ijk}^{eb} \mathcal{F}_e^a
\end{aligned}
\tag{5.26}
$$

CC3:

$$
\begin{aligned}
\mathbf{A}\hat{\Re} = &- \sum_{m} r_m \mathcal{F}_i^m - \frac{1}{2}\sum_{nem} r_{nm}^{e} \mathcal{W}_{ie}^{mn} + \sum_{me} r_{mi}^{e} \mathcal{F}_e^m + \frac{1}{4}\sum_{mnef} r_{mni}^{ef} \langle mn||ef\rangle \\
&- P(ij)\sum_{me} r_{im}^{e} \mathcal{W}_{je}^{ma} - P(ij)\sum_{m} r_{mj}^{a} \mathcal{F}_i^m + \sum_{e} r_{ij}^{e} \mathcal{F}_e^a - \sum_{m} r_m \mathcal{W}_{ji}^{ma} \\
&+ \frac{1}{2}\sum_{mn} r_{mn}^{a} \mathcal{W}_{ji}^{nm} - \frac{1}{2}\sum_{mnef} r_{nm}^{e} t_{ij}^{af} \langle mn||fe\rangle + \sum_{me} r_{mij}^{ea} \mathcal{F}_e^m \\
&- \frac{1}{2}P(ij)\sum_{mne} r_{min}^{ea} \mathcal{W}_{ej}^{mn} - \frac{1}{2}\sum_{mnef} r_n t_{imj}^{aef} \langle mn||ef\rangle + \frac{1}{2}\sum_{mef} r_{mij}^{ef} \mathcal{W}_{ef}^{ma} \\
&+ P(jk/i)\sum_{mn} r_m t_{ni}^{ba} \mathcal{W}_{kj}^{mn} - P(ij/k)P(ab)\sum_{em} r_m t_{ji}^{ea} \mathcal{W}_{ke}^{mb} \\
&- P(ij/k)P(ab)\sum_{m} r_{mk}^{b} \mathcal{W}_{ji}^{ma} + P(jk/i)\sum_{e} r_{jk}^{e} \mathcal{W}_{ei}^{ba} \\
&- P(jk/i)\sum_{m} r_{mjk}^{ab} \mathcal{F}_i^m + P(ab)\sum_{e} r_{ijk}^{eb} \mathcal{F}_e^a
\end{aligned}
\tag{5.27}
$$

In these equations the intermediates ($\mathcal{F}$, $\mathcal{W}$) and integrals ($\langle..||..\rangle$) are identical to those given in Ref. 10 and Ref. 101; note that they include more terms than the intermediates given in chapter 2 since we now throw in the triple excitation operator. The antisymmetric permutation operator P(pq) is defined *via* $P(pq)Z(pq) = Z(pq) - Z(qp)$ as stated earlier and the cyclic permutation operator $P(pq/r)$ is defined *via* $P(pq/r)Z(pqr) = Z(pqr) + Z(qrp) + Z(rpq)$.

Table 5.1: Coupled cluster amplitude equations for CC3 and truncated CCSDT-X methods.

CC methods	amplitude equations
Singles equations	
CCSDT-3	$\langle \Psi_i^a \vert \bar{H} + \hat{W}_N \hat{T}_3 \vert \Psi_0 \rangle = 0$
CC3	$\langle \Psi_i^a \vert \bar{H} + \hat{W}_N \hat{T}_3 \vert \Psi_0 \rangle = 0$
CCSDT-2	$\langle \Psi_i^a \vert \bar{H} + \hat{W}_N \hat{T}_3 \vert \Psi_0 \rangle = 0$
CCSDT-1b	$\langle \Psi_i^a \vert \bar{H} + \hat{W}_N \hat{T}_3 \vert \Psi_0 \rangle = 0$
CCSDT-1a	$\langle \Psi_i^a \vert \bar{H} + \hat{W}_N \hat{T}_3 \vert \Psi_0 \rangle = 0$
Doubles equations	
CCSDT-3	$\langle \Psi_{ij}^{ab} \vert \bar{H} + \hat{W}_N \hat{T}_3 + \hat{W}_N \hat{T}_1 \hat{T}_3 \vert \Psi_0 \rangle = 0$
CC3	$\langle \Psi_{ij}^{ab} \vert \bar{H} + \hat{W}_N \hat{T}_3 + \hat{W}_N \hat{T}_1 \hat{T}_3 \vert \Psi_0 \rangle = 0$
CCSDT-2	$\langle \Psi_{ij}^{ab} \vert \bar{H} + \hat{W}_N \hat{T}_3 + \hat{W}_N \hat{T}_1 \hat{T}_3 \vert \Psi_0 \rangle = 0$
CCSDT-1b	$\langle \Psi_{ij}^{ab} \vert \bar{H} + \hat{W}_N \hat{T}_3 + \hat{W}_N \hat{T}_1 \hat{T}_3 \vert \Psi_0 \rangle = 0$
CCSDT-1a	$\langle \Psi_{ij}^{ab} \vert \bar{H} + \hat{W}_N \hat{T}_3 \vert \Psi_0 \rangle = 0$
Triples equations	
CCSDT-3	$\langle \Psi_{ijk}^{abc} \vert \bar{H} + \hat{F}_N \hat{T}_3 + \hat{W}_N \hat{T}_2 + \frac{1}{2} \hat{W}_N \hat{T}_2^2 + W_N \hat{T}_1 \hat{T}_2 + \frac{1}{2} \hat{W}_N \hat{T}_1^2 \hat{T}_2 + \frac{1}{2} \hat{W}_N \hat{T}_1 \hat{T}_2^2 + \frac{1}{6} \hat{W}_N \hat{T}_1^3 \hat{T}_2 \vert \Psi_0 \rangle = 0$
CC3	$\langle \Psi_{ijk}^{abc} \vert \bar{H} + \hat{F}_N \hat{T}_3 + \hat{W}_N \hat{T}_2 + \hat{W}_N \hat{T}_1 \hat{T}_2 + \frac{1}{2} \hat{W}_N \hat{T}_1^2 \hat{T}_2 + \frac{1}{6} \hat{W}_N \hat{T}_1^3 \hat{T}_2 \vert \Psi_0 \rangle = 0$
CCSDT-2	$\langle \Psi_{ijk}^{abc} \vert \bar{H} + \hat{F}_N \hat{T}_3 + \hat{W}_N \hat{T}_2 + \frac{1}{2} \hat{W}_N \hat{T}_2^2 \vert \Psi_0 \rangle = 0$
CCSDT-1b	$\langle \Psi_{ijk}^{abc} \vert \bar{H} + \hat{F}_N \hat{T}_3 + \hat{W}_N \hat{T}_2 \vert \Psi_0 \rangle = 0$
CCSDT-1a	$\langle \Psi_{ijk}^{abc} \vert \bar{H} + \hat{F}_N \hat{T}_3 + \hat{W}_N \hat{T}_2 \vert \Psi_0 \rangle = 0$

$\bar{H}$ is the similarity transformed Hamiltonian $e^{-\hat{T}} \hat{H} e^{\hat{T}}$ where $\hat{T} = \hat{T}_1 + \hat{T}_2$. $\hat{W}_N$ and $\hat{F}_N$ are the one- and two-electron part of the normal-ordered Hamiltonian, respectively.

Figure 5.3: Diagrammatic representation of $\bar{H}\hat{\mathcal{R}}$ for the EOMIP-CCSDT-3 and EOMIP-CC3 methods projected onto the singles and doubles space in the antisymmetrized Brandow formalism.

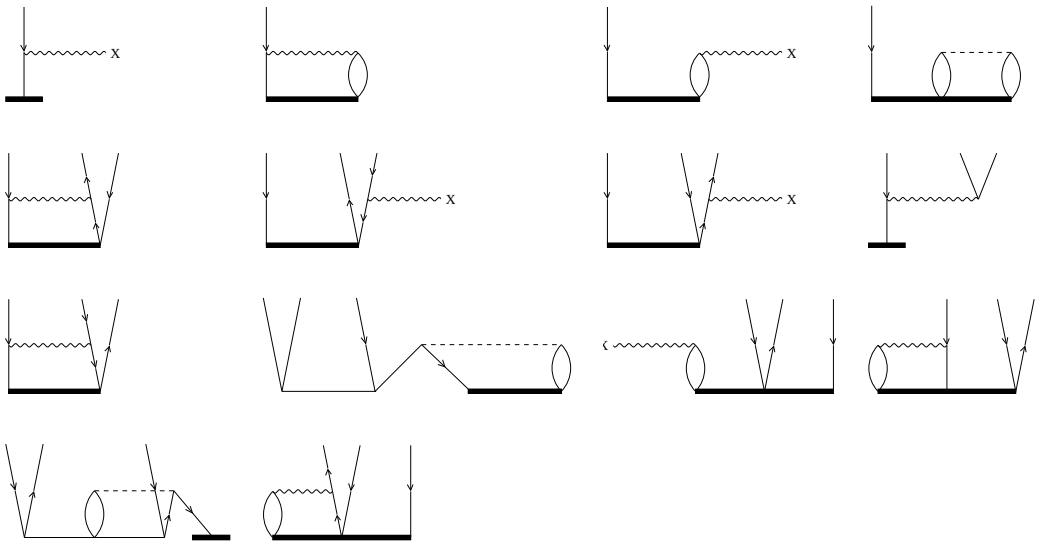

The squiggly lines and the dashed lines represent intermediates and integrals (defined in chapter 2 and Ref. 101), respectively, while the thick and thin amplitude vertices correspond to the $\hat{\mathcal{R}}$ and $\hat{T}$ operators.

Figure 5.4: Diagrammatic representation of $\bar{H}\hat{\mathcal{R}}$ for the EOMIP-CCSDT-3 and EOMIP-CC3 methods projected onto the triples space in the antisymmetrized Brandow formalism. The last three contributions are not included in EOMIP-CC3.

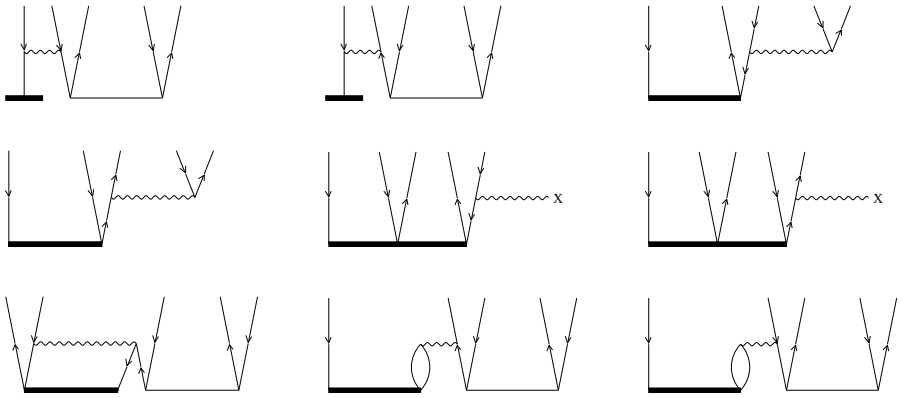

The squiggly lines and the dashed lines represent intermediates and integrals (defined in chapter 2 and Ref. 101), respectively, while the thick and thin amplitude vertices correspond to the $\hat{\mathcal{R}}$ and $\hat{T}$ operators.

5.4 Benchmark and Application to Diatomic Radicals

The harmonic force constants and equilibrium bond lengths were calculated numerically for the BO, CN, N_2^+ and CO^+ molecules using a variety of approaches. In addition to the EOMIP-CC3 and EOMIP-CCSDT-3 methods that are the primary focus of this chapter, we included EOMIP-CCSDT[44,102,103] and EOMIP-CCSDTQ[68], the single-reference CCSD(T)[19,20] and CCSDT methods and, finally, multireference configuration interaction (MRCI) and the related multireference averaged quadratic coupled cluster (MR-AQCC) method. All EOM-based calculations were performed with an excitation energy code, in conjunction with the continuum orbital trick proposed by Stanton *et al.* in Ref. 105. The single-reference calculations used unrestricted Hartree-Fock orbitals (UHF) for all states except the deep Σ^+ states of BO and CN which are not accessible due to variational collapse. For them, the quasi-restricted HF (QRHF) orbitals[96] were used. Active spaces for the MRCI and MRAQCC calculations were full valence active space (CAS) except in the case of the deep $B^2\Sigma$ state of BO where the valence CAS space was augmented by two pairs of π orbitals. In addition, full configuration interaction (FCI) calculations were done for some of the more difficult states. All calculations except EOMIP-CCSDTQ, FCI[68], MRCI and MRAQCC[106,107] were done with a local version of ACES II[67] . Calculations with the two MR-based methods were performed with the Columbus package[108,109], and the string-based many-body code of Kállay[68,103,110] was used for EOMIP-CCSDTQ and FCI. All calculations were performed with the cc-pVDZ basis set[45] and the core

electrons were not correlated. Results of our calculations are given in Tables 5.2-5.5.

From Tables 5.2-5.5 it can be seen that EOMIP-CCSDTQ is very close to FCI and that the former can here be taken as a reference for comparison with the approximate triples methods. For the two lowest states of each molecule, EOMIP-CCSDT-3 and EOMIP-CC3 seem to be performing well and the geometries and vibrational frequencies are in most cases comparable to the ones obtained with EOMIP-CCSDTQ. The biggest discrepancies for these low-lying states were found for the $^2\Pi_u^+$ state of N_2^+ and were around 60 cm^{-1} and 139 cm^{-1} for EOMIP-CCSDT-3 and EOMIP-CC3, respectively. It appears that EOMIP-CC3 introduces more error in the determination of the bond lengths (r) and the vibrational frequencies (ω) than EOMIP-CCSDT-3. Both methods perform better than UHF-CCSD(T) which tends to underestimate the triples effect. It is nevertheless more difficult to consider that EOMIP-CC3 is as consistent as UHF-CCSDT-3. In fact, the latter is always closer to CCSDT. The most challenging cases for any of these methods are the deep $^2\Sigma$ states, apart for N_2^+, EOM-CCSDT-3 and EOM-CC3 predict the bond lengths and frequencies as well or better than QRHF-CCSDT and definitely better than QRHF-CCSD(T). Although, among these examples there is one case where EOM-CC3 shows its limitations and its tendency to overestimate the triples effect. For the deep $^2\Sigma$ state of BO the EOM-CC3 frequency is 200 cm^{-1} too low and the corresponding bond length is 0.02 $\mathring{A}$ too long while EOM-CCSDT-3 is within 20 cm^{-1} and 0.002 $\mathring{A}$ and closer to EOM-CCSDTQ

than any other methods.

The two MR-based methods mentioned in this chapter appear to be extremely reliable in most cases except, again, for the deep $^2\Sigma$ state of BO where a larger reference space had to be used. This was motivated by inspection of the MR-AQCC wavefunction where large coefficients of the configuration describing excitations to these orbitals could be seen. Also, the larger than usual difference for the MRCI and MR-AQCC results indicated that the wavefunction with a valence CAS reference space was not converged. EOM methods are even better than the MR methods for higher level of theory (EOM-CCSDTQ), in our view the EOM approach can provide the same or better treatment for radicals than MR based methods. In this study, however, we were interested in approximate triples methods, because of their low computational cost. As described earlier, the EOM-CCSDT-3 method appears to be in most cases more reliable than EOM-CC3 and compares pretty well to MR methods. The deep $^2\Sigma$ state of BO is a clear example of the great performance and advantage of EOM-CCSDT-3 over MR approaches, the EOM calculations were performed in the same manner for all the examples including the latter whereas the reference space had to be modified for the MR methods which makes them more complicated and less predictable methods.

In most cases, EOMIP-CC3 and EOMIP-CCSDT-3 methods seem to behave better than UHF and QRHF based methods, but they also provide a decent alternative to MR-based methods considering they only scale as $n_{occ}^4 * n_{vir}^3$ and that they can be used in a more systematic way. The advantage of these

methods becomes obvious when considering polyatomic radicals. Even though they have limitations, they are well suited for large radicals when more accuracy is needed. It is clear that analytical first and second derivatives would be a great improvement and would help getting more insight on electronic spectra and chemical properties of radicals.

Table 5.2: Equilibrium geometries and vibrational frequencies of the three lowest states of N_2^+ calculated at the CCSD(T), CCSDT, EOM-CC3, EOM-CCSDT-3, EOM-CCSDT, EOM-CCSDTQ, MR-CISD, MR-AQCC and FCI levels with the cc-pVDZ basis set. The core electrons were not correlated. Internuclear distances are given in Ångströms and vibrational frequencies in cm^{-1}

		UHF		EOM(LR)						
State		CCSD(T)	CCSDT	CC3	CCSDT-3	CCSDT	CCSDTQ	MR-CISD[a]	MR-AQCC[a]	FCI
$\tilde{X}^2\Sigma_u^+$	r	1.1371	1.1366	1.1378	1.1355	1.1349	1.1384	1.1390	1.1395	1.139
	ω	2184	2188	2165	2196	2213	2174	2164	2158	2163
$\tilde{A}^2\Pi_u^+$	r	1.1932	1.1931	1.2058	1.1984	1.1913	1.1940	1.1956	1.1964	1.196
	ω	1899	1904	1755	1834	1919	1894	1873	1868	1872
$\tilde{B}^2\Sigma_g^+$	r	1.0948	1.0956	1.0939	1.0915	1.0957	1.1006	1.1011	1.1018	1.101
	ω	2410	2386	2434	2479	2412	2340	2321	2311	2316

[a] Full valence Complete Active Space (CAS) reference space was used along with corresponding MCSCF orbitals

Table 5.3: Equilibrium geometries and vibrational frequencies of the three lowest states of CO^+ calculated at the CCSD(T), CCSDT, EOM-CC3, EOM-CCSDT-3, EOM-CCSDT, EOM-CCSDTQ, MR-CISD, MR-AQCC and FCI levels with the cc-pVDZ basis set. The core electrons were not correlated. Internuclear distances are given in Ångströms and vibrational frequencies in cm^{-1}

		UHF		EOM(LR)					
State		CCSD(T)	CCSDT	CC3	CCSDT-3	CCSDT	CCSDTQ	MR-CISD[b]	MR-AQCC[b]
$\tilde{X}^2\Sigma$	r	1.1277	1.1323	1.1373	1.1334	1.1319	1.1328	1.1331	1.1337
	ω	2260	2175	2106	2150	2176	2167	2167	2161
$\tilde{A}^2\Pi$	r	1.2602	1.2613	1.2590	1.2575	1.2589	1.2618	1.2618	1.2626
	ω	1545	1533	1546	1558	1550	1535	1529	1526
$\tilde{B}^2\Sigma$	r	1.1767[a]	1.1841[a]	1.1899	1.1840	1.1883	1.1952	1.1956	1.1964
	ω	1846[a]	1757[a]	1666	1751	1731	1649	1619	1616

[a]Single-reference CCSD(T) and CCSDT calculations based on QRHF orbitals.
[b]Full valence Complete Active Space (CAS) reference space was used along with corresponding MCSCF orbitals

Table 5.4: Equilibrium geometries and vibrational frequencies of the three lowest states of CN calculated at the CCSD(T), CCSDT, EOM-CC3, EOM-CCSDT-3, EOM-CCSDT, EOM-CCSDTQ, MR-CISD, MR-AQCC and FCI levels with the cc-pVDZ basis set. The core electrons were not correlated. Internuclear distances are given in Ångströms and vibrational frequencies in cm^{-1}

		UHF		EOM(LR)					
State		CCSD(T)	CCSDT	CC3	CCSDT-3	CCSDT	CCSDTQ	MR-CISD[b]	MR-AQCC[b]
$\tilde{X}^2\Sigma$	r	1.1904	1.1941	1.1969	1.1946	1.1943	1.1963	1.1968	1.1975
	ω	2090	2053	2016	2037	2048	2027	2021	2017
$\tilde{A}^2\Pi$	r	1.2536	1.2549	1.2591	1.2552	1.2520	1.2553	1.2561	1.2567
	ω	1821	1786	1747	1781	1813	1785	1778	1774
$\tilde{B}^2\Sigma$	r	1.1715[a]	1.1729[a]	1.1738	1.1713	1.1749	1.1790	1.1794	1.1803
	ω	2161[a]	2141[a]	2139	2174	2132	2080	2064	2059

[a]Single-reference CCSD(T) and CCSDT calculations based on QRHF orbitals.
[b]Full valence Complete Active Space (CAS) reference space was used along with corresponding MCSCF orbitals

Table 5.5: Equilibrium geometries and vibrational frequencies of the three lowest states of BO, calculated at the CCSD(T), CCSDT, EOM-CC3, EOM-CCSDT-3, EOM-CCSDT, EOM-CCSDTQ, MR-CISD, MR-AQCC and FCI levels with the cc-pVDZ basis set. The core electrons were not correlated. Internuclear distances are given in Ångströms and vibrational frequencies in cm^{-1}

		UHF		EOM(LR)						
State		CCSD(T)	CCSDT	CC3	CCSDT-3	CCSDT	CCSDTQ	MR-CISD[b]	MR-AQCC[b]	FCI
$\tilde{X}^2\Sigma$	r	1.2196	1.2211	1.2261	1.2224	1.2208	1.2217	1.2221	1.2229	
	ω	1852	1833	1787	1817	1834	1820	1832	1825	
$\tilde{A}^2\Pi$	r	1.3758	1.3761	1.3784	1.3767	1.3780	1.3777	1.3758	1.3780	
	ω	1215	1211	1181	1194	1199	1201	1211	1203	
$\tilde{B}^2\Sigma$	r	1.3180[a]	1.3292[a]	1.3592	1.3388	1.3345	1.3408	1.3393[c]	1.3404[c]	1.340
	ω	1348[a]	1272[a]	1047	1187	1241	1216	1205[c]	1203[c]	1213

[a]Single-reference CCSD(T) and CCSDT calculations based on QRHF orbitals.
[b]Except noted, full valence Complete Active Space (CAS) reference space was used along with corresponding MCSCF orbitals
[c]The full valence CAS reference space has been augmented by two pairs of π orbitals. See text.

5.5 Conclusion

The applications shown in the previous section had the following goals: a comparison of the performance and applicability of approximate EOMIP-CCSDT-3 and EOMIP-CC3 methods with traditional coupled cluster methods and multireference techniques and an assessment of the quality of the triples excitation approximation.

When the reference function is well-behaved, the traditional coupled cluster method, CCSD(T), works well and seems to be the best compromise between cost and accuracy. Indeed, CCSD(T) is well known to provide an accurate treatment of triple excitations. Although, when there is significant mixing between zeroth-order Slater determinants the traditional CCSDT and CCSD(T) methods seem highly challenged. On the other hand the equation-of-motion based methods often use a closed-shell reference function thus avoiding the problems associated with studying radicals, or generally speaking, molecules plagued with spin contamination, (pseudo) Jahn-Teller effects, and symmetry breaking problems. They treat nondynamic electron correlation effects fairly well[111,112] by obtaining strongly interacting Slater determinants by removal of one electron from, in most cases, a closed-shell determinant. There are of course drawbacks to using EOMIP; the treatment of dynamic correlation is not as accurate as it is with traditional coupled cluster methods.

Methods such as FCI and MRCI can treat both nondynamic and dynamic correlation at once; but they are usually significantly expensive and more complicated to use. This is why the EOMIP-based methods seem more amenable to

"black-boxing" than any of the methods originally designed to treat open-shell systems with problematic behaviors. Like its conceptually similar counterparts, EOMEE and EOMEA, the EOMIP approach offers a good alternative to multirefrence methods and costly FCI.

Chapter 6

Using Vibronic Coupling Together with Equation-of-Motion Coupled Cluster Theory to Simulate Absorption Spectra

In theoretical spectroscopy it is a common practice to assume that the vibrational wavefunction has its maximum amplitude in the region of the classical turning points[113]. Therefore, in most cases the vertical excitation energy is assumed to be equal to the energy corresponding to the maximum of absorption. However, in some well-known cases such as the $^1B_{2u}$ state of ethylene there exists a significant difference between the best known vertical excitation energy and the maximum of the absorption profile[114]. Given that some electronic structure methods, among them, equation-of-motion coupled cluster theory[36] are now recognized to provide accuracies within 0.5 eV, it seems that the former assumptions are not sufficiently rigorous, and that one should consider that comparing the vertical excitation energy and the maximum of the absorption spectrum may not be a viable approach.

The presence of excited states close in energy to the excited state of interest can produce vibronically induced interactions that can modify the position of the maximum in the absorption profile. Some of these interactions are now recognized to arise from vibronic coupling between two or more

excited states through an unsymmetrical vibrational mode. The model developed by Cederbaum and co-workers[115] to treat vibronic coupling used with equation-of-motion coupled cluster theory seems to provide an accurate yet simple treatment of these interactions[116].

We will present the basics of the vibronic coupling model and provide a study of the controversial case of the $^1B_2 \leftarrow {}^1A_1$ transition in cyclopentadiene (CP) whose vertical excitation energy is still a source of conflict in the quantum chemistry community.

6.1 Basics of the Vibronic Coupling Model

One should keep in mind that this section is not an exhaustive discussion about vibronic coupling theory but rather a short introduction to the important elements that constitute the vibronic coupling model.

In cases where excited states are close in energy and in the vicinity of avoided crossings (conical intersections) the Born–Oppenheimer approximation (adiabatic basis) no longer holds and interactions between excited states have to be taken into account. For two interacting excited states and one coupling mode the full Hamiltonian can be written as follows

$$\hat{\mathbf{H}} = \begin{pmatrix} T_{11} & 0 \\ 0 & T_{22} \end{pmatrix} + \begin{pmatrix} V_{11} & V_{12} \\ V_{12} & V_{22} \end{pmatrix} \tag{6.1}$$

where the non-diagonal terms are now included in the electronic Hamiltonian;

T_{11} and T_{22} being the usual kinetic operators for nuclei. From now on, we will only consider the potential

$$\hat{\mathbf{V}} = \begin{pmatrix} V_{11} & V_{12} \\ V_{12} & V_{22} \end{pmatrix} \tag{6.2}$$

Within the vibronic coupling framework the elements of $\hat{V}$ assume the following forms

$$\begin{aligned} V_{11} &= E_1 + \frac{1}{2}\sum_{i\in s}\omega_i q_i^2 + \sum_{i\in s} K_i^{(1)} q_i + \sum_{i,j\in s} K_{ij}^{(1)} q_i q_j \\ V_{11} &= E_2 + \frac{1}{2}\sum_{i\in s}\omega_i q_i^2 + \sum_{i\in s} K_i^{(2)} q_i + \sum_{i,j\in s} K_{ij}^{(2)} q_i q_j \\ V_{22} &= \lambda q_u \end{aligned} \tag{6.3}$$

where E_1 and E_2 are the (vertical) electronic energies of the two excited states with respect to the ground state energy; q_i and q_u are the reduced normal coordinates corresponding to the symmetrical and unsymmetrical vibrational modes, respectively. The harmonic vibrational frequencies at the ground state in the diabatic basis are defined as ω_s; the gradients and hessian elements of the final states in the normal coordinate representation of the ground state are K_i and K_{ij}, respectively. The linear interstate vibronic coupling constant is λ. Eigenvalues corresponding to the upper and lower states (the adiabatic

energies) are the following

$$\begin{aligned} E^{+} &\cong V_{11} + \frac{\lambda^2 q_u^2}{E_1 - E_2} + (\theta(q_u^3)) \\ E^{-} &\cong V_{22} - \frac{\lambda^2 q_u^2}{E_1 - E_2} + (\theta(q_u^3)) \end{aligned} \tag{6.4}$$

which implies that the harmonic force constants of the unsymmetrical mode on the upper and lower surface in the adiabatic basis are

$$\begin{aligned} f^{+} &= \frac{2\lambda^2}{\Delta} + \omega_{u_{ref}} \\ f^{-} &= -\frac{2\lambda^2}{\Delta} + \omega_{u_{ref}} \end{aligned} \tag{6.5}$$

where $\Delta = E_2 - E_1$ is the so-called vertical gap between the two excited states and $\omega_{u_{ref}}$ is the harmonic vibrational frequency of the unsymmetrical mode at the ground state geometry on the surface of reference in the diabatic basis; it should be noted that f^{+} and f^{-} are also equal to $\frac{\omega_{u_+}\omega_{u_+}}{\omega_{u_{ref}}}$ and $\frac{\omega_{u_-}\omega_{u_-}}{\omega_{u_{ref}}}$. The contributions ω_{u_+} and ω_{u_-} are the harmonic vibrational frequencies of the unsymmetrical mode on the upper and lower excited state surfaces in the diabatic basis, respectively. Therefore the coupling constant can be seem to be

$$\lambda \cong \pm\frac{1}{2}\sqrt{\Delta(f^{+} - f^{-})} = \frac{1}{2}\sqrt{\Delta(\frac{\omega_{u_+}\omega_{u_+}}{\omega_{u_{ref}}}) - \Delta(\frac{\omega_{u_-}\omega_{u_-}}{\omega_{u_{ref}}})} \tag{6.6}$$

One should note that coupling only occurs if the excited states and the vibrational mode involved in the transition satisfy the following condition

$$\Gamma_1 \times \Gamma_u \times \Gamma_2 \subset \Gamma_s \tag{6.7}$$

where Γ_1 and Γ_2 are the irreducible representations of the two excited states, Γ_u is the irreducible representation of the vibrational coupling mode and Γ_s is defined as the totally symmetric irreducible representation.

All of these parameters can be evaluated using traditional and equation-of-motion coupled cluster methods. The combination of these methods constitute a powerful simulation package to study electronic spectra.

6.2 Application to Cyclopentadiene

6.2.1 "Brute Force" Coupled Cluster Approach

The vertical excitation energy corresponding to the $(^1B_2 \leftarrow^1 A_1)\ \pi \rightarrow \pi^*$ transition in cyclopentadiene has been refined several times during the last two decades. These studies always assumed that the vertical excitation energy should be compared to the maximum in the absorption profile which from the most recent gas phase experiments[117,118,119,120] is around 5.30±0.02 eV. Quantum chemical calculations by the Lund group using the CASPT2 method[121,122] and a relatively modest basis set augmented with molecule-centered Rydberg functions found a vertical separation of 5.27 eV[123]. In another study, MRPT2 and the ostensibly more accurate (and similar to CASPT2) quasidegenerate MCQD approaches in conjunction with a slightly larger basis set give 5.19 and 5.26 eV, respectively[124]. The first and third of these values compare quite favorably with the "experimental" value and have therefore been assumed to

attest of the accuracy of the corresponding theoretical methods. Calculations with a basis set similar to that of Ref. 123 using EOM-CC were reported, and gave a vertical separation of 5.65 eV at the CCSD level[125]. However, addition of a noniterative correction for triple excitations known as EOM-CCSD($\tilde{\mathrm{T}}$)[126] lowered this value significantly; the resulting separation of 5.30 eV is indeed close to both "experiment" and the CASPT2 result. Subsequently, the closely-related SAC-CI method[127,128] of Nakatsuji was applied to this problem using a relatively large basis set (180 functions) and gives a value of 5.54 eV[129], 0.21 eV below a result obtained years earlier with the same method in a smaller basis set[130]. Hence, it seems that basis set augmentation acts to lower the excitation energy of cyclopentadiene and that methods based on coupled cluster response theory provide predictions which are roughly 0.4 eV higher than CASPT2.

In this study the vertical excitation corresponding to the $\pi \rightarrow \pi^*$ electronic transition was calculated at the ground state geometry optimized at the CCSD(T)[19,20] level of theory with a cc-pVQZ basis set[45] (See Table 6.1) while the geometry of the ground and excited states used in section 6.2.2 were evaluated at the CCSD[14] and EOM-CCSD[42,31] level using the TZ2P set[131] (See Tables 6.2 and 6.4). We used the cc-pVXZ (X=D,T,Q) and aug-cc-pVXZ series (X=D,T,Q)[45,132]; the latter includes diffuse functions required to describe Rydberg character in excited states. In the calculations with diffuse functions, the aug-cc-pVXZ set was used on the carbon atoms only. The hydrogen atoms were described with the corresponding cc-pVXZ basis; the composite basis

is denoted here as aug-cc-pVXZ'. We also calculated the vertical transition energy with various coupled cluster methods including EOM-CCSD, EOM-CCSDT-3 and EOM-CCSDT. The results are given in Table 6.3; it should be noted that some of these calculations represent a real challenge in the sense that they are done with a large number of basis functions at a somewhat expensive level of theory (580 basis functions for the aug-cc-pVXZ' basis with the CCSD method). The core electrons were correlated in most cases except for the ones performed with the augmented basis sets and with the computationally expensive CCSDT method. However, the effect of not correlating the core electrons was found to be negligible (less than 0.01 eV)[133]. All of these calculations were performed with the quantum chemistry package ACES II[67]. By inspecting Table 6.3, it is obvious that something is missing from our analysis and that the vertical excitations obtained are not really comparable with the experimental maximum of absorption which, in our view, doesn't necessarily mean that the vertical excitation energies are not calculated accurately. These calculations are the most computationally demanding that have ever been done for this particular transition. Using the results of table 6.3, the vertical excitation energy can be further refined by compensating for the basis sets incompleteness by using the formula advocated by Helgaker *et al.* for correlation energies, *viz.*

$$E_X = E_\infty - \frac{a}{X^3}$$

where X is the cc-pVXZ (D=2, T=3, *etc.*) energy and E_∞ is the corresponding estimate in the complete basis[76]. Using the cc-pVXZ series (X=T and Q), one

obtains a result of 5.69 eV for the valence-only basis set limit[133], which then needs to be augmented with an estimate for diffuse functions. A plausible estimate is −0.03 eV, which gives a total EOM-CCSD basis set limit estimate of 5.66 eV. Similarly, the aug-cc-pVTZ' and aug-cc-pVQZ' results can be extrapolated, which gives a value of 5.67 eV. Hence, it seems that the EOM-CCSD basis set limit is indeed very close to 5.66 eV. Given the consistency of data in the table, the triple excitation contribution at the basis set limit is probably around −0.11 eV, so that a "best estimate" value of the vertical energy gap between the ground and $^1B_2$ states of CP at the geometry given in Table 6.1 is 5.55±0.05 eV (see Figure 6.1 for a graphical comparison to other theoretical estimates) at the EOM-CCSDT level with an exhaustive basis set. This is still 0.20 to 0.25 eV above the absorption maximum, which is a very disappointing result if one assumes that the transition is one for which the vertical excitation energy can be equated with the absorption maximum.

6.2.2 Simulations Based on Vibronic Coupling Theory

In order to address the concerns mentioned in the previous section, the vibronic coupling model was used to simulate the $^1B_2 \leftarrow ^1A_1$ absorption spectrum of cyclopentadiene. It was recognized that there is a significant coupling between the $^1B_2$ state and a higher-lying $^1A_2$ state in cyclopentadiene that forces the $^1B_2$ state to be nonplanar[135]. The parameters used in the simulations were obtained from quantum-chemical calculations using the same electronic structure package as in Section 6.2.1. The derivatives required in

the simulation were calculated analytically[136], with the exception of second derivatives of the excited state, which were determined by finite difference of analytic first derivatives[42]; all of these were done with the TZ2P basis set at the CCSD and EOM-CCSD level of theory. Two types of simulations were carried out: one with intrastate quadratic coupling (equivalent to a Franck-Condon simulation with full treatment of Duschinsky mixing) and another one adding interstate linear vibronic coupling mentioned in Section 6.1 and developed by Cederbaum *et al.*[115]. For both simulations, it was found that only six vibrational modes exhibited significant Franck-Condon activity which still translated into 63 thousand and 50 million basis functions, respectively, using 2500 Lanczos recursions (each Lanczos iteration was completed in less than 80 seconds when 50 million basis functions were used). The results of the simulations are given in Figures 6.2-6.3 and in Figure 6.4 where the simulated absorption spectrum from Figure 6.2 is compared to the experimental absorption profile of Ref. 119. The two simulations differ not only in the density of states but also in the position of the maximum of absorption. In the simulation where vibronic coupling (this simulation is supposed to reproduce more accurately the physical phenomena involved in this transition) is included, the maximum is found to lie 0.13 eV below the vertical excitation energy used in the model Hamiltonian (5.55 ev). This estimate is based on the following. The simulations are faithful to the experiment in the sense that they give two closely spaced features with comparable intensities in the vicinity of the maximum in the absorption profile (See Figure 6.3). The profile of this simulated

absorption spectrum does match the experimental profile in a striking manner. Experimentally, the center of the two peaks is located at 5.30 eV, and the distance from the vertical excitation energy used in the simulation and the corresponding feature is 0.13 eV, with the latter at lower energy. However, even though the simulations seem almost perfect there is a crucial approximation that was overlooked in the process. The simulations were done assuming that the ground and first excited states zero-point energies were comparable in energy (at least for the vibrational modes not accounted for in the simulation). By inspecting the ground and excited state of cyclopentadiene more carefully it can be found that their zero-point energies differ by more than 2 kcal mol^{-1} (0.09ev). These zero-point energies for the ground and excited states are 58.78 kcal mol^{-1} and 56.44 kcal mol^{-1}, respectively. They were calculated in a consistent manner, at an optimized geometry obtained with the TZ2P basis set at the CCSD (Table 6.2) and EOM-CCSD (Table 6.4) level of theory. Thus, it is plausible to think that the absorption spectrum simulated in this section should be shifted by an amount – equal or similar – to the difference between the zero-point energies mentioned which would subsequently lower the maximum of absorption to being around 5.32 eV (The maximum absorption was estimated earlier to be found at 5.42 eV which including the previous correction of 2.34 kcal mol^{-1} should now be located at around 5.32 eV). This is only 0.02 eV higher than the position of the maximum in the experimental spectrum but within the error bars assigned to the transition. Hence, it seems likely that the true vertical excitation energy of CP is above

the absorption maximum at 5.30±0.02 eV by such an amount. This energy separation is therefore estimated to be 5.53±0.05 eV, where the assigned error bars are conservative.

Table 6.1: Geometry of cyclopentadiene (C_{2v}) optimized at the CCSD(T) level of theory with a cc-pVQZ basis set. The molecule is in the principal axis system, and the atomic Cartesian coordinates are given in bohr.

Atom	x	y	z
C	0.00000000	0.00000000	2.32960111
C	0.00000000	2.21904113	0.56764638
C	0.00000000	−2.21904113	0.56764638
C	0.00000000	−1.38511451	−1.83599457
C	0.00000000	1.38511451	−1.83599457
H	−1.65585728	0.00000000	3.56379397
H	1.65585728	0.00000000	3.56379397
H	0.00000000	4.16096961	1.17926827
H	0.00000000	−4.16096961	1.17926827
H	0.00000000	−2.54613233	−3.51013832
H	0.00000000	2.54613233	−3.51013832

Table 6.2: Geometry of cyclopentadiene (C_{2v}) optimized at the CCSD level of theory with a TZ2P basis set. The molecule is in the principal axis system, and the atomic Cartesian coordinates are given in bohr.

Atom	x	y	z
C	0.00000000	0.00000000	2.34183615
C	0.00000000	2.22647796	0.56211098
C	0.00000000	−2.22647796	0.56211098
C	0.00000000	−1.39337960	−1.83597018
C	0.00000000	1.39337960	−1.83597018
H	−1.65786063	0.00000000	3.56933488
H	1.65786063	0.00000000	3.56933488
H	0.00000000	4.16982399	1.16606714
H	0.00000000	−4.16982399	1.16606714
H	0.00000000	−2.55302850	−3.50969971
H	0.00000000	2.55302850	−3.50969971

Table 6.3: Vertical transition energies (in eV) for the $^1B_2 \leftarrow ^1 A_1$ transition of cyclopentadiene, calculated using linear-response CC methods and various basis sets. The calculations were obtained at the geometry given explicitly in Table 6.1.

Basis Set	Number of Functions	CCSD	CCSDT-3	CCSDT
cc-pVDZ	100	6.01	5.90	5.90
cc-pVTZ	234	5.81	5.80	—
cc-pVQZ	455	5.74		
aug-cc-pVDZ'	169	5.73	—	—
aug-cc-pVTZ'	368	5.68	—	—
aug-cc-pVQZ'	580	5.68	—	—

Figure 6.1: Comparison of coupled cluster theory to other theoretical estimates. The black bar represents the vertical energy evaluated in this work with the corresponding error bars.

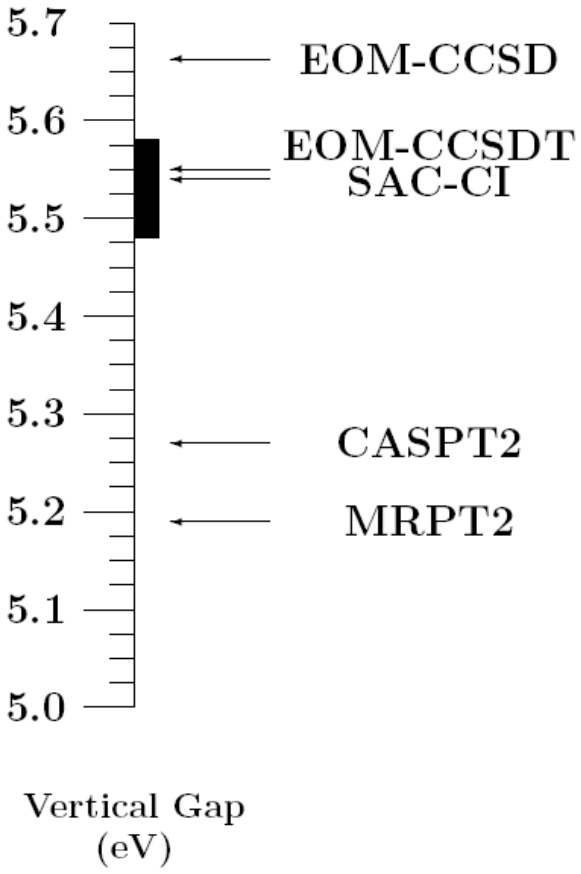

Figure 6.2: Absorption spectrum simulation of cyclopentadiene without inclusion of linear vibronic coupling in eV (Top). Enlargement of the maximum of absorption region (Bottom).

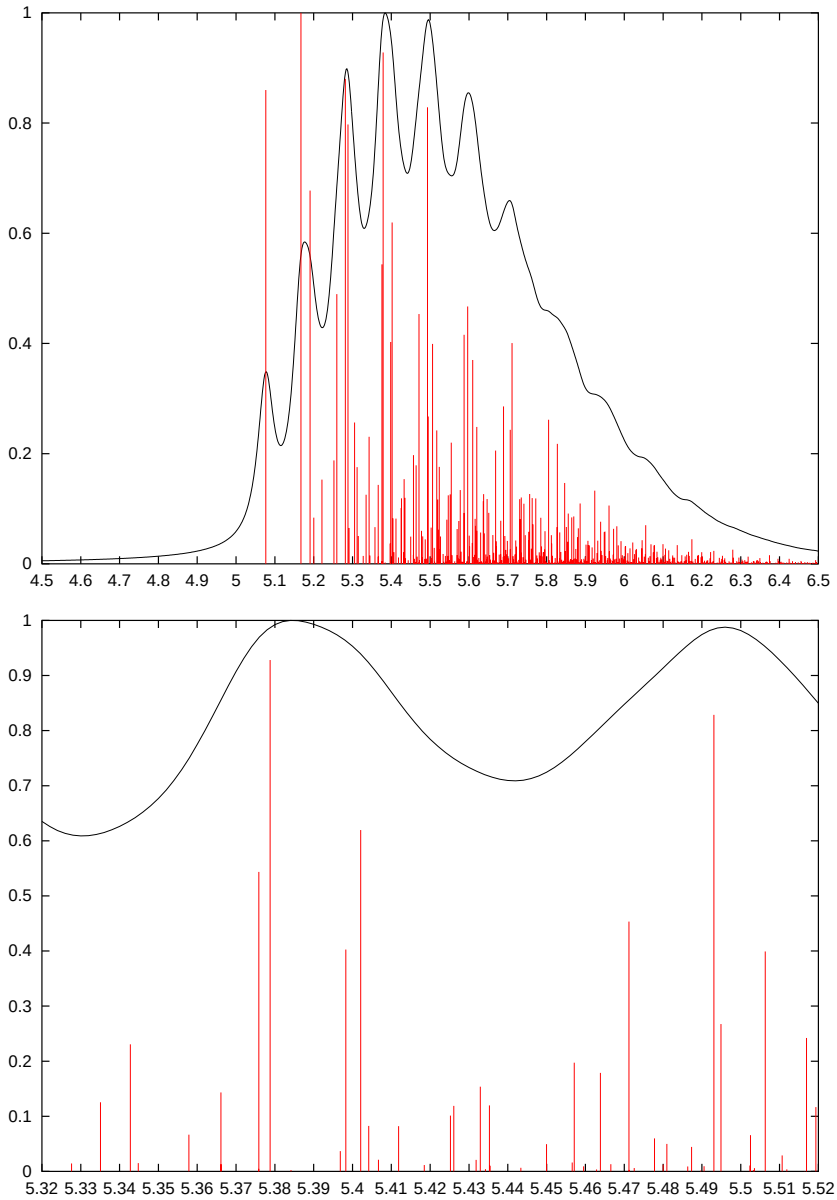

Figure 6.3: Absorption spectrum simulation of cyclopentadiene including linear vibronic coupling in eV (Top). Enlargement of the maximum of absorption region (Bottom).

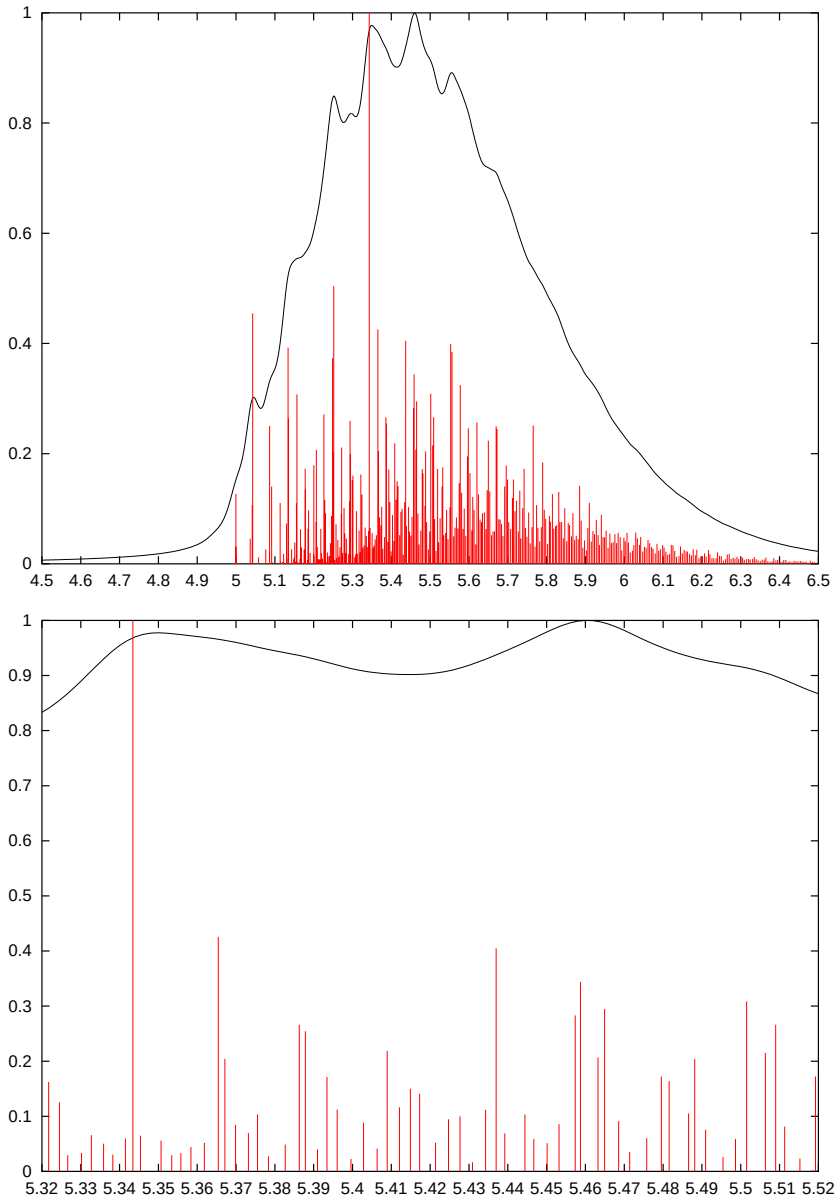

Figure 6.4: Comparison of the absorption spectrum simulation including linear vibronic coupling with the experimental absorption profile.

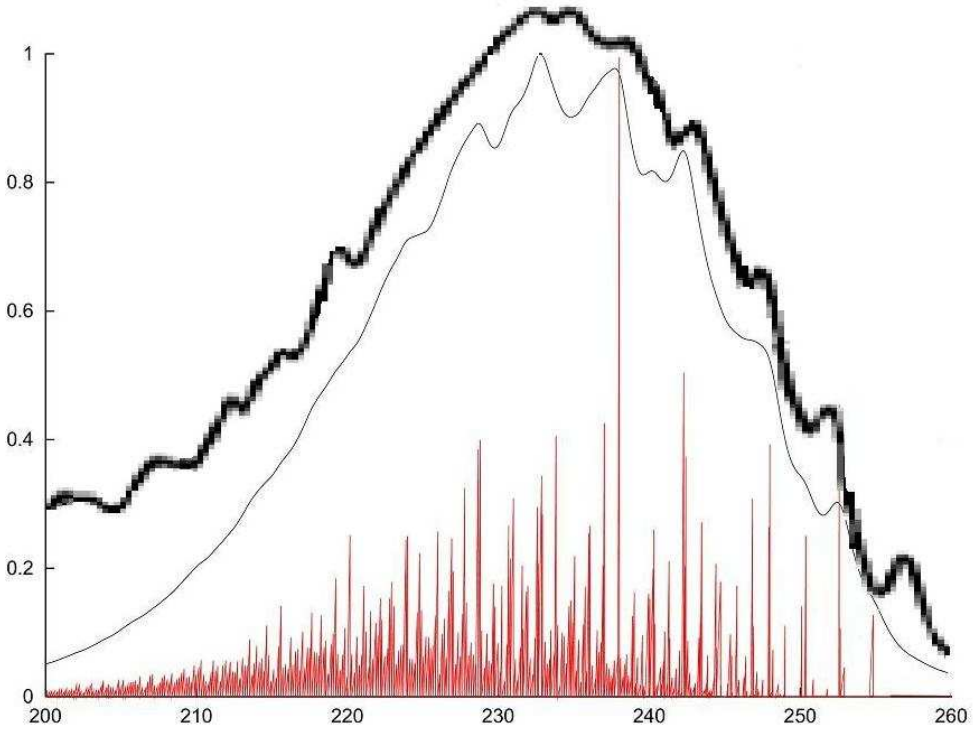

Table 6.4: Geometry of the $^1B_2$ excited state (C_S) of cyclopentadiene optimized at the EOM-CCSD level of theory with a TZ2P basis set. The molecule is in the principal axis system, and the atomic Cartesian coordinates are given in bohr.

Atom	x	y	z
C	0.38886490	0.00000000	2.39890594
C	-0.31557943	2.09753396	0.61141179
C	-0.31557943	-2.09753396	0.61141179
C	0.13635545	-1.32294126	-1.90656452
C	0.13635545	1.32294126	-1.90656452
H	-0.63879122	0.00000000	4.17759154
H	2.43863975	0.00000000	2.79930985
H	-1.28307919	3.79789630	1.18850194
H	-1.28307919	-3.79789630	1.18850194
H	0.20207026	-2.53636150	-3.53747193
H	0.20207026	2.53636150	-3.53747193

6.2.3 Conclusion

With the data at hand, it is appropriate to evaluate the accuracy of multireference perturbation theory and coupled cluster approaches for studying this particular electronic transition. It seems that the former is too low, and the latter probably slightly too high. We believe that inclusion of connected quadruple excitations will probably lower the vertical excitation energy but by a small amount. On the other hand, CASPT2 appears to be about 0.15 eV too low. If one assumes that basis set effects in the CC and CASPT2 calculations are comparable (which is a plausible approximation), then the difference between the extrapolated EOM-CCSD energy of 5.66 eV and that calculated with the same level of theory using the basis set from Ref. 123 (5.79 eV)[137] suggests that CASPT2 would give a value somewhere near 5.15 eV with a large basis set. It should be noted that this is about 0.3 eV below the vertical excitation energy estimated here. CASPT2 is too low, which is not surprising. The excitation energy predicted at the CASSCF level is more than 2 eV above the CASPT2 result, and second-order perturbation theory is notorious for overestimating correlation effects when they are significant in magnitude. Using the highly accurate but expensive EOM-CCSDT method coupled with basis sets of acceptable size seems to have paid off and provided together with the linear vibronic coupling model, an accurate treatment of this electronic transition. We feel that the model presented here should be used to study similar problems where there is an appreciable coupling between excited states; these problems include, but are not limited to, molecules such as

pyrrole and furan.

Chapter 7

Why Is Size Consistency Important?

7.1 Introduction

In electronic structure theory, size consistency is an important characteristic of a quantum chemical method; quoting Pople[138], it is a sign of a well-constructed method. In the previous chapters, it was shown that truncated configuration interaction methods are not size-consistent in contrast to coupled cluster methods that are thanks to the exponential nature of the excitation operator. Therefore, as we mentioned earlier, using coupled cluster theory the energy of a supersystem AB (where A and B don't interact) must be equal to the sum of the energies of the two non-interacting A and B systems placed at an infinite distance from each other.

The CCSD(T) method is known to have problems describing the potential energy surface when the bond of the molecule is stretched, more precisely when multireference character of the wavefunction[139,140] is present. Thus, the CCSD(T) method, widely recognized for its cost/accuracy ratio is not a good choice for "bond breaking" problems. Some time ago an alternative to CCSD(T) was proposed by Piecuch *et al.*[49,50], the so called R-CCSD(T) where R stands for renormalized. The method is based on the method-of-moment idea and was said to perform better than traditional CCSD(T) for "bond

breaking" problems and avoid the tendency of CCSD(T) to overestimate the triples effect by the use of a "damping factor". However, it is possible to prove, with careful inspection, that this former method is not size-consistent.

A brief overview of the method and some conclusive tests will be given in the next section to point out the problems encountered if the R-CCSD(T) method is used without caution.

7.2 The R-CCSD(T) Model

The noniterative triples correction to the CCSD energy $\Delta E_{(T)}$ (See Chapter 3) can be written in spin orbital form as follows

$$\begin{aligned}\Delta E_{(T)} =& \frac{1}{4}\sum_{ijkabc} D_{ijk}^{abc}[\sum_{ef} t_{ae}^{ij} t_{ij}^{af} \langle fk||bc\rangle\langle bc||ek\rangle - \sum_{mn} t_{ab}^{im} t_{in}^{ab} \langle mc||jk\rangle\langle jk||nc\rangle \\ & 2\sum_{e} t_{ij}^{ae} t_{a}^{i} \langle jk||bc\rangle\langle bc||ek\rangle - 2\sum_{m} t_{im}^{ab} t_{a}^{i} \langle jk||bc\rangle\langle mc||jk\rangle]\end{aligned} \tag{7.1}$$

where D_{ijk}^{abc} is equivalent to the denominator seen in Chapter 3 *viz.*

$$D_{ijk}^{abc} \equiv \frac{1}{f_{ii} + f_{jj} + f_{kk} - f_{aa} - f_{bb} - f_{cc}} \tag{7.2}$$

It should be noted that as in Chapter 3 only the diagonal terms of the Fock matrix are used to describe the zeroth-order determinant. Using the spin-orbital form of the $\Delta E_{(T)}$ correction it can be shown that the R-CCSD(T) correction to the CCSD energy namely $\Delta E_{R-(T)}$ can be written as

$$\Delta E_{R-(T)} = D^{-1} \Delta E_{(T)}. \tag{7.3}$$

Here, D is the "damping" factor or denominator used in R-CCSD(T) to control the amplitude of the triples excitations and can be shown to assume the following form

$$D = 1 + \sum_{ia} t_a^i t_i^a + \sum_{abij} (t_{ab}^{ij} t_{ij}^{ab} + t_{ab}^{ij} t_i^a t_j^b) + \sum_{ijkabc} (t_{abc}^{ijk} t_{ij}^{ab} t_k^c + t_{abc}^{ijk} t_i^a t_j^b t_k^c) \tag{7.4}$$

The diagrammatic representation of the $\Delta E_{R-(T)}$ correction in the antisymmetrized Brandow formalism is shown below.

$\Delta E_{R-(T)} =$ 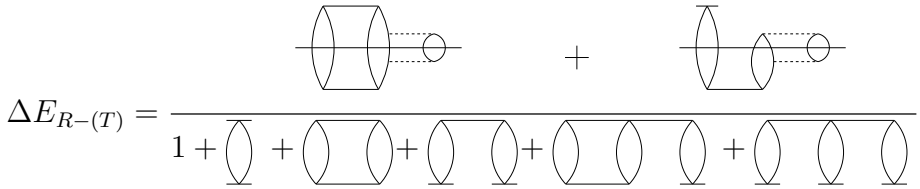 (7.5)

$\Delta E_{R-(T)}$ can be in a simple form assumed as being equivalent to $\frac{\Delta E_{(T)}}{1+A}$ where A scales with the size of the system. The correlation energy obtained with the R-CCSD(T) method is consequently always intermediate between CCSD and CCSD(T). Thus, it is evident that if the system studied gets larger then A will also become larger. This phenomena can be a problem if A becomes too large and "overdamps" the (T) correction; hypothetically the triples corrections could become negligible if the size of the molecule becomes too large. Furthermore, one can notice that the energy of a supersystem A-A ($E_{AA} \equiv \frac{2\Delta E_{(T)}}{1+2A}$) is not equal to twice the energy of the individual system A ($E_A \equiv \frac{\Delta E_{(T)}}{1+A}$). This method is for that reason not size-consistent. The same analysis can be done for the analytical gradients corresponding to the R-CCSD(T). This would also

show that the harmonic vibrational frequencies and equilibrium geometries are always found to be between CCSD and CCSD(T).

In the following section we will present some numerical evidence of the size consistency problem mentioned above for the R-CCSD(T) method.

7.3 Results and Discussion

It is interesting to assess the general performance of the method previously mentioned in order to determine the effect of the "damping" factor. This was done using an exhaustive set of molecules, some of them known to be challenging for most theoretical approaches. The results of these calculations are shown in Tables 7.1-7.6; they were carried on a local version of the ACES II program package. The harmonic force constants were calculated numerically from analytical gradients and the equilibrium bond lengths were calculated analytically. The gradients for the R-CCSD(T) method were recently implemented in ACES II, facilitating this analysis. The cc-pVQZ basis set[45] was used in all cases except stated otherwise and the core electrons were always correlated. The experimental results used in parts of the benchmark presented here can be found in Ref. 141 and were used for comparison purposes.

From looking at Table 7.1-7.4 it is clear that the equilibrium bond lengths calculated with R-CCSD(T) are always intermediate between CCSD and CCSD(T); this is of course expected and is due to the fact that the (T) correction is scaled down by the denominator in R-CCSD(T). The same observation is true for the bond angles. There are not any significant discrepancies

between the performance of CCSD(T) and R-CCSD(T), however, CCSD(T) is in all cases closer to the experimental results with a maximum error of 0.0030 Å *v.* 0.0065 Å and a RMS of barely 0.0010 Å. *v.* 0.0017 Å. The same behavior is seen when the harmonic vibrational frequencies are calculated at the geometries shown in Tables 7.1-7.2; meaning that the results obtained with R-CCSD(T) are always between CCSD and CCSD(T) with the latter being larger in magnitude (Tables 7.5-7.6). One could argue that it is a consequence of shorter R-CCSD(T) bond lengths, compared to CCSD(T), but this phenomenon is present even when the same equilibrium geometry is used. This is consistent with results shown in Tables 7.1-7.2; the entire set of values obtained with R-CCSD(T) is always between CCSD and CCSD(T). These examples owe their relevance to the fact that they provided numerical evidence that the extra denominator in the renormalized version of CCSD(T) slightly degrades the quality of the triples effect. Given the fact that R-CCSD(T) was created with the intent of studying bond breaking problems, the degradation of the solution appears acceptable. Nevertheless, the examples given earlier didn't challenge the lack of size consistency in R-CCSD(T); it is interesting to study how R-CCSD(T) could handle calculations on an extended molecular system. The results of the study are shown in Table 7.7 and Figures 7.1-7.2; in this case the DZP basis set was used[142]. The harmonic vibrational frequency calculations were done at the corresponding equilibrium geometries. The problem of size consistency in R-CCSD(T) is often overlooked by its fervent users, but its magnitude is clearly shown in this example. From a careful

inspection of the R-CCSD(T) correction shown in section 7.2, one expects the R-CCSD(T) correction to become smaller as the size of the wavefunction *i.e* the molecular system gets larger and thus, hypothetically, disappear in the case of a large molecule. The latter statement would mean that a complicated noniterative n^7 method could be used on a very large molecule to get the simpler n^6 CCSD correlation energy. Figures 7.1-7.2 show the difference between the CCSD(T) and R-CCSD(T) bond lengths and harmonic frequencies of the C-N bond, respectively, for a set of molecules with an increasing length of carbon chain. As the carbon chain gets longer, the difference between CCSD(T) and R-CCSD(T) gets larger meaning that the R-CCSD(T) method converges slowly to CCSD. One should keep in mind that while CCSD(T) has problems in "bond breaking" situation it provides an accurate description of the triples effect close to equilibrium geometry. The R-CCSD(T) method has without any doubts the wrong behavior as one would expect the effect of a higher-order correction to CCSD to increase when the system size increases.

Table 7.1: Bond lengths calculated with CCSD, CCSD(T) and R-CCSD(T) using the cc-pVQZ basis set in Ångströms and their empirical estimates.

Species	Bond	Emp	CCSD	CCSD(T)	R-CCSD(T)
HF	R_{FH}	0.9169	0.9126	0.9152	0.9149
H_2O	R_{OH}	0.9575	0.9536	0.9562	0.9559
HOF	R_{OH}	0.9678	0.9613	0.9648	0.9640
HNC	R_{NH}	0.9949	0.9915	0.9941	0.9935
NH_3	R_{NH}	1.0116	1.0078	1.0101	1.0098
HNO	R_{NH}	1.0517	1.0471	1.0510	1.0499
C_2H_2	R_{CH}	1.0618	1.0595	1.0613	1.0618
HCN	R_{CH}	1.0652	1.0625	1.0645	1.0639
N_2	R_{NN}	1.0977	1.0909	1.0981	1.0967
CH_2O	R_{CH}	1.1007	1.0974	1.0996	1.0990
CH_2	R_{CH}	1.1063	1.1036	1.1052	1.1049
CO	R_{CO}	1.1284	1.1219	1.1289	1.1276
HCN	R_{CN}	1.1534	1.1464	1.1538	1.1522
CO_2	R_{CO}	1.1601	1.1530	1.1601	1.1584
HNC	R_{CN}	1.1687	1.1622	1.1693	1.1679
C_2H_2	R_{CC}	1.2035	1.1975	1.2041	1.2027
CH_2O	R_{CO}	1.2047	1.1974	1.2042	1.2028
HNO	R_{NO}	1.2086	1.1971	1.2082	1.2057
O_3	R_{OO}	-	1.2413	1.2663	1.2566
F_2	R_{FF}	1.4124	1.3885	1.4111	1.4059
HOF	R_{FO}	1.4344	1.4125	1.4324	1.4279

Table 7.2: Bond angles calculated with CCSD, CCSD(T) and R-CCSD(T) using the cc-pVQZ basis set and their empirical estimates.

Species	Bond angle	Emp	CCSD	CCSD(T)	R-CCSD(T)
H_2O	HOH	104.51	104.53	104.25	104.28
HOF	HOF	97.54	98.63	97.86	98.02
HNO	HNO	108.27	108.35	108.09	108.15
NH_3	HNH	107.25	106.64	106.36	106.40
CH_2O	HCH	116.74	116.39	116.44	116.43
CH_2	HCN	102.44	102.12	102.11	102.44
O_3	OOO	-	117.78	117.16	117.37

Table 7.3: Statistical analysis of the errors in the bond lengths from Table 7.1 in Ångströms

Methods	CCSD	CCSD(T)	R-CCSD(T)
Mean signed error	−0.0071	−0.0007	−0.0021
Mean absolute error	0.0071	0.0010	0.0021
Maximum error	0.0239	0.0030	0.0065
RMS	0.0058	0.0010	0.0017

Table 7.4: Statistical analysis of the errors in the bond angles from Table 7.2

Methods	CCSD	CCSD(T)	R-CCSD(T)
Mean signed error	−0.02	−0.27	−0.23
Mean absolute error	0.41	0.38	0.39
Maximum error	1.09	0.89	0.85
RMS	0.60	0.38	0.43

Table 7.5: Harmonic vibrational frequencies calculated with CCSD, CCSD(T) and R-CCSD(T) using the cc-pVQZ basis set at the corresponding geometries given in Tables 7.1-7.2 in cm^{-1}.

Species	Mode	Symmetry	CCSD	CCSD(T)	R-CCSD(T)
HF	HF stretch	Σ^+	4210	4167	4172
N2	NN stretch	Σ^+	2448	2368	2386
CO	CO stretch	Σ^+	2248	2177	2192
F_2	FF stretch	Σ^+	1021	925	950
H_2O	HOH bend	A_1	1675	1663	1664
	OH stretch	A_1	3894	3853	3859
	OH stretch	B_2	3998	3960	3965
CH_2O	Umbrella	B_1	1220	1195	1201
	OCH bend	B_2	1295	1279	1282
	HCH bend	A_1	1563	1545	1549
	CO stretch	A_1	1843	1791	1803
	CH stretch	A_1	2974	2945	2952
	CH stretch	B_2	3045	3015	3022
HCN	HCN bend	Π	751	723	730
	CN stretch	Σ^+	2199	2134	2150
	HC stretch	Σ^+	3473	3444	3451
HOF	FO stretch	$A^{'}$	1002	926	945
	HOF bend	$A^{'}$	1446	1403	1413
	OH stretch	$A^{'}$	3836	3786	3799
NH_3	Umbrella	A_1	1083	1082	1082
	HNH bend	E	1699	1685	1687
	NH stretch	A_1	3527	3495	3500
	NH stretch	E	3653	3623	3627

Table 7.6: Harmonic vibrational frequencies calculated with CCSD, CCSD(T) and R-CCSD(T) using the cc-pVQZ basis set at the corresponding geometries given in Tables 7.1-7.2 in cm^{-1}.

Species	Mode	symmetry	CCSD	CCSD(T)	R-CCSD(T)
HNO	HNO bend	$A^{'}$	1594	1554	1565
	NO stretch	$A^{'}$	1689	1611	1629
	NH stretch	$A^{'}$	3026	2966	2983
C_2H_2	HCC bend	Π_g	639	597	607
	HCC bend	Π_u	777	757	761
	CC stretch	Σ^+	2060	2013	2025
	CH stretch	Σ^-	3437	3416	3422
	CH stretch	Σ^+	3535	3509	3516
CO_2	OCO bend	Π_u	698	673	679
	CO stretch	Σ^+	1405	1360	1373
	CO stretch	Σ^-	2451	2411	2423
HNC	HNC bend	A_1	503	483	488
	CN stretch	Σ^+	2131	2067	2082
	NH stretch	Σ^+	3870	3831	3840
CH_2	HCH bend	A_1	1423	1407	1409
	CH stretch	A_1	2958	2938	2941
	CH stretch	B_2	3028	3012	3014
O_3	OOO bend	A_1	776	728	749
	OO stretch	A_1	1299	1174	1232
	OO stretch	B_2	1289	1088	1302

Table 7.7: Bond lengths and harmonic vibrational frequencies corresponding to the C-N bond calculated with CCSD, CCSD(T) and R-CCSD(T) using the DZP basis set in Ångströms and cm^{-1}, respectively.

Species	Bond length	CCSD	CCSD(T)	R-CCSD(T)
HCN	R_{CN}	1.1710	1.1771	1.1759
CH3CN	R_{CN}	1.1714	1.1777	1.1774
CH3CH2CN	R_{CN}	1.1718	1.1783	1.1763
CH3CH2CH2CN	R_{CN}	1.1718	1.1784	1.1761
Species	Mode	CCSD	CCSD(T)	R-CCSD(T)
HCN	CN stretch	2140	2087	2099
CH3CN	CN stretch	2336	2280	2295
CH3CH2CN	CN stretch	2327	2269	2288
CH3CH2CH2CN	CN stretch	2326	2268	2290

Figure 7.1: Difference between the CCSD(T) and R-CCSD(T) bond length of the C-N bond in Ångströms.

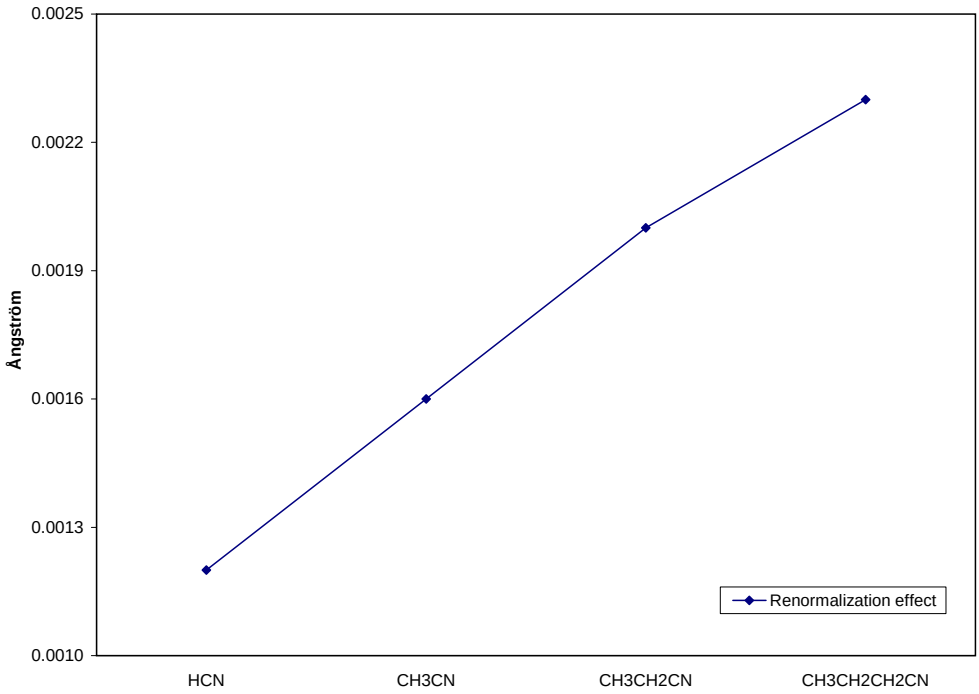

Figure 7.2: Difference between the CCSD(T) and R-CCSD(T) harmonic vibrational frequencies of the C-N stretch in cm^{-1}.

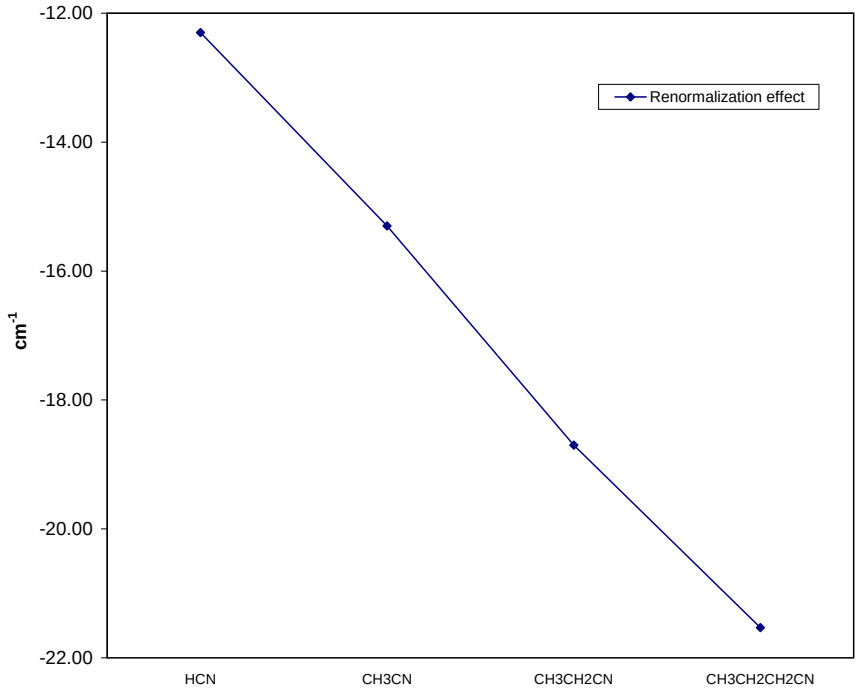

7.4 Conclusion

The renormalized coupled cluster method with inclusion of noniterative triple excitations (R-CCSD(T)) has been, since its implementation, presented as being superior to CCSD(T). However, based on the previous analysis it is important to exercise caution when using R-CCSD(T); its superiority to CCSD(T) in "bond breaking" problems is incontestable and well reported in the literature[49,50] although the problems arising with the lack of size-consistency are miraculously almost nonexistent in the literature.

Chapter 8

Conclusion

In retrospect, we have demonstrated that the new approach for approximating quadruple excitations [CCSDT(Q)] is a robust and powerful method, yet allowing the evaluation of the quadruple excitations in a relatively inexpensive noniterative manner. Compared to its predecessor – obtained from applying perturbation theory on a Hartree-Fock determinant (CCSDT[Q]) – CCSDT(Q) is vastly superior and does not exhibit the rather strange basis-set dependence seen for CCSDT[Q]. The set of molecules used to evaluate the performance of CCSDT(Q) includes cases known to exhibit pathological behaviors, yet CCSDT(Q) performed well and compared favorably to coupled cluster methods including higher excitation levels (CCSDTQP) and even to full configuration interaction. The CCSDT(Q) method has now been incorporated into the high accuracy extrapolated ab initio thermochemistry (HEAT) protocol. This work shows the potential of CCSDT(Q) as being an alternative to the significantly more expensive CCSDTQ and even CCSDTQP. It is expected that CCSDT(Q) will be widely used, and enjoy the sucess that CCSD(T) experienced a few years ago.

In the previous chapters, we also showed the good performance of new alternatives for studying radicals, EOMIP-CCSDT-X (X=1a, 1b, 2, 3) and

CC3, where approximate triple excitations are used in the equation-of-motion framework for ionization potentials. For several problematic cases, such as the CN radical, these methods allow a good description of the excited states potential energy surface by avoiding the usual problems of spin contamination and properly treating pseudo Jahn-Teller effects. Indeed, since the target state is obtained by diagonalization, these methods provide a better description of multireference character than do traditional coupled cluster methods without the complexity common to multireference methods. One of the drawbacks of these approaches is their inferior treatment of dynamic correlation compared to traditional coupled cluster. EOMIP-CCSDT-3 provides a better description of the dynamic correlation and should be preferred to EOMIP-CC3 which overshoots the triple excitation effects significantly in some cases.

Also, equation-of-motion coupled cluster methods, already developed for excited states, were successfully applied in conjunction with vibronic coupling theory to describe the contested $^1B_2 \leftarrow {}^1A_1$ transition in cyclopentadiene. It was determined that the first $^1B_2$ excited state is nonplanar due to the presence of a higher-lying state. The coupling between these two states was shown to be important for the accurate description of this transition. The equation-of-motion methods are within 0.05 eV of the vertical excitation energy inferred from this work. It was also shown that the vertical excitation energy calculated with CASPT2 is too low when a large basis set is used. The machinery for studying excited states is well-established and this template should be used to approach similar problems where there is an appreciable

coupling between excited states. These problems include, but are not limited to, conjugated π systems such as pyrrole and furan.

Additionally, one key aspect of any ab initio methods, size consistency, was discussed in the context of a recent variant of coupled cluster theory. The renormalized version of CCSD(T) was shown to lack size-consistency because the effect of triple excitations calculated with R-CCSD(T) decreases as the size of the molecular system is increased while this is not the case for regular CCSD(T).

Finally, coupled cluster methods have been around for more than thirty years and have been enormously successful. However, they are even more important when accuracies of less than a kJ per mole is sought from ab initio methods. Thus, it is essential to develop new methods based on the model of CCSDT(Q) and invest time in researching the adaptation of parallel computing to coupled cluster calculations in order to achieve this type of accuracy for larger molecules.

Appendices

Appendix A

Mathematical Model for Self-Assembling Dimers

A.1 Introduction

Simplified models are often used in supramolecular chemistry to understand mechanisms involved in larger biological systems[143,144,145]. Among them, the syntheses of stable self assemblies in aqueous solutions play a vital role, since such processes allow more insight in biological applications[146,147]. The types of interactions that usually occur in aqueous media are either ionic or hydrophobic. It is essential to achieve the syntheses of supramolecules involving several types of non-covalent interactions; describing at a small scale what could happen in nature. The main goal of this work was to analyze the formation of stable dimers and the creation of higher-order stable self assemblies via ionic and hydrophobic interactions. The original experimental data did not provide an unambiguous picture of the stoichiometry of these assemblies. A better understanding of these interactions can be obtained by developing a robust mathematical model.

A.2 Experimental Details and Mathematical Model

The attractive interactions of thiophenyl substituents between two adjacent molecules – leading to tight packing of dimers – is reported in the literature[148]. The 2,4,6-substituted 1,3,5-tristhiophenyl benzenes **1**, **2**, **3** were chosen to obtain controlled dimerization in protic media by exploiting both ionic and hydrophobic interactions (Figure A.1). They were reported to account for binding energies of 5 kJ per mol[149] and 3 kJ per mol[150], respectively. These self-assembling processes were studied by electrospray ionization mass spectroscopy (ESI-MS) and ^{1}H NMR titration in a D2O-CD3OD solution. Both these experimental studies showed the possible creation of **1**/**3** and **2**/**3** dimers as well as the self dimerization of **3** but without unequivocal evidence[151]. The mathematical procedure used in this study aims at modelling the NMR titration data provided by the experimental studies. The model includes the possible binding of **1** with **3**, and **2** with **3**, but also the self dimerization of **3**. General equilibria with associated K_{AA} and K_{AB} values are expressed in Eq. A.1, where A is **3** and B is either **1** or **2**, in our analysis. We follow the chemical shift of B (δ_{obs}), hence Eq. A.2 results[152]. Using mass balance and equilibria expressions, [AB] and [B] can be related to [A] (Eq. A.3 and Eq. A.4). Finally, [A] can be determined by solving Eq. A.5. The variables used in this analysis but not explicitly defined are self explanatory or defined in Ref. 153.

Figure A.1: Alternating hexasubsituted benzene derivative **1**, **2**, **3** used as monomeric species.

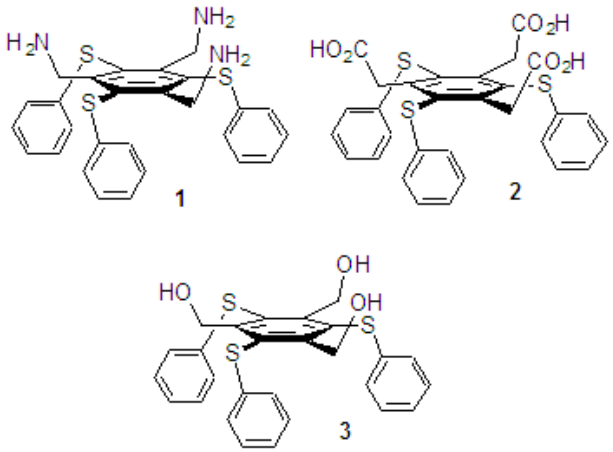

$$A_2 \rightleftharpoons 2A \rightleftharpoons AB \tag{A.1}$$

$$\delta_{obs} = \delta_{AB}\frac{[AB]}{[B]_t} + \delta_B\frac{[B]}{[B]_t} \tag{A.2}$$

$$[AB] = \frac{K_{AB}[A][AB]_t}{1 + K_{AB}[A]} \tag{A.3}$$

$$[B] = [B]_t - \frac{K_{AB}[A][B]_t}{1 + K_{AB}[A]} \tag{A.4}$$

$$2K_{AA}K_{AB}[A]^3 + (2K_{AA} + K_{AB})[A]^2 + (K_{AB}[B]_t + 1 - K_{AB})[A] - [A]_t \tag{A.5}$$

From the previous set of equations it can be seen that δ_{obs} is a function of the following set of variables, δ_B, δ_{AB}, K_{AA}, K_{AB}, $[A]$, $[A]_t$, and $[B]_t$ where only $[A]_t$ and $[B]_t$ are experimentally controllable. The non-linear least-square method is usually a good choice for optimizing these types of systems; in this case the system needs to be optimized for these variables: K_{AA}, K_{AB}, δ_B, δ_{AB}. In this process the gradient vector (G) and the Hessian matrix (H) are calculated from the residual (R)

$$R = \sum_i (\delta^i_{calc} - \delta^i_{obs})^2. \tag{A.6}$$

The Newton-Raphson step is then calculated,

$$r = GH^{-1} \tag{A.7}$$

and the new set of parameters is evaluated,

$$X_{new} = X_{old} - r. \tag{A.8}$$

This procedure is repeated until convergence. Unfortunately, the latter method is not sufficient due to the presence of local minima; this problem is common when solving coupled non-linear systems. A method was developed by Pulay *et al.* in the eighties to expand the search space and avoid the problem of local minima, the so-called direct inversion of the iterative subspace method (DIIS)[51]. Used in most Hartree-Fock self consistent field and coupled cluster algorithms to speed up the conversion process it will, in this study, be adapted to the problem mentioned above.

In the adapted DIIS framework, the error matrix will be formed from the previous n gradients (G^1, G^2, ..., G^n).

$$E = \begin{pmatrix} 2E_{11} & 2E_{12} & 2E_{13} & . & . & . & -1 \\ 2E_{12} & 2E_{22} & 2E_{23} & . & . & . & -1 \\ 2E_{13} & 2E_{23} & 2E_{33} & . & . & . & -1 \\ . & . & . & . & . & . & -1 \\ . & . & . & . & . & . & -1 \\ -1 & -1 & . & . & . & . & 0 \end{pmatrix} \tag{A.9}$$

where

$$E_{ij} = \langle G^{(i)} | G^{(j)} \rangle \tag{A.10}$$

and, therefore,

$$||G^{n+1}|| = \sum_{i=0}^{n} \sum_{j=0}^{m} C_i C_j E_{ij}. \tag{A.11}$$

with C_1, C_2, ..., C_n being expansion coefficients. One can solve the linear system derived from the Lagrange undetermined multiplier method to obtain these expansion coefficients

$$\begin{pmatrix} 2E_{11} & 2E_{12} & 2E_{13} & . & . & . & -1 \\ 2E_{12} & 2E_{22} & 2E_{23} & . & . & . & -1 \\ 2E_{13} & 2E_{23} & 2E_{33} & . & . & . & -1 \\ . & . & . & . & . & . & -1 \\ . & . & . & . & . & . & -1 \\ -1 & -1 & . & . & . & . & 0 \end{pmatrix} \begin{pmatrix} C_1 \\ C_2 \\ C_3 \\ . \\ C_n \\ \lambda \end{pmatrix} = \begin{pmatrix} 0 \\ 0 \\ 0 \\ 0 \\ 0 \\ -1 \end{pmatrix} \tag{A.12}$$

Of course several conventional non-linear least-square steps have to be performed before starting the DIIS algorithm in order to create the necessary

basis. It is now possible to expand the new DIIS gradient vector in the basis spanned by the previous n gradient vectors *viz*

$$G_{DIIS}^{(n+1)} = \sum_{i=0}^{n} C_i G^{(i)} \tag{A.13}$$

the new DIIS solution vector is

$$X_{DIIS}^{(n+1)} = \sum_{i=0}^{n} C_i X^{(i)} \tag{A.14}$$

Finally, the solution vector of interest is evaluated as follows

$$X^{(n+1)} = \sum_{i=0}^{n} C_i X^{(i)} + G_{DIIS}^{(n+1)^{\dagger}} (H^{(n)})^{-1} \tag{A.15}$$

It should be noted that a non-zero term ($G_{DIIS}^{(n+1)^{\dagger}}(H^{(n)})^{-1}$) is added to avoid linear dependence. $X^{(n+1)}$ is then used to recalculate the least-square residual, gradient, and Hessian. The DIIS method provides a faster convergence but also a crucial expansion of the search space essential for solving this problem. The theoretical NMR titration curves obtained using this model and their experimental counterparts are shown in Figures A.2 and A.3. The curve fits are not perfect as the experimental data levels out to a constant chemical shift earlier in the titration than do the simulated curves. This could be due to the precipitation of A making the chemical shift of B less sensitive to any addition of A. However, the general shape of the titration curve is correct in the theoretical model. This advanced curve fitting technique also allow the determination of the reaction rates of Reaction A.1. This model gives us insight in the stoichiometry of the assemblies but also how fast these assemblies are forming.

Figure A.2: Shift of the thiophenyl protons of **1** in D2O-CD3OD(1:1, c=0.01M), buffered at pD 7.5, upon addition of **3** (c=0.12M in CD3OD). Closed circles are experimental data, and open circles are calculated data. $K_{AB} = 1.9 \times 10^3 M^{-1}$; $K_{AA} = 2.3 \times 10^3 M^{-1}$; $\delta_{AB} = 7.096$; $\delta_B = 7.129$. As stated in the text, these affinity constants are not very accurate because of precipitation toward the end of the titrations.

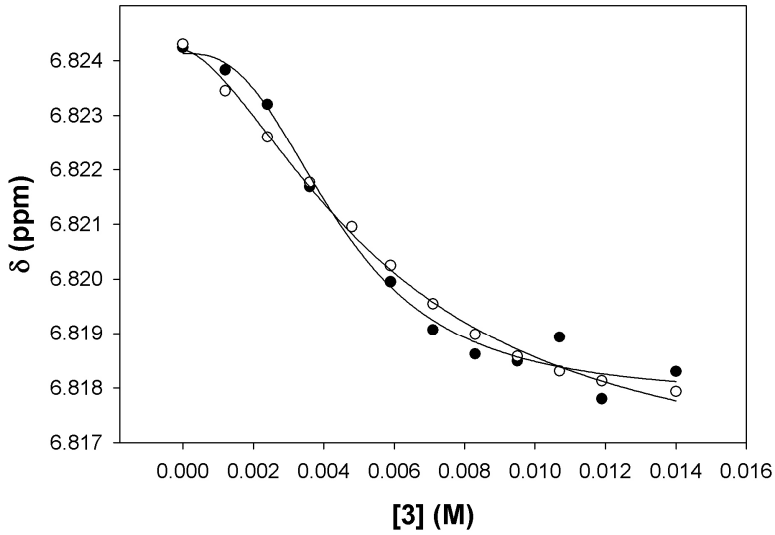

Figure A.3: Shift of the thiophenyl protons of **2** in D2O-CD3OD(1:1, c=0.01M), buffered at pD 7.5, upon addition of **3** (c=0.12M in CD3OD). Closed circles are experimental data, and open circles are calculated data. $K_{AB} = 8.6 \times 10^3 M^{-1}$; $K_{AA} = 2.7 \times 10^3 M^{-1}$; $\delta_{AB} = 6.817$; $\delta_B = 6.824$. As stated in the text, these affinity constants are not very accurate because of precipitation toward the end of the titrations.

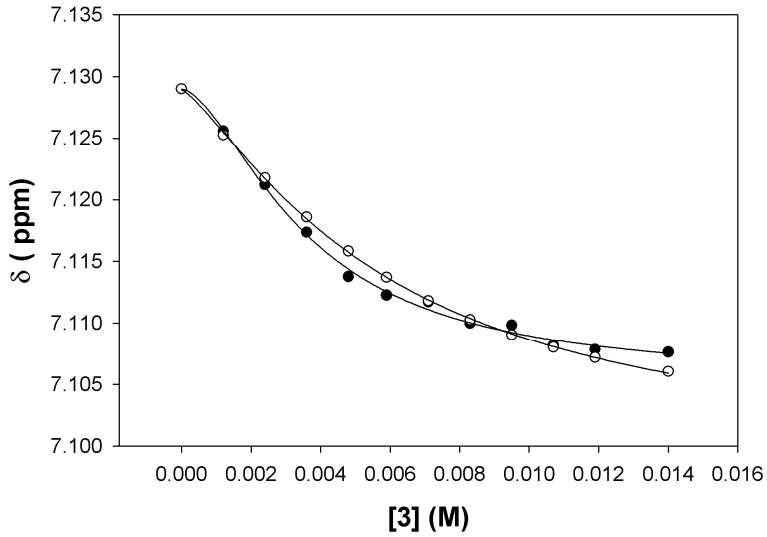

Appendix B

Mathematics for Threshold Detection and Application to the Analysis of Malate in Pinot Noir Grapes

B.1 Overview of Threshold Detection Techniques

Several alternatives can be designed to achieve qualitative colorimetric analysis. The most commonly used, is based on a standard host-guest model where one can assume the indicator to be a host for a proton guest. The following reaction is considered between the analyte (guest (G)) and the recognition moiety (host (H)) with a 1:1 stoichiometry

$$H + G \rightleftharpoons HG \tag{B.1}$$

The equilibrium constant is defined as being equal to the ratio of product over reactants

$$K_{HG} = \frac{[HG]}{[H][G]} \tag{B.2}$$

The colorimetric analysis are followed by absorbance which depends on the concentrations of both the host and host-guest complex, and by Beer's law, is

$$A = \epsilon_H b[H] + \epsilon_{HG} b[HG] \tag{B.3}$$

where b is the path length of light and the ϵ's are the molar absorptivities. Using equation B.2 one can write the concentration of the host-guest complex ($[HG]$) as a function of the total host concentration ($[H]_t$) and total guest concentration ($[G]_t$) as follows

$$K_{HG}[HG]^2 - [HG](K_{HG}[H]_t + K_{HG}[G]_t + 1) + K_{HG}[H]_t[G]_t = 0. \quad \text{(B.4)}$$

After solving this quadratic equation, the evaluation of the host concentration ([H]) and consequently the absorbance is straightforward. This simplistic model allows a faithful simulation of the experimental binding isotherm.

An alternative to a covalently attached indicator is a competition between an indicator (I) and an analyte (guest (G)) for the binding pocket of a receptor (host (H))[154,155,156] supposedly allowing for a more responsive color change than with a regular host-guest approach. The process now involves an equilibrium between four entities as shown in the following equation

$$HI + G \rightleftharpoons HG + I \quad \text{(B.5)}$$

the binding constant K for the indicator-displacement process is now

$$K = \frac{[HG][I]}{[HI][G]} \quad \text{(B.6)}$$

of course other equilibria occurring during this process have to be considered

$$H + I \rightleftharpoons HI \quad \text{(B.7)}$$

and

$$H + G \rightleftharpoons HG \quad \text{(B.8)}$$

The absorbance is in the framework of the indicator-displacement assay written as

$$A = \epsilon_I b[I] + \epsilon_{HI} b[HI]. \tag{B.9}$$

With these relations in hand it is tedious but trivial[157] to write the host-guest concentration ($[HG]$) as a function of the total host ($[H]_t$), total guest ($[G]_t$), and total indicator ($[I]_t$) concentrations as the following cubic equation

$$\begin{aligned} &K_{HG}(1-K)[HG]^3 + (K_{HG}K[G]_t + K_{HG}[I]_t - (1-K) - K_{HG}[G]_t(1-K) \\ &- K_{HG}[H]_t(1-K))[HG]^2 + (K_{HG}[H]_t[G]_t(1-K) - K_{HG}K[G]_t^2 \\ &+ K_{HG}[I]_t[G]_t - K_{HG}K[H]_t[G]_t - K[G]_t)[HG] + K_{HG}K[H]_t[G]_t^2 = 0 \end{aligned} \tag{B.10}$$

B.2 Discussion

Both the standard host-guest and indicator-displacement approaches require solution of a set of non-linear equations, quadratic and cubic, respectively. Several straightforward algorithms are well known for dealing with such systems. One of the most used of these approaches being Newton's method; but analytic formulas are available and allow the creation of a simpler interface. The quadratic equation B.4 has two well-known roots,

$$[HG]_1 = \frac{\sqrt{-(K_{HG}[H]_t + K_{HG}[G]_t + 1)^2 - 4K_{HG}^2[H]_t[G]_t}}{2K_{HG}} + \frac{(K_{HG}[H]_t + K_{HG}[G]_t + 1)}{2K_{HG}} \tag{B.11}$$

and

$$[HG]_2 = -\frac{\sqrt{-(K_{HG}[H]_t + K_{HG}[G]_t + 1)^2 - 4K_{HG}^2[H]_t[G]_t}}{2K_{HG}} + \frac{(K_{HG}[H]_t + K_{HG}[G]_t + 1)}{2K_{HG}} \tag{B.12}$$

However, Equation B.10 is a cubic equation and the analytical solutions are harder to characterize; the method of Viéte[158] is in this example used to obtain the cubic roots. The following set of variable has to be defined before introducing the expression for the cubic roots

$$T = K_{HG}(1 - K) \tag{B.13}$$

$$N = K_{HG}K[H]_t[G]_t^2 \tag{B.14}$$

$$S = K_{HG}K[G]_t + K_{HG}[I]_t - (1 - K) - K_{HG}[G]_t(1 - K) - K_{HG}[H]_t(1 - K) \tag{B.15}$$

$$F = K_{HG}[H]_t[G]_t(1 - K) - K_{HG}K[G]_t^2 + K_{HG}[I]_t[G]_t - K_{HG}K[H]_t[G]_t - K[G]_t \tag{B.16}$$

$$p = \frac{\frac{3F}{T} - \frac{S^2}{T^2}}{3} \tag{B.17}$$

$$Q = \frac{\frac{2S^3}{T^3} - \frac{9SF}{T^2} + \frac{27N}{T}}{27} \tag{B.18}$$

$$\Phi = \arccos\left(\frac{-0.5Q}{\sqrt{\frac{P^3}{27}}}\right) \tag{B.19}$$

$$Temp = 2\sqrt{\frac{p}{3}} \tag{B.20}$$

Using these definitions equation B.10 can be rewritten as

$$T[HG]^3 + S[HG]^2 + F[HG] + N \tag{B.21}$$

The solutions corresponding to this equation are

$$\begin{aligned} [HG]_1 &= Temp \times \cos\frac{\Phi}{3} - \frac{S}{3T} \\ [HG]_2 &= -Temp \times \cos\frac{\Phi + \pi}{3} - \frac{S}{3T} \\ [HG]_3 &= -Temp \times \cos\frac{\Phi - \pi}{3} - \frac{S}{3T} \end{aligned} \tag{B.22}$$

if and only if

$$\left(\frac{Q^2}{4} + \frac{P^3}{27}\right) < 0 \tag{B.23}$$

In our problem, two of the roots can be discarded as they do not represent realistic values of the concentration [HG]. It is noteworthy to mention that the selected solution oscillates between two roots depending on the value of the binding constant K (the cutoff point being K=1). This mathematical model allows some flexibility in the manipulation of the system parameters (*i.e.* concentrations, equilibrium constants, and molar absorptivities). The computer program was designed to simulate binding isotherms (concentration of guest *vs.* absorbance). Figure B.1 shows a comparison between the isotherm binding curve for a traditional guest-host model (classical sensor system) and the corresponding isotherm for an indicator-displacement assay process. In order to test the latter, we generated the binding isotherm corresponding to the indicator-displacement assay for tartrate[159] and compared it to an independent experimental study (Figures B.2 and B.3). The mathematical model performs well and the theoretical binding curves agree favorably with experiment. The real motivation for developing this mathematical model was to allow the simulation and optimization of indicator-displacement systems by varying the different parameters (concentrations, equilibrium constants, and molar absorptivities) as an alternative to brute force experimental trials. This is further discussed in Ref. 157.

The previous computer program allowed the optimization of an assay for the analysis of tartrate and malate in Pinot Noir grapes. The concentrations are important in determining the maturity of the grapes[160]. While both

tartaric and malic acids are present when the grapes are picked (before the ripening period) the concentration of malic acid then decreases but the concentration of tartaric acid remains constant during Véraison . The experimental studies together with the theoretical model can help predicting the state of ripeness of the Pinot Noir grapes (Figures B.4 and B.5). During Véraison, the malic acid is consumed as an energy source; the optimal state of ripeness is at the end of Véraison meaning when the steepest inflexion is found in Figure B.5, around fifty-six days.

Figure B.1: Comparison of the theoretical isotherm binding curve for an indicator displacement assay process (cubic) with the theoretical binding isotherm for a classical sensor system (quadratic).

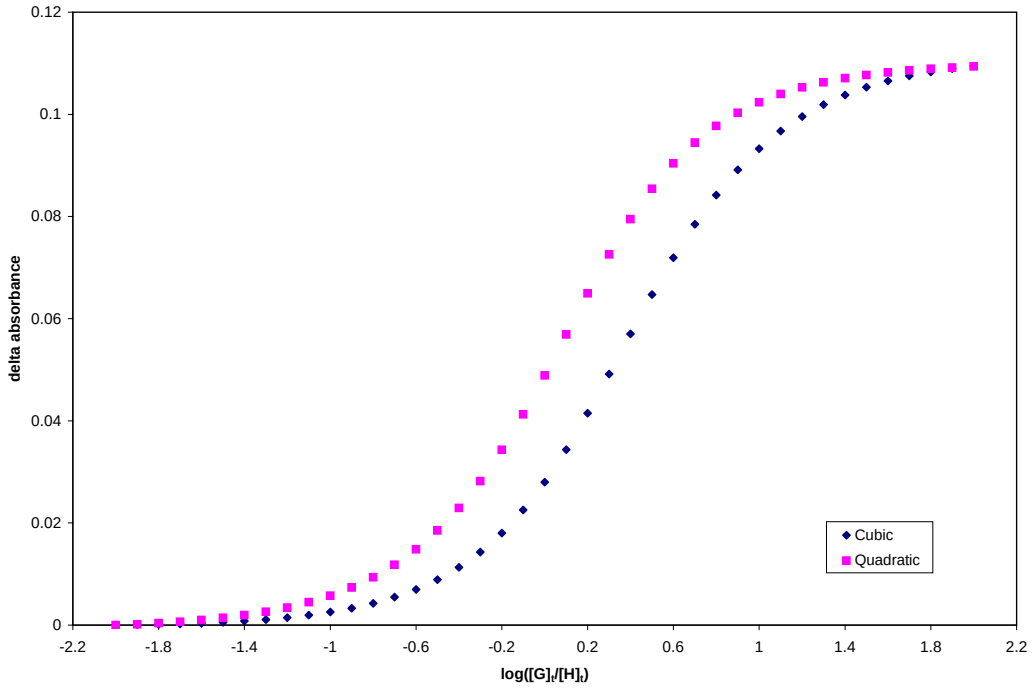

Figure B.2: Comparison of theoretical and experimental binding isotherms for an indicator displacement assay; guest concentration (1.58mM), host concentration (185 M), indicator concentration (150 M).

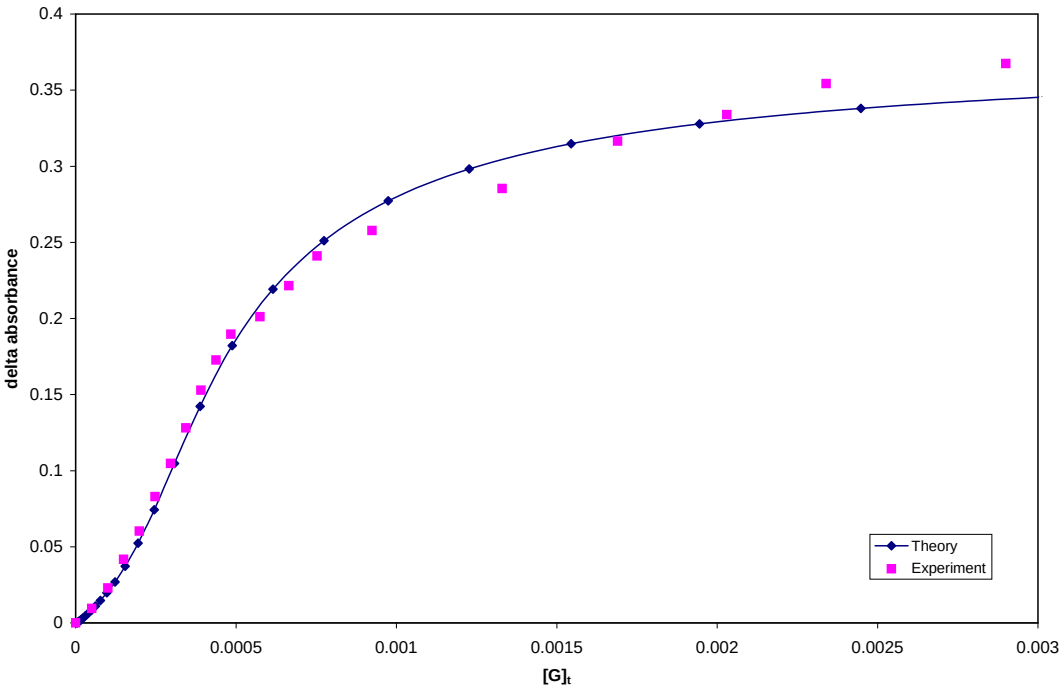

Figure B.3: Comparison of theoretical and experimental binding isotherms for an indicator displacement assay; guest concentration (1.58mM), host concentration (185 M), indicator concentration (150 M).

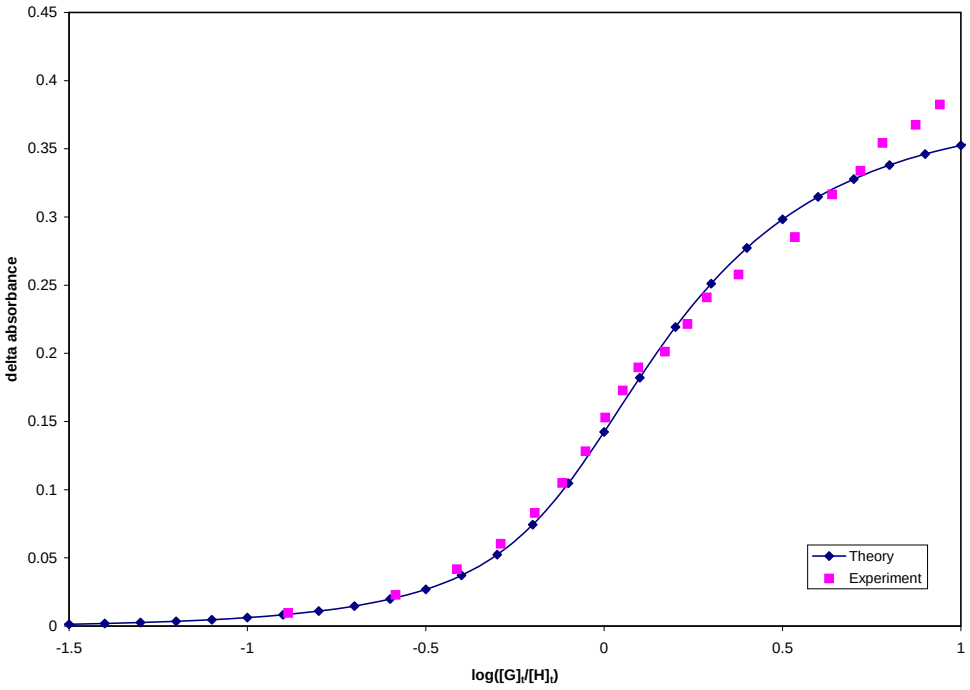

Figure B.4: Binding isotherms for the indicator displacement titration of malic acid. Tartaric acid and must were added for the grape juice analysis.

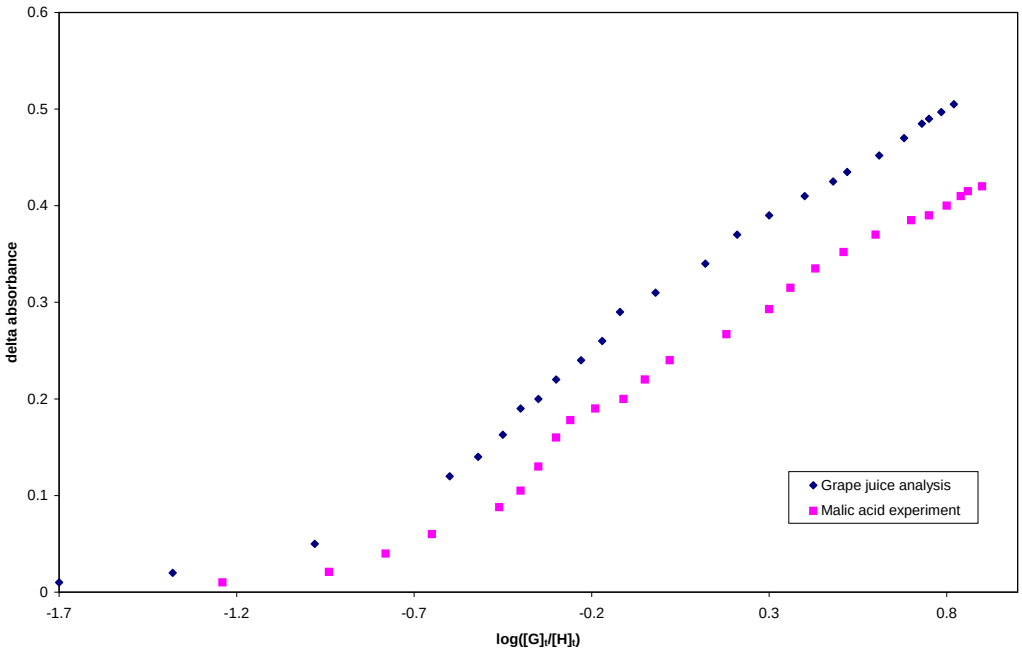

Figure B.5: Comparison of the concentration of malate from the literature and from experiment during Véraison.

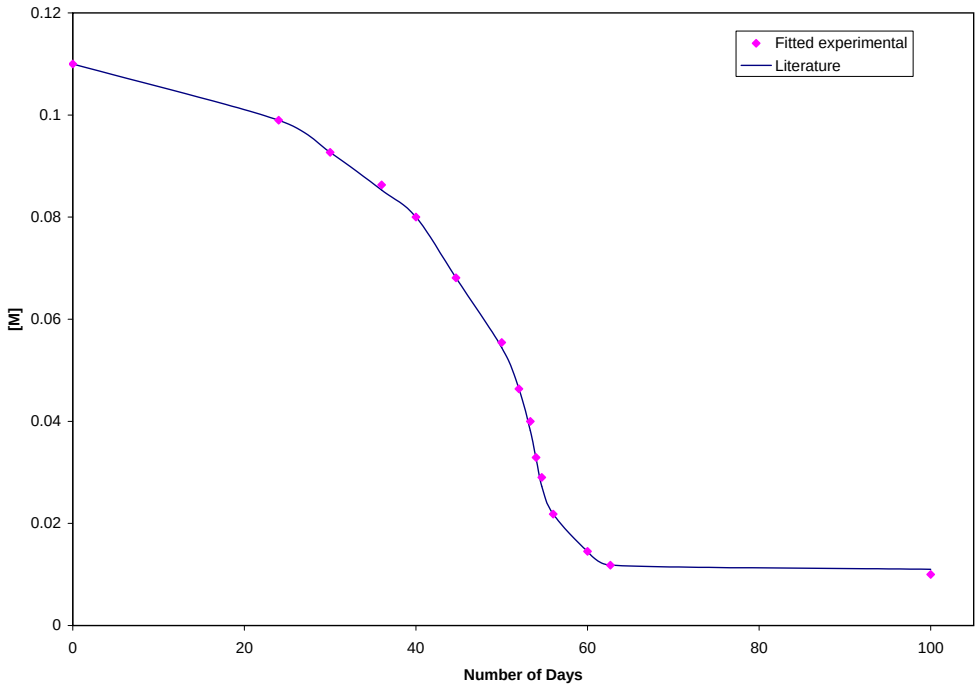

Appendix C

List of Publications

1. Anna M. Piatek, Yannick J. Bomble, Sheryl L. Wiskur, and Eric V. Anslyn, "Threshold Detection Using Indicator-Displacement Assays: An Application in the Analysis of Malate in Pinot Noir Grapes", *J. Am. Chem. Soc.* 126, 6072 (2004).

2. Yannick J. Bomble, Kurt W. Sattelmeyer, John F. Stanton, and Jürgen Gauss, "On the Vertical Excitation Energy of Cyclopentadiene", *J. Chem. Phys.* 121, 5236 (2004).

3. Gunther Hennrich, Wendi M. David, Yannick J. Bomble, Eric V. Anslyn, Jennifer S. Brodbelt, and John F. Stanton, "Self-Assembling Dimeric and Trimeric Aggregates Based on Solvophobic and Charge-Pairing Interactions", *Supramolecular Chemistry* 16, 521 (2004).

4. Yannick J. Bomble, Jamal C. Saeh, John F. Stanton, Péter G. Szalay, Mihály Kállay, and Jürgen Gauss, "Equation-of-Motion Coupled-Cluster Methods for Ionized States with an Approximate Treatment of Triple

Excitations", *J. Chem. Phys.* 122, 154107 (2005).

5. Yannick J. Bomble, John F. Stanton, Mihály Kállay, and Jürgen Gauss, "Coupled Cluster Methods Including Noniterative Approximate Quadruple Excitation Corrections", *J. Chem. Phys.* 123, 054101 (2005).

6. Yannick J. Bomble, "Computer Software Review: ADF 2005 (Amsterdam Density Functional 2005)", *J. Am. Chem. Soc.* 128, 3103 (2006).

7. Yannick J. Bomble, Juana Vázquez, Mihály Kállay, Christine Michauk, Péter G. Szalay, Attila G. Császár, Jürgen Gauss, and John F. Stanton, "HEAT: High Accuracy Extrapolated Ab Initio Thermochemistry II: Minor Improvements to the Protocol and a Vital Simplification", accepted for publication in *J. Chem. Phys.* (2006).

8. Steven E. Wheeler, Kenneth A. Robertson, Wesley D. Allen, Henry F. Schaefer, Yannick J. Bomble, and John F. Stanton, "Thermochemistry of Key Soot Formation Intermediates: Isomers of C_3H_3", to be submitted to *J. Chem. Phys.* (2006).

9. Michael H. Cortez, Nicole R. Brinkmann, William F. Polik, Yannick J. Bomble, Peter R. Taylor, and John F. Stanton, "Factors Con-

tributing to the Accuracy of Harmonic Force Field Calculations", *in preparation.* (2006).

10. Sébastien Villaume, Alain Strich, Chantal Daniel, S. Ajith Perera, Rodney J. Bartlett, Yannick J. Bomble, and John F. Stanton, "Electronic Spectroscopy of $Cr(CO)_6$ and $Cr(CO)_5$: Coupled Cluster Calculations", *in preparation.* (2006).

Appendix D

Threshold Detection Using Indicator-Displacement Assays: An Application in the Analysis of Malate in Pinot Noir Grapes

Anna M. Piatek, Yannick J. Bomble, Sheryl L. Wiskur, and Eric V. Anslyn

Abstract

The mathematics for modeling indicator-displacement assay isotherms is presented and contrasted to the classical host-guest binding isotherm. It is shown that the signal response can be tuned to occur closer to 1 equiv of guest relative to a standard binding algorithm. This delay in response leads to a better triggering protocol for threshold detection schemes. The determination of malate in Pinot Noir must was calculated using this new mathematical model, which demonstrates how a color change can be tuned to occur near a desired concentration of analyte.

J. Am. Chem. Soc. 126, 6072 (2004)

Appendix E

On the Vertical Excitation Energy of Cyclopentadiene

Yannick J. Bomble, Kurt W. Sattelmeyer, John F. Stanton, and Jürgen Gauss

Abstract

The vertical excitation energy for the lowest valence $\pi \rightarrow \pi^*$ transition of cyclopentadiene is investigated. Using a combination of high-level theoretical methods and spectroscopic simulations, the vertical separation at the ground state geometry is estimated to be 5.43±0.05 eV. This value is intermediate between those calculated with coupled-cluster and multireference perturbation theory methods and is about 0.13 eV higher than the observed maximum in the absorption profile.

J. Chem. Phys. 121, 5236 (2004)

Appendix F

Self-Assembling Dimeric and Trimeric Aggregates Based on Solvophobic and Charge-Pairing Interactions

Gunther Hennrich, Wendi M. David, Yannick J. Bomble, Eric V. Anslyn, Jennifer S. Brodbelt, and John F. Stanton

Abstract

Self-assembly processes based on shape complementarity and noncovalent binding interactions are widely recognized as a fundamental principle in nature. Besides charge pairing and hydrogen bonding, hydrophobic interactions play a crucial role in water. Here we report the self-assembly of structurally simple monomers to yield defined dimeric and trimeric aggregates in highly polar media, based on ionic and solvophobic interactions. NMR, mass spectrometry and curve fitting were used to characterize these supramolecular assemblies in watermethanol solutions.

Supramolecular Chemistry 16, 521 (2004)

Appendix G

Equation-of-Motion Coupled-Cluster Methods for Ionized States with an Approximate Treatment of Triple Excitations

Yannick J. Bomble, Jamal C. Saeh, John F. Stanton, Péter G. Szalay, Mihály Kállay, and Jürgen Gauss

Abstract

The accuracy of geometries and harmonic vibrational frequencies is evaluated for two equation-of-motion ionization potential (EOMIP) coupled-cluster methods including CC3 and CCSDT-3 triples corrections. The first two Σ states and first Π state of the N_2^+, CO^+, CN, and BO diatomic radicals are studied. The calculations show a tendency for the CC3 variant to overestimate the bond lengths and to underestimate the vibrational frequencies, while the CCSDT-3 variant seems to be more reliable. It is also demonstrated that the accuracy of such methods is comparable to sophisticated traditional multireference approaches and the full configuration interaction method.

J. Chem. Phys. 122, 154107 (2005)

Appendix H

Coupled Cluster Methods Including Noniterative Approximate Quadruple Excitation Corrections

Yannick J. Bomble, John F. Stanton, Mihály Kállay, and Jürgen Gauss

Abstract

A new method is presented for treating the effects of quadruple excitations in coupled-cluster theory. In the approach, quadruple excitation contributions are computed from a formula based on a non-Hermitian perturbation theory analogous to that used previously to justify the usual non-iterative triples correction used in the coupled cluster method known as CCSD(T). The method discussed in this paper plays a parallel role in improving energies obtained with the full singles, doubles and triples method (CCSDT), and is known as CCSDT(Q). The method is tested for an extensive set of examples, and is shown to provide total energies that compare favorably with those obtained with the full singles, doubles, triples and quadruples (CCSDTQ) method.

J. Chem. Phys. 123, 054101 (2005)

Appendix I

Computer Software Review: ADF 2005 (Amsterdam Density Functional 2005)

Yannick J. Bomble

Abstract

The quantum chemistry package ADF 2005 was tested on two different platforms (Linux and Windows XP). The performance of this package as well as its relevance for chemical applications were assessed. ADF was found to be, while limited to density functional theory (DFT) based methods, a useful tool for studying chemical problems.

J. Am. Chem. Soc. 128, 3103 (2006)

Appendix J

HEAT: High Accuracy Extrapolated Ab Initio Thermochemistry II: Minor Improvements to the Protocol and a Vital Simplification

Yannick J. Bomble, Juana Vázquez, Mihály Kállay, Christine Michauk, Péter G. Szalay, Attila G. Császár, Jürgen Gauss, and John F. Stanton

Abstract

The recently-developed HEAT method for theoretical thermochemistry, which is intimately related to other high-precision protocols such as the Weizmann-3 (W3) and focal-point approaches, is revisited. Some minor improvements in theoretical rigor are introduced which do not lead to any significant additional computational overhead, but are shown to have a negligible overall effect on the accuracy. In addition, the method is extended to completely treat electron correlation effects up to pentuple excitations. The use of an approximate treatment of quadruple and pentuple excitations is suggested; the former as a pragmatic approximation for standard cases, and the latter when extremely high accuracy is required. For a test suite of molecules that have rather precisely known enthalpies of formation (as taken from Ruscic's Active

Thermochemical Tables (ATcT)), the largest deviations between theory and experiment are 0.52, −0.70 and 0.51 kJ mol^{-1} for the latter three methods, respectively. Some perspective is provided on this level of accuracy, and sources of remaining systematic deficiencies in the approaches are discussed.

accepted for publication in *J. Chem. Phys.* (2006)

Appendix K

Thermochemistry of Key Soot Formation Intermediates: Isomers of C_3H_3

Steven E. Wheeler, Kenneth A. Robertson, Wesley D. Allen, Henry F. Schaefer, Yannick J. Bomble, and John F. Stanton

Abstract

Accurate standard enthalpies of formation for allene, propyne, and four C_3H_3 isomers important in the formation of soot during combustion have been determined through systematic extrapolations of ab initio energies within the focal point method of Allen and co-workers. Further corrections have been applied for zero-point vibrational energy and core-valence correlation, non-Born-Oppenheimer, and scalar relativistic effects. Electron correlation has been accounted for through second-order Z-averaged perturbation theory (ZAPT2) and restricted open-shell coupled cluster theory through approximate connected quadruple excitations [ROCCSD, ROCCSD(T), ROCCSDT, and UCCSDT(Q)] utilizing the correlation-consistent hierarchy of basis sets, cc-pVXZ (X = D,T,Q,5,6). All geometries were fully optimized using ROCCSD(T) with the TZ(2d1f,2p1d) basis set. Our recommended values for

the enthalpies of formation are as follows: (propargyl) = 84.7, (1 propynyl) = 126.6, (cycloprop 1 enyl) = 125.7, (cycloprop 2 enyl) = 117.3, (allene) = 47.2, and (propyne) = 46.2 kcal mol^{-1}. The corresponding energies for C_3H_3 isomers 1 propynyl, cycloprop 1 enyl, and cycloprop 2 enyl, relative to propargyl radical, are 41.9, 40.9, and 32.7 kcal mol^{-1}. These isomerization energies are roughly 1 kcal mol^{-1} larger than previous coupled cluster predictions and several kcal mol^{-1} below those previously predicted using density functional theory. Predicted bond dissociation energies for the methyl and acetelynic C-H bonds in propyne are 90.2 and 132.1 kcal mol^{-1}, respectively.

to be submitted to *J. Chem. Phys.* (2006)

Appendix L

Factors Contributing to the Accuracy of Harmonic Force Field Calculations

Michael H. Cortez, Nicole R. Brinkmann, William F. Polik, Yannick J. Bomble, Peter R. Taylor, and John F. Stanton

Abstract

The major factors affecting the accuracy of computations for the harmonic force field of water are presented. By systematically varying the level of approximation in basis set, electron correlation, electron interactions, and relativistic effects, the error associated with each of these factors on the computation of harmonic frequencies for water was characterized. Analysis of this data resulted in the quantification of the underlying sources of error in theoretical computations of harmonic vibrational frequencies for water. The error associated with the cc-pVQZ Hartree-Fock wavefunction was 1.6 cm^{-1}, as determined from extending the computations to larger basis sets. Since the average absolute difference between computed vibrational frequencies at the CCSD(T) and CCSDT levels of theory was 0.3 cm^{-1}, the CCSD(T) theory was chosen for computational efficiency. The error from valence electron interactions was addressed by adding diffuse functions to the basis set and found to

be 3.7 cm^{-1} when using the aug-cc-pVQZ basis set. The error associated with freezing core electrons was 5 cm^{-1} and with neglecting relativistic effects was 2 cm^{-1}. Due to a fortuitous cancellation among the various sources of error, the harmonic frequencies for H_2O computed using the CCSD(T)/aug-cc-pVQZ model chemistry were on average within 2 cm^{-1} of experimental vibrational frequencies.

in preparation (2006)

Bibliography

1. R. J. Harrison and N. C. Handy, *Chem. Phys. Lett.* 95, 386 (1983)

2. C. W. Bauschlicher and P. R. Taylor, *J. Chem. Phys.* 85, 2779 (1986)

3. C. W. Bauschlicher, S. R. Langhoff, P. R. Taylor, and H. Partridge, *Chem. Phys. Lett.* 126, 436 (1986)

4. R. J. Bartlett, *Ann. Rev. Phys. Chem.* 32, 359 (1981)

5. K. A. Bruekner, *Phys. Rev.* 97, 1353 (1954)

6. K. A. Bruekner, *Phys. Rev.* 100, 36 (1955)

7. J. Goldstone, *Proc. R. Soc. London Ser. A.* 239, 267 (1957)

8. J. Cízek, *J. Chem. Phys.* 45, 4256 (1966)

9. R. J. Bartlett, *J. Phys. Chem.* 93, 1697 (1989)

10. T. D. Crawford and H. F. Schaefer, in *Reviews of Computational Chemistry*, Vol X, ed K. B. Lipkowitz and D. B. Boys, VCH, New York, p.33 (1999)

11. This is not entirely true, the first implementation of coupled cluster theory was done by Cízek in 1966. This work is shown in Ref. 8 where the CCSDT method is presented.

12. J. A. Pople, R. Krishnan, H. B. Schlegel, and J. S. Binkley, *Int. J. Quantum Chem. Symp.* 14, 545 (1978)

13. R. J. Bartlett and G. D. Purvis, *Int. J. Quantum Chem.* 14, 561 (1978)

14. G. D. Purvis and R. J. Bartlett, *J. Chem. Phys.* 76, 1910 (1982)

15. J. Gauss, J. F. Stanton, and R. J. Bartlett, *J. Chem. Phys.* 95, 2623 (1991)

16. M. Kállay and P. R. Surján, *J. Chem. Phys.* 113, 1359 (2000); S. Hirata, M. Nooijen, and R. J. Bartlett, *Chem. Phys. Lett.* 326, 255 (2000); S. A. Kucharski, M. Wloch, M. Musial, and R. J. Bartlett, *J. Chem. Phys.* 115, 8263 (2001); H. Larsen, K. Hald, J. Olsen, and P. Jørgensen, *J. Chem. Phys.* 115, 3015 (2001); K. Kowalski and P. Piecuch, *J. Chem. Phys.* 115, 643 (2001) [excited state]; J. Noga and R. J. Bartlett, *J. Chem. Phys.* 86, 7041 (1987) [ground state].

17. S. A. Kucharski and R. J. Bartlett, *J. Chem. Phys.* 97, 4282 (1992)

18. M. Musial, S. A. Kucharski, and R. J. Bartlett, *J. Chem. Phys.* 116, 4382 (2002)

19. K. Raghavachari, G. W. Trucks, J. A. Pople, and M. Head-Gordon, *Chem. Phys. Lett.* 157, 479 (1989)

20. R. J. Bartlett, J. D. Watts, S. A. Kucharski, and J. Noga, *Chem. Phys. Lett.* 165, 513 (1990)

21. J. F. Stanton, *Chem. Phys. Lett.* 281, 130 (1997)

22. Y. J. Bomble, J. F. Stanton, M. Kállay, and J. Gauss, *J. Chem. Phys.* 123, 054101 (2005)

23. R. J. Bartlett, J. D. Watts, S. A. Kucharski, and J. Noga, *Chem. Phys. Lett.* 165, 513 (1990)

24. S. A. Kucharski, and R. J. Bartlett, *J. Chem. Phys.* 108, 9221 (1998)

25. S. Hirata, M. Nooijen, I. Grabowski, and R. J. Bartlett, *J. Chem. Phys.* 114, 3919 (2001)

26. S. Hirata, P.-D. Fan, A. A. Auer , M. Nooijen, and P. Piecuch, *J. Chem. Phys.* 121, 12197 (2004)

27. A. Tajti, P. G. Szalay, A. G. Csaszar, M. Kállay, J. Gauss, E. F. Valeev, B. A. Flowers, J. Vazquez, and J. Stanton, *J. Chem. Phys.* 121, 11599 (2004)

28. B. A. Flowers, P. G. Szalay, J. F. Stanton, M. Kállay, J. Gauss, and A. G. Császár, *J. Phys. Chem. A* 108, 3195 (2004)

29. J. F. Stanton, *J. Chem. Phys.* 115, 10382 (2001)

30. L. Farnell, J. A. Pople, and L. Radom, *J. Phys. Chem.* 87, 79 (1983)

31. J. Geertsen, M. Rittby, and R. J. Bartlett, *Chem. Phys. Lett.* 164, 57 (1989)

32. D. Mukherjee and P. K. Mukherjee, *Chem. Phys.* 39, 325 (1979)

33. K. Emrich, *Nucl. Phys. A* 351, 379 (1981)

34. H. Sekino and R. J. Bartlett, *Int. J. Quantum Chem. Symp.* 18, 255 (1984)

35. L. Meissner and R. J. Bartlett, *J. Chem. Phys.* 94, 6670 (1991)

36. J. F. Stanton and R. J. Bartlett, *J. Chem. Phys.* 98, 7029 (1993)

37. R. J. Bartlett and J. F. Stanton, *Rev. Comput. Chem.* 5, 65 (1994)

38. M. Nooijen and J. G. Snijders, *Int. J. Quantum. Chem Quantum. Chem. Symp.* 26, 55 (1992)

39. M. Nooijen and J. G. Snijders, *Int. J. Quantum. Chem.* 48, 15 (1993)

40. J. F. Stanton and J. Gauss, *J. Chem. Phys.* 101, 8938 (1994)

41. J. F. Stanton and J. Gauss, *J. Chem. Phys.* 111, 8785 (1999)

42. J. F. Stanton, *J. Chem. Phys.* 99, 8840 (1993); J. F. Stanton and J. Gauss, *J. Chem. Phys.* 100, 4695 (1994)

43. M. Nooijen and R. J. Bartlett,*J. Chem. Phys.* 102, 3629 (1995)

44. M. Musiał, S. A. Kucharski, and R. J. Bartlett, *J. Chem. Phys.* 118, 1128 (2003)

45. T. H. Dunning, *J. Chem. Phys.* 90, 1007 (1989)

46. J. D. Watts and R. J. Bartlett, *Chem. Phys. Lett.* 258, 581 (1996) [excitation energies]; J. Noga, R. J. Bartlett, and M. Urban, *Chem. Phys. Lett.* 134, 126 (1987) [ground state].

47. H. Koch, O. Christiansen, P. Jørgensen, A.M.S de Meras, and T. Helgaker, *J. Chem. Phys.* 106, 1808 (1997)

48. O. Christiansen, H. Koch, and P. Jørgensen, *J. Chem. Phys.* 103, 7429 (1995)

49. K. Kowalski and P. Piecuch, *J. Chem. Phys.* 113, 18 (2000)

50. K. Kowalski and P. Piecuch, *J. Chem. Phys.* 113, 5644 (2000)

51. P. Csaszar and P. Pulay, *J. Mol. Struc.* 114, 31 (1984)

52. M. Head-Gordon, R. J. Rico, M. Oumi, and T. J. Lee, *Chem. Phys. Letter.* 219, 21 (1994)

53. M. Urban, J. Noga, S. J. Cole, and R. J. Bartlett, *J. Chem. Phys.* 83, 4041 (1986)

54. J. Noga, R. J. Bartlett, and M. Urban, *Chem. Phys. Lett.* 134, 126 (1987)

55. S. A. Kucharski and R. J. Bartlett, *Adv. Quantum. Chem.* 18, 281 (1986)

56. S. A. Kucharski, J. Noga, and R. J. Bartlett, *J. Chem. Phys.* 90, 7282 (1989)

57. S. A. Kucharski and R. J. Bartlett, *Chem. Phys. Lett.* 158, 550 (1989)

58. S. A. Kucharski and R. J. Bartlett, *Chem. Phys. Lett.* 206, 574 (1993)

59. CCSDT[Q][23 24 25 26] was initially designated as CCSDT(Q) by Bartlett and Kucharski but is referred to as CCSDT[Q] here because of its formal similarity to CCSD[T].

60. J. F. Stanton, W. N. Lipscomb, D. H. Magers, and R. J. Bartlett, *J. Chem. Phys.* 90, 1077 (1989)

61. $\mathcal{L}$ is the lambda vector that plays a central role in coupled cluster gradient theory[62].

62. L. Adamowicz, W. D. Laidig, and R. J. Bartlett, *Int. J. Quantum. Chem.* 18, 245 (1984)

63. P. O. Löwdin *J. Math. Phys.* 3, 969 (1962)

64. T. D. Crawford and J. F. Stanton, *Int. J. Quantum. Chem.* 70, 601 (1998)

65. S. A. Kucharski and R. J. Bartlett, *J. Chem. Phys.* 108, 5243 (1998)

66. S. R. Gwaltney and M. Head-Gordon, *J. Chem. Phys.* 115, 2014 (2001)

67. J. F. Stanton, J. Gauss, J. D. Watts, W. J. Lauderdale, and R. J. Bartlett, *Int. J. Quantum Chem. Symp.* 26, 879 (1992)

68. M. Kállay and P. R. Surján, *J. Chem. Phys.* 115, 2945 (2001)

69. G. von Laszewski, B. Ruscic, P. Wagstrom, S. Krishnan, K. Amin, S. Nijsure, S. Bittner, R. Pinzon, J. C. Hewson, M. L. Morton, and A. Wagner, in "Lecture Notes in Computer Science, Vol 2536" pp. 25-38, M. Parashar, ed. (Springer, Berlin, 2002)

70. B. Ruscic, R. E. Pinzon, M. L. Morton, G. von Laszevski, S. J. Bittner, S. G. Nijsure, K. A. Amin, M. Minkoff, and A. F. Wagner, *J. Phys. Chem. A* 108, 9979 (2004)

71. L. Farnell, J. A. Pople, and L. Radom, *J. Phys. Chem.* 87, 79 (1983)

72. P. J. Szalay, J. Vázquez, C. Simmons, and J. F. Stanton, *J. Chem. Phys.* 121, 7624 (2004)

73. This error occurs for the problematic CN molecule. When CN is excluded, the maximum absolute error becomes 0.228 mE_H (for N_2).

74. R. A. Kendall and T. H. Dunning, *J. Chem. Phys.* 96, 6796 (1992)

75. D. Feller, *J. Chem. Phys.* 96, 6104 (1992)

76. T. Helgaker, W. Klopper, H. Koch, and J. Noga, *J. Chem. Phys.* 106, 9639 (1997)

77. Note that this is not the case when using CCSDT(Q) where the bottleneck calculations involve CCSDT with large basis sets.

78. R. D. Cowan and M. Griffin, *J. Opt. Soc. Am.* 66, 1010 (1976)

79. R. L. Martin, *J. Phys. Chem.* 87, 750 (1983)

80. W. Klopper, *J. Comp. Chem.* 18, 20 (1997)

81. A. G. Császár, W. Klopper, and H. M. Quinney, *Mol. Phys.* 99, 1769 (2001)

82. H. Sellers and P. Pulay, *Chem. Phys. Lett.* 103, 463 (1984)

83. N. C. Handy, Y. Yamaguchi, and H. F. Schaefer, *J. Chem. Phys.* 84, 4481 (1986)

84. N. C. Handy and A. M. Lee, *Chem. Phys. Lett.* 252, 425 (1996)

85. W. Kutzelnigg, *Mol. Phys.* 90, 909 (1997)

86. I. M. Mills, in *Modern Spectroscopy: Modern Research*, edited by K. N. Rao and C. W. Matthews (Academic Press, New York, 1972), pp. 115-140

87. V. Barone, *J. Chem. Phys.* 120, 3059 (2004)

88. M. S. Schuurman, S. R. Muir, W. D. Allen, and H. F. Schaefer, *J. Chem. Phys.* 120, 11586 (2004)

89. Numerical results from all three implementations appear to agree with each other, and a sum-over-states direct summation program [J. Vázquez and J. F. Stanton, *Mol. Phys.* 104, 377 (2006)]. The correct equation is

$$\begin{aligned} G_0 &= -\frac{1}{4}\sum_{\alpha} B_e^{\alpha} + \frac{1}{64}\sum_{k} \phi_{kkkk} - \frac{7}{576}\sum_{k} \frac{\phi_{kkk}^2}{\omega_k} \\ &+ \frac{3}{64}\sum_{k\neq l} \frac{\omega_l \phi_{kkl}^2}{4\omega_k^2 - \omega_l^2} - \frac{1}{4}\sum_{k<l<m} \frac{\phi_{klm}^2 \omega_k \omega_l \omega_m}{D_{klm}} \\ &- \frac{1}{8}\sum_{k\neq l}\sum_{\alpha} B_e^{\alpha} \left(\zeta_{kl}^{\alpha}\right)^2 . \end{aligned}$$

See Ref. 27 for a definition of the symbols in this equation. In Ref. 27, the fifth and sixth terms were in error. Further, the kinetic energy elements in Ref. 90 were in error, which was addressed to some degree in Ref. 87.

90. V. Barone and C. Minishino, *J. Mol. Struct. (THEOCHEM)* 330, 365 (1995)

91. In the course of this research, we have noted a similar property of the CCSD[T] and the CCSD(T) methods. For the same set of molecules and atoms the error with respect to CCSDT in CCSD[T] grows with the size of the basis set, while that of CCSD(T) becomes sligtly smaller. The magnitude of this effect is not as large as in the corresponding quadruples methods, but is still significant: respective errors are 0.450 and 0.482 mE_H with cc-pVDZ and 0.624 and 0.452 mE_H with cc-pVTZ for CCSD[T] and CCSD(T).

92. J. Noga, R. J. Bartlett, and M. Urban, *Chem. Phys. Lett.* 134, 146 (1987)

93. U. Kaldor, *Chem. Phys. Lett.* 185, 131 (1991)

94. E. R. Davidson and W. T. Borden, *J. Phys.Chem.* 87, 4783 (1983)

95. J. F. Stanton and J. Gauss, *Adv. Chem. Phys.* 125, 101 (2003)

96. M. Rittby and R. J. Bartlett, *J. Phys. Chem.* 92, 3033 (1988)

97. J. D. Watts and R. J. Bartlett, *Chem. Phys. Lett.* 233, 81 (1995)

98. K. W. Sattelmeyer, J. F. Stanton, J. Olsen, and J. Gauss, *Chem. Phys. Lett.* 347, 499 (2001)

99. K. Hirao and H. Nakatsuji, *J. Comp. Phys.* 45, 246 (1982)

100. E. R. Davidson, *J. Comp. Phys.* 17, 87 (1975)

101. J. Gauss and J. F. Stanton, *Phys. Chem. Chem. Phys.* 2, 2047 (2000)

102. The same method was implemented earlier with a non-proper scaling by Hirata *et al.*[104].

103. M. Kállay and J. Gauss, *J. Chem. Phys.* 121, 9257 (2004)

104. S. Hirata, M. Nooijen, and R. J. Bartlett, *Chem. Phys. Lett.* 328, 459 (2000)

105. J. F. Stanton and J. Gauss, *J. Chem. Phys.* 111, 8785 (1999)

106. P. G. Szalay and R. J. Bartlett, *Chem. Phys. Lett.* 214, 481 (1993)

107. P. G. Szalay and R. J. Bartlett, *J. Chem. Phys.* 103, 3600 (1995)

108. H. Lischka, R. Shepard, I. Shavitt, F. B. Brown, R. M. Pitzer, R. Ahlrichs, H.-J. Böhm, A. H. H. Chang, D. C. Comeau, R. Gdanitz, H. Dachsel, M. Dallos, C. Erhard, M. Ernzerhof, G. Gawboy, P. Höchtl, S. Irle, G. Kedziora, T. Kovar, Th. Müller, V. Parasuk, M. Pepper, P. Scharf, H. Schiffer, M. Schindler, M. Schüler, E. Stahlberg, P. G. Szalay and J.-G. Zhao, COLUMBUS, An ab initio Electronic Structure Program, Release 5.8, (2001)

109. H. Lischka, R. Shepard, R. Pitzer, I. Shavitt, M. Dallos, T. Müller, P. Szalay, M. Seth, G. Kedziora, S. Yabushita, and Z. Zhang, *Phys. Chem. Chem. Phys.* 3, 664 (2001)

110. M. Kállay, J. Gauss, and P. G. Szalay, *J. Chem. Phys.* 119, 2991, (2003)

111. J. F. Stanton, *Chem. Phys. Lett.* 237, 20 (1995)

112. T.D. Crawford and J.F. Stanton, *J. Chem. Phys.* 112, 7873 (2000)

113. E. R. Davidson and A. A. Jarzecki, *Chem. Phys. Lett.* 285, 155 (1998)

114. C. Petrongolo, R. J. Buenker, and S. D. Peyerimhoff, *J. Chem. Phys.* 76, 3655 (1982)

115. H. Köppel, W. Domcke, and L. S. Cederbaum, *Adv. Chem. Phys.* 57, 59 (1984)

116. J. F. Stanton, K. W. Sattelmeyer, J. Gauss M. Allan, T. Skalicky, and T. Bally, *J. Chem. Phys.* 115, 1 (2001)

117. H. Stobbe and F. Dunnhaupt, *Berichte* 52, 1436 (1919)

118. L. W. Pickett, F. Paddock, and E. Sackter, *J. Am. Chem. Soc.* 63, 1073 (1941)

119. A. Sabljic and R. McDiarmid, *J. Chem. Phys.* 93, 3850 (1990)

120. Q.-Y. Shang and B. S. Hudson, *Chem. Phys. Lett.* 183, 63 (1991)

121. K. Andersson, P.-A. Malmqvist, B. O. Roos, A. J. Sadlej, and K. J. Wolinsky, *J. Phys. Chem.* 94, 5483 (1990)

122. K. Andersson, P.-A. Malmqvist, and B. O. Roos, *J. Chem. Phys.* 96, 1218 (1992)

123. L. Serrano-Andres, M. Merchan, I. Nebot-Gil, B. O. Roos, and M. Fulscher, *J. Am. Chem. Soc.* 115, 6184 (1993)

124. H. Nakano, T. Tsuneda, T. Hashimoto, and K. Hirao, *J. Chem. Phys.* 104, 2312 (1996)

125. J. D. Watts, S. R. Gwaltney, and R. J. Bartlett, *J. Chem. Phys.* 105, 6979 (1996)

126. J. D. Watts and R. J. Bartlett *Chem. Phys. Lett.* 258, 581 (1995)

127. H. Nakatsuji and K. Hirao, *J. Chem. Phys.* 68, 2053 (1978)

128. H. Nakatsuji, K. Ohta, and K. Hirao, *J. Chem. Phys.* 75, 409 (1986)

129. J. Wan, M. Ehara, M. Hada, and H. Nakatsuji, *J. Chem. Phys.* 113, 5245 (2000)

130. H. Nakatsuji, O. Kitao, and T. Yonezawa, *J. Chem. Phys.* 83, 723 (1985)

131. The TZ2P basis sets for carbon and hydrogen are fully documented elsewhere [J. Gauss, J. F. Stanton, and R. J. Bartlett, *J. Chem. Phys.* 97, 7825 (1992)].

132. R. A. Kendall, T. H. Dunning, and R. J. Harrison, *J. Chem. Phys.* 96, 6796 (1992)

133. Effects associated with inadequate treatment of core correlation by the cc-pVXZ basis sets were assessed by comparing EOM-CCSD excitation

energies calculated with the cc-pVTZ and cc-pCVTZ[134] basis sets and were entirely negligible (0.005 eV).

134. D. E. Woon and T. H. Dunning, *J. Chem. Phys.* 103, 4572 (1995)

135. M. Z. Gierski and F. Zerbetto, *J. Chem. Phys.* 99, 372 (1993)

136. A. C. Scheiner, G. E. Scuseria, J. E. Rice, T. J. Lee, and H. F. Schaefer, *J. Chem. Phys.* 87, 5361 (1987) (CCSD first derivatives); J. Gauss and J. F. Stanton, *Chem. Phys. Lett.* 276, 70 (1997) (CCSD second derivatives).

137. This calculation was carried out with a local version of the ACES II program package using EOM-CCSD level of theory with the basis set and the experimental geometry from Ref. 123

138. J. A. Pople, R. Krishnan, H. B. Schlegel, and J. S. Binkley, *Int. J. Quantum Chem. Symp.* 14, 545 (1978)

139. J. D. Watts and R. J. Bartlett, Int. J. Quantum Chem. Symp. 27, 51 (1993)

140. J. D. Watts, J. Gauss, and R. J. Bartlett, *J. Chem. Phys.* 98, 8718 (1993)

141. K. L. Bak, J. Gauss, P. Jørgensen, J. Olsen, T. Helgaker, and J. F. Stanton, *J. Chem. Phys.* 114, 6550 (2001)

142. T. H. Dunning, *J. Chem. Phys.* 53, 2823 (1970)

143. J. -M. Lehn, *Science* 295, 2400 (2002)

144. D. N. Reinhoudt and M. Crego-Calama, *Science* 295, 5564 (2002)

145. H. Fraser, J. Rebek, *Jr. Proc. Natl Acad. Sci. USA* 99, 4775 (2002)

146. L. R. MacGillvray and J. L. Atwood, *Nature* 389, 469 (1997)

147. J. De Mendoza, *Chem. Eur. J.* 4, 1373 (1998)

148. T. Grawe, T. Schrader, M. Gurrath, A. Kraft, and F. Osterod, *Org. Lett.* 2, 29 (2000)

149. H. -J. Schneider, *Chem. Soc. Rev.* 227 (1994)

150. D. B. Smithrud and F. Diederich, *J. Am. Chem. Soc.* 112, 339 (1990)

151. More details about the experimental procedure and results can be found in Ref. 153

152. δ_{AB} and δ_B are not resolved due to the time resolution of the NMR instrument.

153. G. Hennrich, W. M. David, Y. J. Bomble, E. V. Anslyn, J. S. Brodbelt, and J. F. Stanton, *Supramolecular Chemistry* 16, 521 (2004)

154. S. L. Wiskur, H. Ait-Haddou, J. J. Lavigne, and E. V. Anslyn, *Acc. Chem. Res.* 34, 963 (2001)

155. H. Ait-Haddou, S. L. Wiskur, V. M. Lynch, and E. V. Anslyn, *J. Am. Chem. Soc.* 123, 11296 (2001)

156. S. C. McCleskey, A. Metzger, C. S. Simmons, and E. V. Anslyn, *Tetrahedron* 58, 621 (2002)

157. A. M. Piatek, Y. J. Bomble, S. L. Wiskur, and E. V. Anslyn, *J. Am. Chem. Soc.* 126, 6072 (2004)

158. F. Viéte, *De aquationum recognitione et emendatione* Chapter VI, (1650)

159. S. L. Wiskur, *Ph.D. thesis, University of Texas, Austin, TX (USA)*, (2003)

160. D. Jackson and P. B. Lombard, *Am. J. Enol. Vitic.* 44, 409 (1993)

Index

Vita

Yannick J. Bomble was born in Grande-Synthe, France on June 21^{st}, 1978. He is the son of Michel Bomble and Mariannick Bomble. He received his High School diploma – scientific stream – from the Lycée du Noordover with honors in 1996. He entered the classes of Mathématiques Supérieures in 1996 and the classes of Mathématiques Spéciales in 1997 at the Lycée Faidherbe, Lille. He then joined the Université des Sciences et Technologies de Lille in 1998 and graduated in 2001 with a Bachelor in Chemistry, minor in Physics, with honors. His last year of Bachelor was completed at the University of Texas through an exchange program sponsored by the Ecole Centrale de Lille and the IMCC Engineering Exchange Program. In August 2001, he began his graduate studies at the University of Texas in the Department of Chemistry and Biochemistry and joined the research group of Professor John F. Stanton to study ab initio electronic structure theory. He married his long-time sweetheart, Florence Lenne, on June 15^{th}, 2002. They are expecting a little baby girl, Olivia, and will soon be moving to California where he recently accepted a research associate position at the Scripps Research Institute in La Jolla.

Permanent address: 1741 Spyglass Dr Apt 127
Austin, Texas 78746

This dissertation was typeset with LaTeX[†] by the author.

[†]LaTeX is a document preparation system developed by Leslie Lamport as a special

version of Donald Knuth's TEX Program.